TRANSMIT OPTIMIZATION FOR MULTICARRIER AND MULTIPLE-INPUT MULTIPLE-OUTPUT WIRELESS COMMUNICATIONS

by

Neng Wang

A thesis submitted to the

Department of Electrical and Computer Engineering

in conformity with the requirements

for the degree of Doctor of Philosophy

Queen's University

Kingston, Ontario, Canada

May 2005

Abstract

To meet growing demand for wireless access to voice, data and multimedia services, current wireless communication technologies need further improvement in spectral efficiency. Many enabling technologies have been proposed, including multicarrier modulation, multiple-input multiple-output (MIMO) and link adaptation. This thesis investigates link adaptation, particularly transmit optimization in multicarrier and MIMO wireless communications.

In the first part of this thesis, we propose a new bandwidth efficient Orthogonal Frequency Division Multiplexing (OFDM) scheme with adaptive zero-padding (AZP-OFDM) for wireless transmission. A new system design criterion based on the channel matrix condition is studied and applied to the design of an AZP-OFDM system. It has been shown that AZP-OFDM offers a more flexible tradeoff between performance, bandwidth efficiency and complexity.

The second part of this thesis investigates power allocation for OFDM. We propose new minimum bit error rate (MBER) and approximate MBER (AMBER) subcarrier power allocation algorithms for cyclic prefix (CP)-OFDM. It is shown both analytically and by simulation that the proposed CP-OFDM with MBER and AMBER power allocation schemes are superior to CP-OFDM without power allocation as well as zero-forcing (ZF)-equalized

single-carrier with CP. BER performance analysis of power allocation with imperfect channel state information is conducted.

Precoding for MIMO spatial multiplexing generally requires high feedback overhead and/or high complexity processing. In the third part of this thesis, simultaneous reduction in complexity and overhead is proposed by imposing a diagonal structural constraint to precoding, i.e., power allocation. MBER is employed as the optimization criterion. It has been shown that interference cancellation and detection ordering with MBER power allocation offer superior performance over previously proposed MBER precoding with ZF equalization as well as over MMSE precoding/decoding. Performance under noisy channels and power feedback is analyzed.

In the fourth part of this thesis, transmit optimization for two-input multiple-output (TIMO) spatial multiplexing systems is investigated. Approximate MBER transmit power allocation for a variety of receiver structures is investigated. An approximate MBER transmit beamforming scheme is proposed, which eliminates error floors in ill-conditioned TIMO channels.

Acknowledgments

First and foremost, I would like to thank my Ph.D. supervisor, Dr. Steven Blostein, for his excellent guidance, insight, encouragement, patience, and generous support throughout this thesis research.

This work is in part sponsored by Natural Sciences and Engineering Research Council, Samsung Electronics AIT, Bell Mobility, Nortel Networks, and Queen's University. Their financial support is greatly appreciated.

I am grateful to my thesis committee members, Dr. David Falconer from Carleton University, Dr. Fady Alajaji from Department of Mathematics and Statistics, Dr. Saeed Gazor and Dr. Mohamed Ibnkahla, for their taking time to review my thesis and for their comments and suggestions with respect to this thesis.

My sincere thanks to all my colleagues and friends at Queen's, for their friendship, help and all the wonderful time we had together. A special thanks to Dr. Wei-Ping Zhu from Concordia University, for his kind assistance and consideration during my graduate study.

Finally, I would like to thank my wife, Lili Zhang, and my family for their encouragement and support throughout my Ph.D. study at Queen's.

Contents

List of Tables

List of Figures

Acronyms

AMBER	Approximate Minimum Bit Error Rate
AWGN	Additive White Gaussian Noise
AZP	Adaptive Zero-Padding
BER	Bit Error Rate
BPSK	Binary Phase Shift Keying
cf.	confer; refer to
CP	Cyclic Prefix
CSI	Channel State Information
CSIT	Channel State Information at Transmitter
DAB	Digital Audio Broadcasting
DVB	Digital Video Broadcasting
DFT	Discrete Fourier Transform
FDD	Frequency Division Duplex
FFT	Fast Fourier Transform
FIR	Finite Impulse Response
IDFT	Inverse Discrete Fourier Transform
IFFT	Inverse Fast Fourier Transform
LOS	Line-Of-Sight
LS	Least Squares

MIMO	Multiple-Input Multiple-Output
MBER	Minimum Bit Error Rate
MC	Multicarrier
ML	Maximum-Likelihood
MMSE	Minimum Mean-Square Error
OFDM	Orthogonal Frequency Division Multiplexing
OSIC	Ordered Successive Interference Cancellation
PAPR	Peak-to-Average Power Ratio
P/S	Parallel-to-Serial
SC	Single-Carrier
SIC	Successive Interference Cancellation
SISO	Single-Input Single-Output
SNR	Signal-to-Noise Ratio
S/P	Serial-to-Parallel
SVD	Singular Value Decomposition
TDD	Time Division Duplex
TIMO	Two-Input Multiple-Output
V-BLAST	Vertical Bell Laboratories Layered Space-Time
w/ and w/o	with and without, respectively
w.l.o.g.	Without loss of generality
ZF	Zero-Forcing
ZP	Zero-Padding

List of Important Symbols

$\stackrel{\text{def}}{=}$	Defined as
$\star$	Linear convolution
$\otimes$	Circular convolution
$(\cdot)^T$	Matrix or vector transpose
$(\cdot)^*$	Complex conjugate
$(\cdot)^H$	Matrix or vector conjugate transpose
$(\cdot)^\dagger$	Matrix Moore-Penrose pseudo-inverse
$[\cdot]_m$	m-th entry of a vector
$[\cdot]_{m,n}$	(m,n)-th entry of a matrix
$\lvert x\rvert$	Absolute value (modulus) of the scalar x
$\lVert\boldsymbol{x}\rVert$	A norm of a vector $\boldsymbol{x}$
$\lVert\boldsymbol{x}\rVert_2$	2-norm of a vector $\boldsymbol{x}$: $\lVert\boldsymbol{x}\rVert_2 = (\boldsymbol{x}^H\boldsymbol{x})^{1/2}$
$(\cdot)^f$	Frequency-domain variable
$\boldsymbol{\eta}$	Noise vector
$\kappa_2(\boldsymbol{X})$	Condition number of matrix $\boldsymbol{X}$ with respect to 2-norm
$\boldsymbol{\Upsilon}_{\boldsymbol{X}}$	Projection matrix of $\boldsymbol{X}$
$\boldsymbol{\Upsilon}_{\boldsymbol{X}}^{\perp}$	Orthogonal projection matrix of $\boldsymbol{X}$
$\det(\cdot)$	Determinant of a matrix
$\text{diag}(\boldsymbol{x})$	Diagonal matrix with diagonal entries given by $\boldsymbol{x}$

$\mathbb{E}\{\cdot\}$	Expectation of random variables
$\boldsymbol{H}$	Channel matrix
$\hat{\boldsymbol{H}}$	Estimate of channel matrix $\boldsymbol{H}$
$\boldsymbol{I}_N$	$N \times N$ identity matrix
$\mathfrak{I}(\cdot)$	Imaginary part of a complex number
N	Block size of block transmission
N_t	Number of transmit antennas
N_r	Number of receive antennas
$\boldsymbol{P}$	Power allocation or precoding matrix
$\boldsymbol{r}$	Received signal vector
$\mathfrak{R}(\cdot)$	Real part of a complex number
$\boldsymbol{s}$	Transmitted signal vector
$\text{trace}(\cdot)$	Trace of a matrix

Chapter 1

Introduction

1.1 Motivation

Over past decades, wireless markets have been witnessing unprecedented growth fueled by information explosion and technology revolution. Wireless communications is diverse and ubiquitous in today's world. The continued increase in demand for all types of wireless services (voice, data and multimedia) has driven wireless communications to move from *narrowband* to *wideband* in both *cellular mobile* and *fixed wireless* areas [9, 65]. In this context, wireless communication technologies need further improvement in spectral efficiency to satisfy the ever increasing demand for higher capacity and data rates. Many enabling technologies that improve the spectral efficiency have been proposed and/or standardized, including, e.g., smart antennas, in particular multiple-input multiple-output (MIMO) technology, multicarrier modulation, and link adaptation techniques [9, 14, 17, 39, 98].

1.1.1 Multicarrier Wireless Transmission

Multicarrier transmission is a form of multichannel communications. The frequency band of the multicarrier channel is subdivided into a number of subcarriers over which information is transmitted [10]. As a bandwidth efficient multicarrier scheme, Orthogonal Frequency Division Multiplexing (OFDM) has become a popular technique for transmission of signals over wired and wireless channels [11, 106].

Historically, OFDM was introduced in 1960s [19, 83, 87]. Further development, e.g., [10] and [21] enabled a growing interest in OFDM technology and applications with adoption in wired and wireless standards, such as digital audio and video broadcasting (DAB and DVB) in Europe [29, 30], high speed modem transmissions over copper wires (Asynchronous Digital Subscriber Line, ADSL) [5], wireless Local Area Network (Wireless LAN) standards IEEE 802.11 in North America [46], HIPERLAN/2 in Europe [32] and Multimedia Mobile Access Communication (MMAC) in Japan, and wireless Metropolitan Area Network (Wireless MAN) IEEE 802.16 [47] and HIPERMAN [33]. OFDM is also a potential candidate for dedicated short-range communications (DSRC) for road side to vehicle communications and fourth-generation (4G) wireless mobile systems [98].

Wireless transmission experiences multipath fading due to the nature of radio propagation. Multipath signals cause inter-symbol interference (ISI), which limits system performance and data rate. In single-carrier communications, time-domain equalization (TDE) is generally employed to mitigate ISI. With the increase of system bandwidth, multipath effects become severe and the complexity of TDE increases, which can be prohibitively high in particular wideband systems. On the other hand, by subdividing the channel frequency band, OFDM effectively converts a frequency-selective channel into a number of parallel frequency-flat subchannels. Therefore, equalization in OFDM systems degenerates to scalar gain control, also known as one-tap equalization.

In OFDM systems, subcarriers are separated by the minimum frequency separation required to maintain orthogonality among their corresponding time domain waveforms, while their corresponding signal spectra overlap in frequency. As a result, the channel bandwidth is used efficiently in OFDM. To mitigate the effect of ISI, a guard interval of length no shorter than the channel delay spread is generally inserted between OFDM block signals. The guard interval may be either cyclic prefix (CP) [82] or null [107], referred to as, respectively, CP-OFDM and zero-padding (ZP) OFDM [106]. The baseband modulation/demodualtion of OFDM signals can be implemented efficiently using discrete Fourier transform (DFT) [82]. These properties facilitate OFDM to be a favorable transmission scheme for wideband wireless communications.

Besides its advantages, OFDM transmission experiences some difficulties as well. For example, OFDM signals have high peak-to-average power ratio (PAPR), which increases the cost of linear amplifiers [73]. Compared with its single-carrier counterpart, OFDM is sensitive to frequency offsets and time-varying channels, both of which destroy orthogonality among subcarriers and cause inter-carrier interference (ICI) and irreducible error floors [113]. The problems of PAPR reduction and synchronization in OFDM have been studied in [61, 99, 110].

Though OFDM uses the available frequency band efficiently, the overall system bandwidth efficiency is not necessarily high due to the overhead incurred by guard intervals. When either the channel delay spread or data rate increases, the length of the guard sequence has to be increased accordingly in order to avoid ICI, which reduces system bandwidth efficiency. One method to improve efficiency is to increase the OFDM block size, at the cost of increased latency and implementation complexity. Moreover, CP-OFDM offers simplified equalization at the expense of symbol recovery capability, since subcarriers may encounter channel nulls [106]. These problems comprise our main concerns about OFDM

transmission in this thesis, where link adaptation schemes will be investigated as solutions.

1.1.2 MIMO Wireless Communications

The fundamental work by Foschini and Gans [36] and Telatar [102] suggest that the use of multiple transmit and receive antennas, referred to as a MIMO system, can provide higher data rates over wireless links at no extra expenditure of bandwidth and power. MIMO technologies essentially explore the spatial dimension in wireless communication links to provide a promising means to increase spectral efficiency in future wideband wireless transmission.

MIMO technologies improve wireless system performance with *array gain*, *diversity gain*, *spatial multiplexing gain*, and *interference reduction* capability [79, 80]:

- Array gain results from coherent combining, increases average receive SNR, and can be achieved through processing at the transmit and receive side [4];
- Diversity gain mitigates random fluctuation (or fading) of radio signals, and can be made available at the receiver [50], the transmitter [3, 100, 101], or both;
- Spatial multiplexing offers a linear increase in capacity at no additional expenditure of power or bandwidth, under conducive channel conditions, such as rich scattering [36, 102];
- Interference reduction algorithms cancel or reduce the co-channel interference (CCI) by differentiating between the spatial signatures of the desired and CCI signals, allow aggressive frequency reuse, and therefore improve the system capacity [81].

To achieve these gains afforded by MIMO technologies, appropriate transceiver designs are necessary. We focus on MIMO spatial multiplexing systems in this thesis. Signal

reception in MIMO spatial multiplexing can employ a variety of criteria. While the optimal maximum likelihood (ML) receiver lower bounds the error rate performance of other sub-optimal receivers, ML complexity grows exponentially in the number of the transmitted signal streams. The linear ZF receiver, on the other hand, has low complexity, but generally suffers from noise enhancement problems. Reasonable tradeoffs between performance and complexity can be achieved by other sub-optimal receivers, such as minimum mean squared-error (MMSE), successive interference cancellation (SIC), or ordered SIC (OSIC) as, for example, in the case of the Vertical Bell Laboratories Layered Space-Time (V-BLAST) [37, 79].

When channel knowledge is available at the transmitter, referred to as CSIT, it can be exploited to improve system performance [79]. While obtaining full CSIT is generally expensive, partial CSIT in the form of instantaneous channel parameters or its second-order statistics can be easier to obtain. A variety of factors determine the scheme used to exploit CSIT, such as receiver structure and optimization criterion (e.g., throughput or error rate). Generally, CSIT is exploited by using precoding. A variety of precoding schemes have been proposed for MIMO, including MMSE precoding/decoding [92], minimum bit error rate (MBER) precoding for ZF receiver [28], and limited feedback precoding [58, 59]. As a special case of precoding, transmit antenna selection has also been proposed to reduced the complexity/cost of radio frequency (RF) chains [42, 64, 89]. Nevertheless, general precoding for MIMO has high complexity (in obtaining the precoder) and/or feedback overhead (in feeding back the channel or precoding matrix), which motivates our investigation of new schemes to exploit CSIT with reduced complexity and overhead.

1.1.3 Link Adaptation

Link adaptation refers to algorithms and protocols that dynamically adapt the modulation, coding rate and/or other signal transmission parameters to the changing channel conditions. Good channel conditions result in the transmission of less redundant information and therefore more efficiency [17]. Traditional link adaptation techniques employed in cellular communication systems include *power control*, *adaptive modulation/coding* and *water-filling* [6]:

- Power control adjusts the power of the transmitted signal to *meet* a target carrier-to-interference-plus-noise ratio. It is commonly used in CDMA systems to reduce interference, as well as in some TDMA systems. Downlink power control can be viewed as *power allocation* among all of the active users.

- Adaptive modulation/coding adjusts the modulation level and coding formats to *match* the current received signal quality. It is used in TDMA systems such as the Enhanced Data for GSM Evolution (EDGE) as well as in some CDMA systems.

- Water-filling can be viewed as a combination of adaptive modulation/coding and power allocation [20].

We note that traditional link adaptation techniques are primarily applied to multiuser cellular systems. As additional signal dimensions (space and frequency) are exploited in future wideband communications, a nature question is how to dynamically allocate available resources among these dimensions for each user in order to increase spectral efficiency. As a heuristic solution, each signal stream can be viewed as a virtual user, resulting in a virtual multiuser system. The existing link adaptation techniques then apply directly. Nevertheless, compared with cellular multiuser systems, multicarrier and MIMO system design

poses different technical challenges and provides new degrees of freedom as well. A few examples are given next.

- In the uplink of a multiuser system, each user does not generally have full channel knowledge of other users, but some transmission parameters from the basestation. At the transmitter of a multicarrier or MIMO systems, on the other hand, CSI can be made available to all virtual users. This makes collaboration among virtual users (signal streams) possible.

- Traditional link adaptation in cellular wireless systems generally employ criteria such as system capacity, peak data rate, and/or coverage reliability [6]. These criteria can also be used in link adaptation of multicarrier and MIMO systems. Furthermore, taking into account the nature of optimization of single user performance, other criteria such as error rate can be employed as well.

- In OFDM systems, redundancy is introduced in terms of CP or ZP for simplification of equalization or symbol recovery. Such redundancy is fixed in existing standards. This scheme is not efficient if the channel condition is good, and not robust when the channel delay spread is large.

These motivate our investigation of link adaptation for multicarrier and MIMO systems.

Future wideband wireless networks are expected to support a mix of real-time (delay-sensitive) traffic such as voice, multimedia teleconferencing and games, and data traffic such as Web-browsing, email and file transfers [94]. In this thesis, we assume the transmission rate is fixed and study the redundancy and power aspects of link adaptation, which may find application in real-time applications. Such link adaptation techniques are also referred to as *transmit optimization* in this thesis.

1.2 Thesis Overview

This thesis investigates the transmit optimization problem for wireless multicarrier and MIMO communications. There are seven chapters in this thesis addressing different aspects of this topic.

In Chapter 2, the wireless channel model, including both SISO and MIMO, is first described. Principles of wireless multicarrier and MIMO transmission as well as their related issues are then reviewed, followed by a description of the objectives of this thesis.

Chapter 3 proposes an adaptive zero-padding (AZP) OFDM transmission scheme which offers flexible tradeoffs among performance, bandwidth efficiency and complexity. We first analyze redundancy issues in OFDM schemes using cyclic prefix (CP), zero-padding (ZP) as well as the use of no guard interval. A new system design criterion based on the channel matrix condition is then proposed. Based on this criterion, an AZP-OFDM scheme is proposed, which adjusts the length of guard interval in terms of zero-padding according to the condition number of channel matrix. Performance of the proposed AZP-OFDM scheme is assessed by Monte Carlo simulations.

A framework for analytical performance comparison between CP-based OFDM and siggle-carrier block transmission schemes is presented in Chapter 4. Motivated by the analytical performance comparison, power allocation schemes using a variety of criteria are proposed, including minimization of bit error rate (MBER), as well as an approximate MBER (AMBER) scheme with a closed-form optimum solution and small performance loss. Analytical performance comparison among a variety of schemes is conducted. Performance degradation of power allocation under imperfect CSI estimate/feedback is investigated as well.

In Chapter 5, we apply power allocation to MIMO spatial multiplexing systems. Signal reception methods and performances are first reviewed. An MBER transmit power

allocation scheme is then proposed. It is shown that compared with existing precoding schemes, the proposed MBER transmit power allocation together with detection ordering and interference cancellation improves performance with reduced feedback overhead and complexity. Performance degradation of transmit power allocation using noisy feedback is also investigated, based on which a robust MBER power allocation scheme is proposed, which takes into account both noisy CSI variance and error propagation.

Chapter 6 considers transmit optimization of TIMO spatial multiplexing systems, a special case of MIMO. The MBER transmit power allocation method proposed in Chapter 5 is applied to TIMO channels, with simple closed-form solutions. An approximate MBER transmit beamforming scheme is also proposed, with the capability of mitigating error floors in ill-conditioned TIMO channels.

Finally, Chapter 7 summarizes the conclusions and suggests possible directions for future work.

1.3 Summary of Contributions

The primary contributions of this thesis are summarized as follows.

- Redundancy in OFDM schemes is analyzed. An OFDM system design criterion based on the channel matrix condition number is proposed. Using this criterion, an AZP-OFDM scheme is developed. An algorithm for choice of AZP length is provided.

- MBER and AMBER power allocation schemes and algorithms for CP-OFDM are proposed. Analytical performance comparison among CP-OFDM and single-carrier block transmission is conducted. Performance of power allocation under uncertain CSI feedback/estimate is analyzed.

- MBER power allocation is applied to MIMO spatial multiplexing systems. Performance, complexity and feedback overhead using power allocation are analyzed and compared to general precoding schemes. Performance degradation under noisy CSI and power feedback is analyzed. A robust MBER power allocation using feedback noise variance is proposed. Mitigation of error propagation in interference cancellation receivers is addressed.

- MBER power allocation for TIMO spatial multiplexing is analyzed. An approximate MBER transmit beamforming scheme for ill-conditioned TIMO channels is proposed. Extension of the proposed transmit beamforming to high order modulation schemes is investigated.

Chapter 2

Background and Objectives

2.1 Wireless Channel Model

The mobile radio channel places fundamental limitations on reliability and throughput of wireless communications. The mechanisms behind radio-wave propagation are complicated. Due to scattering, reflection and diffraction of radiated energy from various objects, the transmitted signal arrives the receiver along a number of distinct paths, resulting in *multipath fading*. Multipath signals arrive at the receiver with different time-varying delays, angles of arrival and attenuations. In a single-input single-output (SISO) channel, multipath causes the spreading of signals in time and frequency:

- frequency-nonselective fading due to constructive and destructive interference of multipath signals;
- frequency-selective fading caused by multipath propagation delays;
- time-selective fading (Doppler spread) due to relative movements of the transmitter, receiver and/or scatters.

Radio propagation and wireless channel modelling issues have been covered in detail in [50, 85]. For MIMO communications, multipath propagation results in the spreading of signals in the spatial dimension in addition to time and frequency dimensions, i.e.,

- spatially selective fading due to angle spread.

MIMO channel modelling has been reviewed and studied in detail in [79, 112].

2.1.1 SISO Wireless Channel

Consider a SISO wireless channel. Let $h(\tau,t)$ denote the overall time-varying impulse response of the transmit-filter, continuous channel and receive-filter. Denote $s(t)$ as the transmitted signal. Ignoring the additive white Gaussian noise (AWGN), the received signal $r(t)$ is given by

$$r(t) = \int_{\tau_1}^{\tau_{\tilde{L}}} h(\tau,t)s(t-\tau)d\tau = h(\tau,t) \star s(t), \tag{2.1}$$

where $\star$ denotes convolution; τ_1 and $\tau_{\tilde{L}}$ denote the minimum and maximum path delays, respectively.

2.1.1.1 Frequency-Nonselective Fading

If the delay spread is much less than the symbol period T_s, i.e., $\tau_{\tilde{L}} - \tau_1 \ll T_s$, then (2.1) can be approximated as

$$r(t) \approx h(\tau_1,t)s(t-\tau_1) \stackrel{\text{def}}{=} h(t)s(t-\tau_1). \tag{2.2}$$

The channel is *frequency-nonselective.* When there is a large number of multipath signals with uniformly distributed phase angles on $[0,2\pi]$, the channel amplitude $|h(t)|$ has a Rayleigh distribution,

$$f_{|h(t)|}(\alpha) = \frac{\alpha}{\sigma_h^2} \exp\left\{-\frac{\alpha^2}{2\sigma_h^2}\right\}, \quad \alpha \geq 0, \tag{2.3}$$

where σ_h^2 is the power of the multipath signals. If there is a dominant path, usually a line-of-sight (LOS) path, $|h(t)|$ follows a Ricean distribution,

$$f_{|h(t)|}(\alpha) = \frac{\alpha}{\sigma_h^2} \exp\left\{-\frac{\alpha^2 + A^2}{2\sigma_h^2}\right\} I_0\left(\frac{\alpha A}{\sigma_h^2}\right), \qquad \alpha \geq 0, \tag{2.4}$$

where A is the amplitude of the dominant path, and $I_0(\cdot)$ denotes the zeroth-order modified Bessel function of the first kind. The Ricean K-factor characterizes the dominance of the LOS path and is defined as

$$K \stackrel{\text{def}}{=} \frac{A^2}{2\sigma_h^2}. \tag{2.5}$$

2.1.1.2 Frequency-Selective Fading

With a decrease in symbol duration, or, equivalently, an increase in signal bandwidth, the received signal is a sum of resolvable delayed copies of the original signal,

$$r(t) = \sum_{\tilde{l}=1}^{\tilde{L}} h_{\tilde{l}}(t) s(t - \tau_{\tilde{l}}(t)), \tag{2.6}$$

where $h_{\tilde{l}}(t)$ and $\tau_{\tilde{l}}(t)$ denote, respectively, the channel gain coefficient and delay of the $\tilde{l}$-th path. The frequency response of the channel in (2.6) fluctuates across the signal bandwidth, and (2.6) is *frequency-selective*. Note that in (2.6), when there is no delay spread, i.e., $\tilde{L} = 1$, and the channel frequency response is flat across the signal bandwidth, and (2.6) degenerates to the frequency-nonselective channel (2.2).

A frequency domain parameter related to channel frequency selectivity is *coherence bandwidth* (B_c), which is inversely proportional to the delay spread. Frequency selectivity depends on the bandwidth of signal (B_s) with respect to channel coherence bandwidth B_c. If B_s is relatively small compared to B_c, the signal experiences frequency-nonselective fading; otherwise, fading is frequency-selective. Frequency-selective fading introduces inter-symbol interference (ISI) in single-carrier transmission, and time domain equalization is typically employed to mitigate distortion and improve system performance. Complexity

of time domain equalization increases with the number of channel taps. On the other hand, in multicarrier systems, the total bandwidth is subdivided into narrower (with respect to channel coherence bandwidth) frequency bins for signal transmission. Such frequency division mitigates channel frequency selectivity experienced by the transmitted signal and simplifies equalization.

2.1.1.3 Time-Selective Fading

Scatter or transmitter/receiver relative motion results in variation of channel response in time. In other words, the transmitted signal experiences different fading at different times, which is referred to as *time-selective fading*. Motion results in frequency shift (Doppler spread). Time-selective fading can be characterized by the channel coherence time, T_c, which is inversely proportional to Doppler spread. Most communications systems require channel state information (CSI) at the receiver to decode the transmitted information. For channels with relative small T_c (with respect to T_s), CSI has to be acquired frequently, which increases overhead. In systems with transmit optimization, overhead due to estimation or feedback of CSI or related information at the transmitter increases as well.

2.1.2 MIMO Wireless Channel

Consider a MIMO system with N_t transmit antennas and N_r receive antennas. The MIMO channel matrix is obtained on the basis of SISO channels, i.e.,

$$\boldsymbol{H}(\tau,t) = \begin{bmatrix} h_{1,1}(\tau,t) & h_{1,2}(\tau,t) & \cdots & h_{1,N_t}(\tau,t) \\ h_{2,1}(\tau,t) & h_{2,2}(\tau,t) & \cdots & h_{2,N_t}(\tau,t) \\ \vdots & \vdots & \ddots & \vdots \\ h_{N_r,1}(\tau,t) & h_{N_r,2}(\tau,t) & \cdots & h_{N_r,N_t}(\tau,t) \end{bmatrix}_{N_r \times N_t}, \tag{2.7}$$

where $h_{m,n}(\tau,t)$ denotes the channel response between the n-th ($n = 1,\cdots,N_t$) transmit antenna and the m-th ($m = 1,\cdots,N_r$) receive antenna. For simplicity of notation, we drop the t dependence in (2.7). We also assume frequency-nonselective MIMO channels in this thesis. Due to the introduction of the spatial dimension, compared with SISO channel model, a number of new parameters are added in order to characterize MIMO channels. We consider a general Ricean fading MIMO channel, which can be modelled as the sum of a LOS component and a scattered component [35]

$$\boldsymbol{H} = \sqrt{\frac{K}{1+K}}\boldsymbol{H}_l + \sqrt{\frac{1}{1+K}}\boldsymbol{H}_s, \tag{2.8}$$

where Ricean K-factor is defined as the ratio of LOS-to-scattered power. When $K = 0$, (2.8) degenerates to a Rayleigh fading MIMO channel. $\boldsymbol{H}_l$ and $\boldsymbol{H}_s$ denote $N_r \times N_t$ channel matrices of the LOS and scattered components, respectively.

2.1.2.1 LOS Component

Consider linear transmit and receive antenna arrays. The LOS component $\boldsymbol{H}_l$ can be modelled as [35]

$$\boldsymbol{H}_l = \boldsymbol{a}_r(\theta_r)\,\boldsymbol{a}_t(\theta_t)^T,$$

where

$$\begin{aligned}
\boldsymbol{a}_r(\theta_r) &= \left[1 \;\; e^{-j2\pi d_r \sin(\theta_r)} \;\; \cdots \;\; e^{-j2\pi d_r \sin((N_r-1)\theta_r)}\right]^T, \\
\boldsymbol{a}_t(\theta_t) &= \left[1 \;\; e^{-j2\pi d_t \sin(\theta_t)} \;\; \cdots \;\; e^{-j2\pi d_t \sin((N_t-1)\theta_t)}\right]^T,
\end{aligned}$$

are the array response vectors for the receiver and transmitter antenna arrays; θ_r and θ_t are the angles of arrival and departure of the deterministic component, respectively; d_r and d_t are the receiver and transmitter antenna spacing expressed in terms of wavelengths, respectively.

2.1.2.2 Scattered Component

The entries of the scattered component are modelled as zero-mean complex Gaussian random variables, with cross-correlations determined by antenna array geometry, angle spread, mean direction of signal arrival/departure, etc. Spatial fading correlations indicate the available spatial diversity of a MIMO channel: little spatial diversity gain can be extracted from highly correlated channels, and vice-versa. In [95], the spatial fading correlations were derived for isotropic scattering around the mobile. A space-time fading correlation model for general nonisotropic scattering around the mobile was proposed in [1].

In this thesis, we adopt the spatial fading correlation model given in [1]. A geometric configuration of MIMO channel with local scatterers around the transmitter is illustrated in Fig. 2.1. For isotropic scattering around the transmitter and a small angle spread Δ, the cross-correlation between channel coefficients $h_{p,l}$ and $h_{q,m}$ can be approximated as [1]

$$\begin{aligned}\mathbb{E}\left\{h_{p,l}h_{q,m}^{*}\right\} &\approx \exp\left\{jc_{pq}\cos(\alpha_{pq})\right\} \\ &\quad\times I_0\left(\sqrt{-b_{lm}^2-c_{pq}^2\Delta^2\sin^2(\alpha_{pq})-2c_{pq}b_{lm}\Delta\sin(\alpha_{pq})\sin(\beta_{lm})}\right) \qquad (2.9)\end{aligned}$$

where $j=\sqrt{-1}$; $b_{lm}=2\pi d_{lm}$ and $c_{pq}=2\pi\delta_{pq}$; d_{lm} and δ_{pq} are the antenna spacings at the receiver and transmitter expressed in terms of wavelengths; angles α_{pq} and β_{lm} are shown in Fig. 2.1. With the decrease of angle spread Δ, spatial correlation increases. In a Ricean fading channel (2.8), as the LOS component becomes prominent, i.e., K increases, the spatial correlations increase as well. We note that (2.8) includes both Rayleigh and uncorrelated fading channels as special cases.

2.2 Multicarrier Wireless Communications

Frequency-selective multipath channels introduce ISI, which degrades performance and limits maximum data rate [84]. If single-carrier (SC) modulation is employed, an equalizer

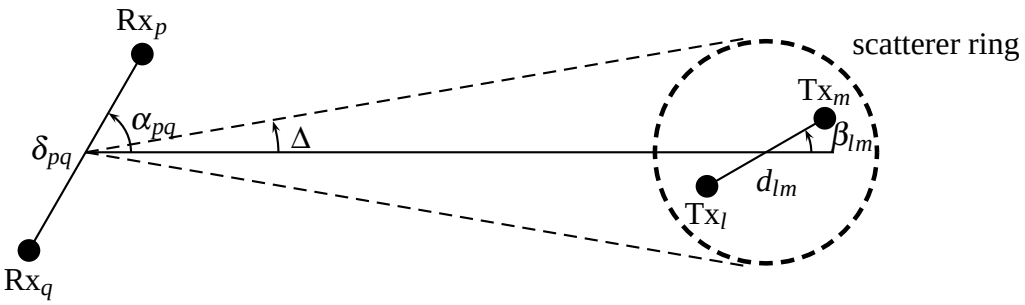

Figure 2.1. Geometric configuration of MIMO channel with local scatterers around the transmitter: Rx$_p$ is the p-th antenna element at the receiver, Tx$_l$ is the l-th antenna element at the transmitter.

is required to compensate for the channel distortion. The complexity of an SC receiver increases as the channel delay spread increases. Alternatively, multicarrier (MC) technologies can be used. In an MC system, the available bandwidth is subdivided into a number of subcarriers, with each subcarrier experiencing nearly frequency-nonselective fading. From a time-domain point of view, the symbol duration of each subcarrier in MC systems is longer than that of SC systems, which increases robustness to channel delay spread and simplifies equalization.

2.2.1 Principle of MC Modulation

Consider an MC system with N subcarriers. To eliminate inter-carrier interference (ICI), subcarriers are chosen to be orthogonal to each other. Denote the symbol period of each subcarrier as T_s. When the frequency separation between subcarriers is $\Delta f = n/T_s, n = 1, 2, \cdots$, subcarriers are orthogonal to each other [84]. The minimum frequency separation between subcarriers for orthogonality is $\Delta f_{\min} = 1/T_s$. Multicarrier modulation with subcarrier frequency separation $\Delta f_{\min}$ is usually referred to as orthogonal frequency division

multiplexing (OFDM), which is also a topic of this thesis.

Denote the baseband frequency of the k-th subcarrier as $f_k = k/T_s, k \in [0, N-1]$. The transmitted signal is modelled as

$$s(t) = \frac{1}{\sqrt{N}} \sum_{k=0}^{N-1} u_k e^{j2\pi kt/T_s}, \quad 0 \le t < T_s, \tag{2.10}$$

where u_k is the information symbol transmitted over the k-th subcarrier. When $s(t)$ is transmitted over a frequency-selective channel, the received signal is given by

$$r_{\mathrm{MC}}(t) = s(t) \star h(t) + \eta(t), \tag{2.11}$$

where $\eta(t)$ denotes the additive white Gaussian noise (AWGN) process. If we assume that the channel is constant over an OFDM block, and varying (slowly) from block to block, (2.11) can be simplified, according to (2.6), as

$$r_{\mathrm{MC}}(t) = \sum_{\tilde{l}=1}^{\tilde{L}} h_{\tilde{l}} s(t - \tau_{\tilde{l}}) + \eta(t). \tag{2.12}$$

In successive transmission, (2.12) experiences inter-block interference (IBI) from previous block. To avoid IBI, a guard interval of duration $T_g \ge \tau_{\tilde{L}}$ in terms of cyclic prefix (CP) or zero-padding (ZP) is usually inserted.

2.2.1.1 CP-OFDM

By inserting a cyclic prefix, the CP-OFDM transmitted signal becomes

$$s_{\mathrm{CP}}(t) = \frac{1}{\sqrt{N}} \sum_{k=0}^{N-1} u_k e^{j2\pi kt/T_s}, \quad -T_g \le t < T_s, \tag{2.13}$$

Denote the sampling period as $T_c = T_s/N$. Sampling the continuous transmitted signal (2.10) at $t_n = nT_c$, the discrete transmitted signal becomes

$$s_n = \frac{1}{\sqrt{N}} \sum_{k=0}^{N-1} u_k e^{j2\pi kn/N}, \quad 0 \le n < N,$$

which is the inverse discrete Fourier transform (IDFT) of $\{u_k\}_{k=0}^{N-1}$. For convenience of notation, we use matrix-vector representation in what follows. The transmitted signal vector is given by

$$\boldsymbol{s} = [s_0\ s_1\ \cdots\ s_{N-1}]^T = \boldsymbol{F}_N^H \boldsymbol{u},$$

where $\boldsymbol{F}_N$ denotes the N-point discrete Fourier transform (DFT) matrix with $[\boldsymbol{F}_N]_{m,n} = \frac{1}{\sqrt{N}} e^{-j2\pi mn/N}$, and $\boldsymbol{u} = [u_0\ \cdots\ u_{N-1}]^T$ denotes the information symbol vector. Choose T_g so that $G = T_g/T_c$ is an integer. The CP-OFDM signal vector is then obtained as

$$\boldsymbol{s}_{\text{CP}} = [\underbrace{s_{N-G}\ \cdots\ s_{N-1}}_{\text{cyclic prefix}}\ \underbrace{s_0\ \cdots\ s_{N-1}}_{\boldsymbol{s}}]^T.$$

The multipath propagation channel can be modelled as a finite impulse response (FIR) filter with tap coefficients $h_0, h_1, \cdots, h_L$. At the receiver, after discarding the first G entries corresponding to the CP, the received signal vector is obtained as,

$$\underbrace{\begin{bmatrix} r_{\text{CP},0} \\ r_{\text{CP},1} \\ \vdots \\ \vdots \\ \vdots \\ r_{\text{CP},N-1} \end{bmatrix}}_{\boldsymbol{r}_{\text{CP}}} = \underbrace{\begin{bmatrix} h_0 & 0 & \cdots & 0 & h_L & \cdots & h_1 \\ h_1 & \ddots & \ddots & & \ddots & \ddots & \vdots \\ \vdots & \ddots & \ddots & \ddots & & \ddots & h_L \\ h_L & & \ddots & \ddots & \ddots & & 0 \\ 0 & \ddots & & \ddots & \ddots & \ddots & \vdots \\ \vdots & \ddots & \ddots & & \ddots & \ddots & 0 \\ 0 & \cdots & 0 & h_L & \cdots & h_1 & h_0 \end{bmatrix}}_{\boldsymbol{H}_{\text{CP}}} \underbrace{\begin{bmatrix} s_0 \\ s_1 \\ \vdots \\ \vdots \\ \vdots \\ s_{N-1} \end{bmatrix}}_{\boldsymbol{s}} + \underbrace{\begin{bmatrix} \eta_0 \\ \eta_1 \\ \vdots \\ \vdots \\ \vdots \\ \eta_{N-1} \end{bmatrix}}_{\boldsymbol{\eta}_N}, \tag{2.14}$$

where $\boldsymbol{H}_{\text{CP}}$ is an $N \times N$ circulant matrix [41], and $\boldsymbol{\eta}_N$ denotes an $N \times 1$ AWGN vector. Note that due to CP insertion, the linear convolution model (2.12) becomes circular convolution [75] in (2.14), i.e.,

$$r_{\text{CP},n} = h_n \otimes s_n + \eta_n,$$

where $\otimes$ denotes circular convolution. Performing MC demodulation via DFT, the frequency-domain received signal vector is obtained as

$$\begin{aligned} \boldsymbol{r}^f &= \boldsymbol{F}_N \boldsymbol{r}_{\mathrm{CP}} \\ &= \boldsymbol{F}_N \boldsymbol{H}_{\mathrm{CP}} \boldsymbol{s} + \boldsymbol{F}_N \boldsymbol{\eta}_N \\ &= \boldsymbol{F}_N \boldsymbol{H}_{\mathrm{CP}} \boldsymbol{F}_N^H \boldsymbol{u} + \boldsymbol{\eta}_N^f, \end{aligned} \tag{2.15}$$

where the superscript ^{f} denotes a frequency-domain variable. By using the well-known property of circulant matrices, we have

$$\boldsymbol{r}^f = \underbrace{\mathrm{diag}\{\boldsymbol{F}_N \boldsymbol{h}\}}_{\stackrel{\mathrm{def}}{=}\boldsymbol{D}_h} \boldsymbol{u} + \boldsymbol{\eta}_N^f, \tag{2.16}$$

where the $N \times 1$ vector $\boldsymbol{h} \stackrel{\mathrm{def}}{=} [h_0\ h_1\ \cdots\ h_L\ 0\ \cdots\ 0]^T$, and $\boldsymbol{D}_h \stackrel{\mathrm{def}}{=} \mathrm{diag}\{H_0, H_1, \cdots, H_{N-1}\}$ with $H_k \stackrel{\mathrm{def}}{=} [\boldsymbol{F}_N \boldsymbol{h}]_k$ denoting the channel frequency response of k-th subcarrier. A block diagram of CP-OFDM system is illustrated in Fig. 2.2. Essentially, by inserting CP and performing MC modulation and demodulation, N effective frequency-nonselective fading channels have been established, i.e.,

$$r_k^f = H_k u_k + \eta_k^f, \qquad k = 0, 1, \cdots, N-1, \tag{2.17}$$

where $r_k^f \stackrel{\mathrm{def}}{=} [\boldsymbol{r}^f]_k$ and $\eta_k^f \stackrel{\mathrm{def}}{=} [\boldsymbol{\eta}_N^f]_k$. This is shown in Fig. 2.3. Equalization required for (2.17) is scalar division, also know as *one-tap equalization*,

$$\hat{u}_k = \frac{r_k^f}{H_k} = u_k + \frac{\eta_k^f}{H_k}, \qquad k = 0, 1, \cdots, N-1, \tag{2.18}$$

where perfect channel state information (CSI) is assumed available at the receiver.

For simplicity of analysis purposes, we assume white input and noise, i.e., $\mathbb{E}\left\{\boldsymbol{u}\boldsymbol{u}^H\right\} = E_s \boldsymbol{I}_N$ and $\mathbb{E}\left\{\boldsymbol{\eta}_N \boldsymbol{\eta}_N^H\right\} = N_0 \boldsymbol{I}_N$. The input signal-to-noise ratio (SNR) is defined as $\gamma_s \stackrel{\mathrm{def}}{=} E_s/N_0$. Note that DFT is a unitary operation, and the statistical properties of $\boldsymbol{\eta}_N^f$ are the

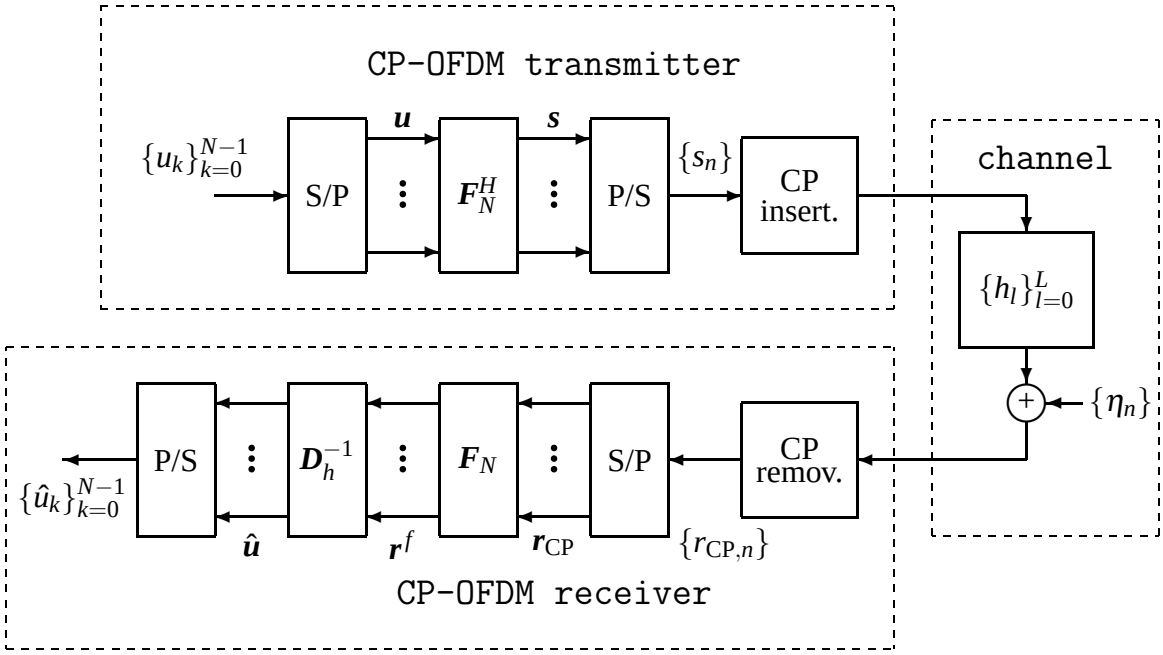

Figure 2.2. Block diagram of CP-OFDM system (S/P: serial-to-parallel conversion, P/S: parallel-to-serial conversion).

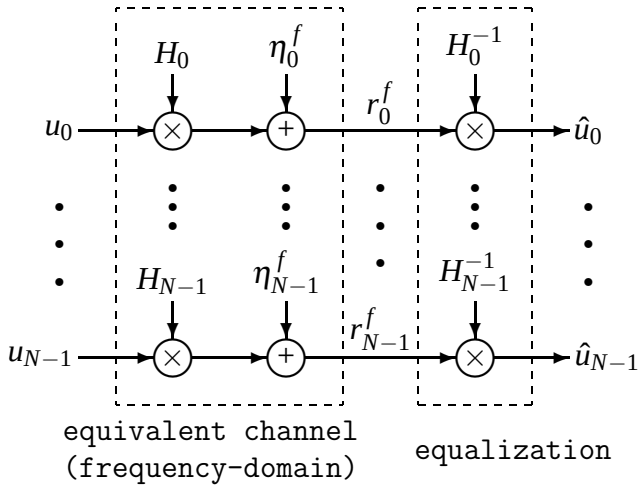

Figure 2.3. Equivalent model of a CP-OFDM system.

same as those of $\boldsymbol{\eta}_N$. From (2.18), the decision-point SNR of the k-th subcarrier is then obtained as

$$\gamma_k = \frac{\mathbb{E}\left\{|u_k|^2\right\}}{\mathbb{E}\left\{\left|\eta_k^f/H_k\right|^2\right\}} = \gamma_s|H_k|^2, \qquad k = 0,1,\cdots,N-1. \tag{2.19}$$

Using the decision-point SNR's (2.19), the instantaneous average probability of error can be readily obtained. For example, using binary phase shift keying (BPSK) modulation, the instantaneous average bit error rate (BER) is given by [84]

$$P_b(\gamma_s;\boldsymbol{h}) = \frac{1}{N}\sum_{k=0}^{N-1} Q\left(\sqrt{2\gamma_s|H_k|^2}\right), \tag{2.20}$$

where $Q(x) \stackrel{\text{def}}{=} \frac{1}{\sqrt{2\pi}}\int_x^\infty e^{-y^2/2}dy$.

2.2.1.2 ZP-OFDM

The ZP-OFDM transmitted signal vector is given by

$$\boldsymbol{s}_{\text{ZP}} = [\underbrace{s_0 \cdots s_{N-1}}_{\boldsymbol{s}} \underbrace{0 \cdots 0}_{G}]^T.$$

Denote $M = N+G$. The received signal vector is obtained as

$$\underbrace{\begin{bmatrix} r_{\text{ZP},0} \\ r_{\text{ZP},1} \\ \vdots \\ \vdots \\ \vdots \\ r_{\text{ZP},M-1} \end{bmatrix}}_{\boldsymbol{r}_{\text{ZP}}} = \underbrace{\begin{bmatrix} h_0 & 0 & \cdots & 0 \\ h_1 & \ddots & \ddots & \vdots \\ \vdots & \ddots & \ddots & 0 \\ h_L & & \ddots & h_0 \\ 0 & \ddots & & h_1 \\ \vdots & \ddots & \ddots & \vdots \\ 0 & \cdots & 0 & h_L \end{bmatrix}}_{\boldsymbol{H}_{\text{ZP}}} \underbrace{\begin{bmatrix} s_0 \\ s_1 \\ \vdots \\ \vdots \\ s_{N-1} \end{bmatrix}}_{\boldsymbol{s}} + \underbrace{\begin{bmatrix} \eta_0 \\ \eta_1 \\ \vdots \\ \vdots \\ \eta_{N-1} \end{bmatrix}}_{\boldsymbol{\eta}_M}, \tag{2.21}$$

where $\boldsymbol{H}_{\text{ZP}}$ is an $M \times N$ tall Toeplitz matrix [41], and $\boldsymbol{\eta}_M$ denotes an $M \times 1$ AWGN vector. Since a tall Toeplitz matrix always has full rank, symbol recovery in (2.21) is guaranteed

[106]. The ZP-OFDM receiver can employ either Zero-Forcing (ZF) or Minimum Mean Squared-Error (MMSE) equalization, i.e.,

$$\boldsymbol{G}_{\mathrm{ZF}} = \boldsymbol{F}_N \boldsymbol{H}_{\mathrm{ZP}}^{\dagger}, \quad \boldsymbol{G}_{\mathrm{MMSE}} = \boldsymbol{F}_N \boldsymbol{H}_{\mathrm{ZP}}^{H} \left(N_0 \boldsymbol{I}_M + \boldsymbol{H}_{\mathrm{ZP}} \boldsymbol{H}_{\mathrm{ZP}}^{H} \right)^{-1}.$$

However, direct ZF or MMSE equalization requires the inversion of an $N \times N$ or $M \times M$ matrix, respectively. The complexity can be reduced by using FFT's [67]. Compared with CP-OFDM, ZP-OFDM improves error rate performance at the expense of complexity.

2.2.2 Advantages of MC

Compared with SC, MC transmission offers a number of advantages in frequency-selective channels, some of which have been mentioned previously.

- Robustness to multipath delay spread, and elimination of IBI by the insertion of a guard interval in terms of CP or ZP.
- Low complexity implementation. As we see from Fig. 2.2, CP-OFDM modulation and demodulation employ IDFT and DFT, which can be efficiently implemented using the fast Fourier transform (FFT) algorithm [75]. ZP-OFDM also enjoys low complexity implementation with FFT's [67].
- Low complexity equalization. For CP-OFDM, this is indicated by (2.18). ZP-OFDM, on the other hand, has higher equalization complexity. Using fast algorithms in [67], equalization complexity can be reduced significantly.
- Adaptive bit loading and/or power allocation across subcarriers to increase throughput [24] or improve reliability [49, 105].

2.2.3 Disadvantages of MC

Disadvantages of MC transmission include:

- Lack of symbol recovery capability in CP-OFDM. As we can see from (2.17), when channel frequency response H_k is very small, symbol recovery of the corresponding subcarrier suffers from noise enhancement problems, resulting in error floors in the overall average performance.

- High peak-to-average power ratio (PAPR). An MC-modulated signal is a summation of a number of sinusoids and is approximately Gaussian [73]. Therefore, highly linear amplifiers with large back-off are required, which increases costs.

- Sensitivity to frequency offsets and time-selective fading. Both time variation of channel response within an MC block and frequency offsets destroy orthogonality among subcarriers, result in ICI, and cause error floors in performance [113].

- Low bandwidth efficiency. When duration of a guard interval is relatively large compared with symbol duration, the BW efficiency is low. For examples, in wireless LAN standards such as HIPERLAN/2, the duration of guard interval is 1/4 of that of the block of symbols, resulting in a bandwidth efficiency of 80% [31].

2.3 MIMO Wireless Communications

By employing multiple antennas at both the transmitter and receiver, known as MIMO, the reliability (quality) and/or throughput of a wireless communication system can be improved. Compared with SISO, MIMO technologies offer a number of improvements [80]: *array gain* and *interference reduction* capability inherited from antenna array technologies; by transmitting the signal over multiple (ideally) independent fading paths in space, *spatial*

diversity gain is achieved to mitigate fading effects; by transmitting independent signals from the individual antennas (or, precisely, over spatially established channels), linear increase in capacity can be achieved without additional power and bandwidth expenditure, which is known as *spatial multiplexing gain*. For MIMO transmission studied in this thesis, we focus on the spatial multiplexing aspect.

2.3.1 MIMO Signal Reception

Consider a MIMO spatial multiplexing communication system with N_t transmit and N_r receive antennas where $N_r \geq N_t$, as shown in Fig. 2.4. In this section, we review receiver structures without transmit processing, i.e., $\boldsymbol{P} = \boldsymbol{I}_{N_t}$. The received signal can be modelled as

$$\boldsymbol{r} = \boldsymbol{H}\boldsymbol{s} + \boldsymbol{\eta}, \tag{2.22}$$

where $\boldsymbol{s}$ is the $N_t \times 1$ transmitted signal vector; $\boldsymbol{H}$ is the $N_r \times N_t$ channel matrix, which is assumed to be generally correlated Ricean fading as in Section 2.1.2; and $\boldsymbol{\eta}$ is an $N_r \times 1$ AWGN vector. For simplification of analysis, we assume white noise and input, i.e., $\mathbb{E}[\boldsymbol{s}\boldsymbol{s}^H] = E_s\boldsymbol{I}_{N_t}$ and $\mathbb{E}[\boldsymbol{\eta}\boldsymbol{\eta}^H] = N_0\boldsymbol{I}_{N_r}$, input SNR $\gamma_s \stackrel{\text{def}}{=} E_s/N_0$.

2.3.1.1 Maximum Likelihood (ML) Receiver

Assuming equiprobable transmitted signal vectors, the ML receiver estimates the transmitted signal vector by

$$\hat{\boldsymbol{s}}_{\text{ML}} = \arg\min_{\boldsymbol{s}} \|\boldsymbol{r} - \boldsymbol{H}\boldsymbol{s}\|^2, \tag{2.23}$$

where the minimization is performed over all possible transmitted signal vector $\boldsymbol{s}$. If the signal transmitted from each antenna is drawn from an M-ary signal constellation, the optimal ML receiver requires search over a total of M^{N_t} signal vectors. The complexity of

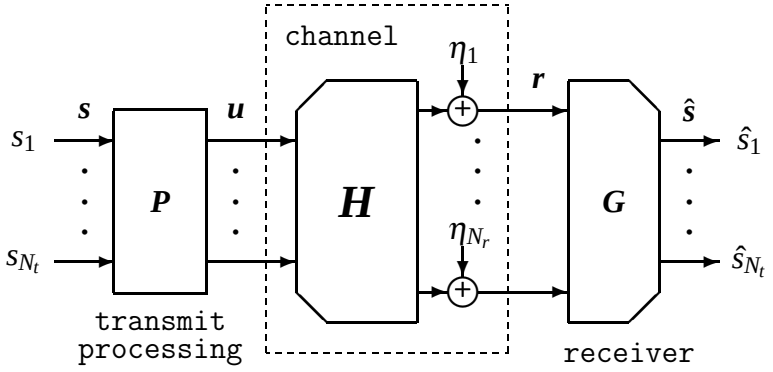

Figure 2.4. Block diagram of a MIMO spatial multiplexing transceiver.

the optimal ML receiver grows exponentially in the number of transmit antennas, N_t. Efforts to reduce the complexity of optimal ML receiver include fast sphere decoding algorithms [26, 43] and detectors that combine linear processing with local ML search [56].

2.3.1.2 Linear Receivers

The complexity of the optimal ML receiver can be significantly reduced by using a linear filter to estimate the transmitted signal vector, as shown in Fig. 2.4. Linear receivers can employ criteria like zero-forcing (ZF) or minimum mean squared-error (MMSE) [37].

- *ZF receiver:* The ZF receive matrix filter is given by

$$\boldsymbol{G}_{\mathrm{ZF}} = \boldsymbol{H}^{\dagger}. \tag{2.24}$$

The output of the ZF receiver is obtained as

$$\hat{\boldsymbol{s}}_{\mathrm{ZF}} = \boldsymbol{G}_{\mathrm{ZF}}\boldsymbol{r} = \boldsymbol{s} + \boldsymbol{H}^{\dagger}\boldsymbol{\eta}. \tag{2.25}$$

From (2.25), it is clear that $\hat{\boldsymbol{s}}_{\mathrm{ZF}}$ is an unbiased estimate of $\boldsymbol{s}$. The ZF receiver decouples the MIMO channel into N_t parallel SISO channels with additive spatially-correlated noise. Each SISO channel is decoded independently which reduces receiver complexity significantly. Compared to the optimal ML decoding, the ZF solution suffers from noise enhancement problem, resulting in significant performance degradation [80].

- *MMSE receiver:* The MMSE receiver minimizes the mean squared-error (MSE), $\mathrm{MSE}(\boldsymbol{G}) = \mathbb{E}\left\{\|\boldsymbol{s} - \boldsymbol{G}\boldsymbol{r}\|^2\right\}$. By using the orthogonality principle [77],

$$\mathbb{E}\left\{(\boldsymbol{G}\boldsymbol{r} - \boldsymbol{s})\,\boldsymbol{r}^H\right\} = \boldsymbol{0},$$

the MMSE matrix filter is obtained as

$$\boldsymbol{G}_{\mathrm{MMSE}} = \left(N_0\boldsymbol{I}_{N_t} + \boldsymbol{H}^H\boldsymbol{H}\right)^{-1}\boldsymbol{H}^H. \tag{2.26}$$

The output of the MMSE receiver

$$\begin{aligned}\hat{\boldsymbol{s}}_{\mathrm{MMSE}} &= \boldsymbol{G}_{\mathrm{MMSE}}\boldsymbol{r} \\ &= \left(N_0\boldsymbol{I}_{N_t} + \boldsymbol{H}^H\boldsymbol{H}\right)^{-1}\boldsymbol{H}^H\boldsymbol{H}\cdot\boldsymbol{s} + \left(N_0\boldsymbol{I}_{N_t} + \boldsymbol{H}^H\boldsymbol{H}\right)^{-1}\boldsymbol{H}^H\boldsymbol{\eta}, \end{aligned} \tag{2.27}$$

which is a biased estimate of $\boldsymbol{s}$. Compared to the ZF solution, the MMSE receiver balances interference mitigation against noise enhancement.

2.3.1.3 Successive Interference Cancellation (SIC) Receiver

Performance and complexity issues of linear receivers can be addressed by employing a multistage interference cancelling structure. Without loss of generality, we assume stream $k = 1$ is detected first; then the interference due to the first stream is regenerated and subtracted, and stream $k = 2$ is detected. This procedure is repeated until all streams are

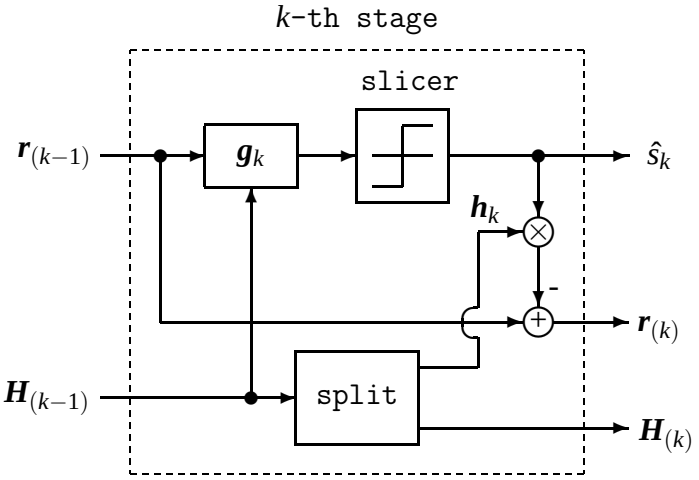

Figure 2.5. Schematic diagram of the k-th stage of an SIC receiver.

detected. A schematic diagram of the k-th stage is illustrated in Fig. 2.5, where $\boldsymbol{H}_{(k)}$ is generated in a recursive fashion by nulling the $(k-1)$-st column of $\boldsymbol{H}_{(k-1)}$ for $k = 2, \cdots, N_t$, and $\boldsymbol{H}_{(1)} \stackrel{\text{def}}{=} \boldsymbol{H}$; $\boldsymbol{h}_k$ denotes the k-th column of $\boldsymbol{H}_{(k-1)}$; $\boldsymbol{r}_{(k)} = \boldsymbol{r}_{(k-1)} - \hat{s}_k \boldsymbol{h}_k$ for $k = 2, \cdots, N_t$, and $\boldsymbol{r}_{(1)} \stackrel{\text{def}}{=} \boldsymbol{r}$; and $\boldsymbol{g}_k$ denotes the k-th row of the linear receiver matrix $\boldsymbol{G}$.

The linear receiver employed in an SIC receiver may be either ZF or MMSE. Ignoring error propagation, the equivalent system after the k-th stage is MIMO with $N_t - k$ transmit and N_r receive antennas. The SIC receiver essentially converts the MIMO channel into N_t parallel channels with increasing diversity order [79].

2.3.1.4 Ordered SIC (OSIC) Receiver

To improve SIC performance, the streams can be reordered, resulting in an ordered SIC (OSIC) receiver, which is used in V-BLAST [37]. This receiver differs from the previous SIC only in the detection ordering. An SNR-based ordering scheme that maximizes minimum SNR appears in [37, 109], and is reproduced in Table 2.1. This ordering scheme has been shown to be optimal for the SIC receiver. Using OSIC with SNR-based ordering, the

decoded stream has an inherent form of selection diversity [79].

Table 2.1. SNR-Based Ordering Algorithm

Initialization	$i = 1$; $\mathbf{H}_{(1)}^{O} = \mathbf{H}$
Recursion	`if` $(i \leq N_t)$
	{
	$k_i = \arg\min_l \left[\left(\left(\mathbf{H}_{(i)}^{O} \right)^H \mathbf{H}_{(i)}^{O} \right)^{\dagger} \right]_{l,l}$;
	`reorder` $\mathbf{H}^O$ `by interchanging its`
	i`-th column and` k_i`-th column`;
	$i \leftarrow i+1$
	}

2.3.2 Transmit Processing

When channel state information (CSI) is available at the transmitter, system performance can be improved. Transmit processing can be linear or nonlinear [16], redundant or non-redundant [57, 72]. Generally speaking, linear transmit processing schemes require low implementation complexity at the expense of performance compared to nonlinear schemes; introducing redundancy in transmit processing improves reliability by means of diversity at the expense of efficiency. In this thesis, we will focus on linear non-redundant transmit processing.

A block diagram of MIMO with linear transmit processing is illustrated in Fig. 2.4. The received signal can be modelled as

$$\boldsymbol{r}_{\mathrm{P}} = \boldsymbol{HPs} + \boldsymbol{\eta}, \tag{2.28}$$

where $\boldsymbol{P}$ is an $N_t \times N_t$ transmit processing matrix. In practice, there is constraint on transmit power. Assuming that the total transmit power is the same for schemes with and without transmit processing, we obtain the equivalent constraint on $\boldsymbol{P}$,

$$\text{trace}\left\{\boldsymbol{P}\boldsymbol{P}^H\right\} = N_t. \tag{2.29}$$

In addition to the total transmit power constraint (2.29), other constraints can be imposed, such as the dynamic range of the power amplifier at each transmit antenna, and the PAPR [76]. If a linear receiver $\boldsymbol{G}$ is employed, the estimate of the transmitted signal vector $\boldsymbol{s}$ is given by

$$\hat{\boldsymbol{s}} = \boldsymbol{G}\boldsymbol{r}_{\text{P}} = \boldsymbol{G}\boldsymbol{H}\boldsymbol{P}\boldsymbol{s} + \boldsymbol{G}\boldsymbol{\eta}. \tag{2.30}$$

We next review several existing precoding schemes.

2.3.2.1 Linear MMSE Precoding/Decoding [92]

The linear MMSE precoding/decoding seeks a precoder $\boldsymbol{P}$ and decoder $\boldsymbol{G}$ that minimizes

$$\begin{aligned}\text{MSE}(\boldsymbol{P},\boldsymbol{G}) &= \mathbb{E}\left\{\|\hat{\boldsymbol{s}} - \boldsymbol{s}\|^2\right\} \\ &= \text{trace}\left\{E_s\left(\boldsymbol{G}\boldsymbol{H}\boldsymbol{P} - \boldsymbol{I}\right)\left(\boldsymbol{G}\boldsymbol{H}\boldsymbol{P} - \boldsymbol{I}\right)^H + N_0\boldsymbol{G}\boldsymbol{G}^H\right\}.\end{aligned}$$

Denote the eigenvalue decomposition $\boldsymbol{H}^H\boldsymbol{H} = \boldsymbol{W}\boldsymbol{\Lambda}\boldsymbol{W}^H$. The MMSE precoder using total transmit power constraint (2.29) can be derived as

$$\boldsymbol{P}_{\text{MMSE}} = \boldsymbol{W}\boldsymbol{\Phi}, \tag{2.31}$$

where $\boldsymbol{\Phi}$ is an $N_t \times N_t$ diagonal matrix with (k,k)-th entry satisfies

$$\left|[\boldsymbol{\Phi}]_{k,k}\right|^2 = \left(\frac{N_t + \sum_{n=1}^{\bar{N}} \lambda_n^{-1}}{\gamma_s \lambda_k^{1/2} \sum_{n=1}^{\bar{N}} \lambda_n^{-1/2}} - \frac{1}{\gamma_s \lambda_k}\right)_+,$$

with $\lambda_k \overset{\text{def}}{=} [\boldsymbol{\Lambda}]_{k,k}$, and $\bar{N} \leq N_t$ is such that $\left|[\boldsymbol{\Phi}]_{k,k}\right| > 0$ for $n \in [1,\bar{N}]$ and $\left|[\boldsymbol{\Phi}]_{k,k}\right| = 0$ for all other n. The corresponding MMSE decoder is given by

$$\boldsymbol{G}_{\text{MMSE}} = \boldsymbol{P}_{\text{MMSE}}^H \boldsymbol{H}^H \left(\boldsymbol{H}\boldsymbol{P}_{\text{MMSE}}\boldsymbol{P}_{\text{MMSE}}^H\boldsymbol{H}^H + \frac{1}{\gamma_s}\boldsymbol{I}_{N_r}\right)^{-1}. \tag{2.32}$$

A generalization of this method was given in [88] where a weighted MMSE is used as the optimization criterion.

2.3.2.2 MBER Precoding for ZF Equalization [28]

The MBER precoding for block transmission with ZF equalization given in [28] can be readily applied to MIMO systems. Using a ZF receiver, the MBER precoding matrix is given by

$$\boldsymbol{P}_{\text{MBER-ZF}} = \sqrt{\frac{N_t}{\text{trace}\left(\boldsymbol{\Lambda}^{-1/2}\right)}}\boldsymbol{W}\boldsymbol{\Lambda}^{-1/4}\boldsymbol{F}_{N_t}, \tag{2.33}$$

where $\boldsymbol{F}_{N_t}$ is the $N_t \times N_t$ DFT matrix.

2.3.2.3 Precoding with Reduced Feedback

When CSI is unavailable at the transmitter, it is desirable to perform transmit processing with limited feedback in order to reduce the feedback overhead [58]. Existing precoding with reduced feedback can be categorized into two types, namely, *CSI quantization* and *limited feedback signal design* [59]. Precoding using CSI quantization, by its name, performs transmit processing based on a quantized version of CSI feedback [52, 69]. Limited feedback signal design methods optimize the transmitted signal at the receiver and feed it back to the transmitter [44,55]. Recently, a hybrid limited feedback precoding scheme with quantized precoding codebook was proposed in [59].

2.3.2.4 Transmit Antenna Selection

By using multiple antennas, MIMO systems offer significant gains in quality and/or capacity. While antenna elements and digital signal processing are usually cheap, the RF components are expensive [64]. A cost-effective solution is to perform transmission over a

selected subset of available antenna elements [13, 42, 44, 89, 108]. Transmit antenna selection can be viewed as a special precoding scheme. Suppose N out of N_t transmit antennas are to be selected. The $N_t \times N$ precoding matrix $\boldsymbol{P}$ for transmit antenna selection consists of N column vectors drawn from $\boldsymbol{I}_{N_t}$. The solution is a function of the signaling scheme, receiver structure and available CSI. A variety of optimization criteria can be employed, such as information rate and error rate [79].

2.3.3 Implementation Issues

As stated above, MIMO technologies improve quality and/or capacity of wireless communication systems at the expense of transceiver complexity, and, thus, cost. Moreover, exploiting channel knowledge at the transmitter by means of transmit processing requires related information to be fed back, which increases feedback overhead.

2.3.3.1 Transceiver Complexity/Cost

The performance of the ML receiver lower bounds all suboptimal receivers, while its implementation complexity is exponential in the number of transmit antennas. Reasonable tradeoffs between performance and complexity can be achieved via linear (ZF, MMSE) or nonlinear (SIC, OSIC) suboptimal receivers.

When linear precoding is performed, diagonalization of channel matrix is required, which involves singular value decomposition (SVD) of an $N_r \times N_t$ complex channel matrix $\boldsymbol{H}$ to obtain singular values ($\boldsymbol{\Lambda}$) and right singular vectors ($\boldsymbol{W}$). The complexity to compute

such an SVD is given by either [41][1]

$$\begin{cases} 32N_rN_t^2+64N_t^3 \quad (\text{flops}) & (\text{Golub-Reinsch SVD}) \\ 16N_rN_t^2+88N_t^3 \quad (\text{flops}) & (R-\text{SVD}) \end{cases}.$$

Moreover, linear precoding also requires matrix-matrix and/or matrix-vector multiplications at both the transmitter and the receiver. Limited feedback precoding using a codebook, on the other hand, does not require on-line diagonalization of channel matrix, but matrix multiplications. However, a pre-designed codebook has to be stored, which increases the memory cost.

2.3.3.2 Feedback Overhead

In channels lacking reciprocity in the up- and downlink, such as in frequency division duplex (FDD), full CSI is not available at the transmitter. To enable linear precoding, either the channel or a precoding matrix is required to be fed back. Channel matrix feedback is equivalent to feeding back $2N_tN_r$ real numbers, while a precoding matrix feedback requires $2N_t^2+N_t$ real numbers. Precoding with limited feedback signal design [55], on the other hand, reduces the feedback amount to $2N_t$ real numbers, which is a factor of $1/N_r$ savings.

Precoding using channel quantization reduces feedback overhead significantly [52]. Assuming that N_q bits are used to describe each real element of $\boldsymbol{H}$, the total amount of

[1] Denote the SVD $\boldsymbol{H}=\boldsymbol{U}\boldsymbol{\Lambda}\boldsymbol{V}^H$, and the unitary matrix $\boldsymbol{T}=\frac{1}{\sqrt{2}}\begin{bmatrix} \boldsymbol{I} & j\boldsymbol{I} \\ j\boldsymbol{I} & \boldsymbol{I} \end{bmatrix}$. We have

$$\begin{bmatrix} \boldsymbol{H} & \boldsymbol{0} \\ \boldsymbol{0} & \boldsymbol{H}^* \end{bmatrix} = \boldsymbol{T}\begin{bmatrix} \Re\{\boldsymbol{H}\} & -\Im\{\boldsymbol{H}\} \\ \Re\{\boldsymbol{H}\} & \Im\{\boldsymbol{H}\} \end{bmatrix}\boldsymbol{T}^H = \begin{bmatrix} \boldsymbol{U} & \boldsymbol{0} \\ \boldsymbol{0} & \boldsymbol{U}^* \end{bmatrix}\begin{bmatrix} \boldsymbol{\Lambda} & \boldsymbol{0} \\ \boldsymbol{0} & \boldsymbol{\Lambda} \end{bmatrix}\begin{bmatrix} \boldsymbol{V} & \boldsymbol{0} \\ \boldsymbol{0} & \boldsymbol{V}^* \end{bmatrix}^H.$$

Therefore, computation of the SVD of a complex matrix can be transformed into an equivalent SVD of a real matrix.

feedback is $2N_qN_tN_r$ bits. A quantitative study of feedback overhead for MIMO with adaptive modulation is provided in [96]. Feedback overhead is further reduced in precoding using a codebook [59].

2.4 Objectives

Mathematically, both multicarrier and MIMO can be described by matrix-vector signal models, and multicarrier systems can be viewed as special cases of MIMO with structural channel matrix, as is clear from (2.14), (2.16), (2.21) and (2.22). In practical scenarios, however, they face different difficulties as discussed in the previous sections. The objectives of this thesis are to develop cost-effective transmit optimization techniques for multicarrier and MIMO wireless communications.

2.4.1 Bandwidth Efficient OFDM Wireless Transmission

Existing CP- and ZP-OFDM transmission schemes utilize a fixed-length guard interval. In channels with small delay spread with respect to the duration of guard interval, this limits the system bandwidth efficiency. On the other hand, when channel delay spread is longer than the duration of the guard interval, residual IBI occurs which destroys orthogonality among subcarriers and limits system performance. We develop an adaptive ZP-OFDM scheme that adjusts the guard duration according to the channel condition.

2.4.2 Power Efficient Multicarrier Wireless Transmission

Joint bit loading and power allocation has been widely studied and deployed in wire-line multicarrier communications where the channel is regarded as static. We investigate fixed

rate wireless multicarrier transmission employing power allocation, which could be applicable to delay-sensitive applications. Power allocation for wireless multicarrier systems reduces transceiver complexity, increases system power efficiency, and improves link reliability. To this end, error rate minimization is employed as an optimization criterion. Effects of channel knowledge uncertainty are studied.

2.4.3 Power Efficient MIMO Wireless Transmission

To reduce complexity and/or feedback overhead of existing precoding methods, we apply error-rate-minimizing power allocation to MIMO wireless communications. This scheme could be regarded as an extension of power allocation for OFDM. Specific aspects of MIMO need to be taken into account, such as different transceiver structures, ill-conditioned channels and imperfect feedback.

Chapter 3

Adaptive Zero-Padding OFDM over Frequency-Selective Multipath Channels

3.1 Introduction

Orthogonal Frequency Division Multiplexing (OFDM) has been receiving growing interest in recent years and has been adopted in many standards. For example, OFDM has been chosen as a solution for digital audio and video broadcasting (DAB and DVB) in Europe, and applied for high speed Digital Subscriber Line (DSL) modems over twisted pairs (ADSL, HDSL, and VDSL). Recently, it has also been proposed for Digital Cable Television systems and adopted in new standards for wireless Local Area Networks (wireless LAN) in North America (IEEE 802.11a), in Europe (HIPERLAN/2) and in Asia (MMAC) [106].

All standard OFDM systems are based on insertion of a cyclic prefix (CP) to eliminate inter-block interference (IBI) between successive blocks. A CP of length of no less than the channel order is inserted per transmitted block. Discarding the CP at the receiver not only suppresses IBI, but also converts the linear channel convolution into a circular one, which facilitates the diagonalization of the channel matrix, and makes single-tap equalization using scalar division possible [106]. An obvious problem in CP-OFDM systems is that the

transmitted symbols cannot be recovered when some channel nulls are located on subcarriers. Recently, it has been proposed in [91, 106] to replace CP insertion by zero-padding (ZP) at the end of the block of symbols to be transmitted. The padded zeros deterministically suppress the IBI but lead to a larger number of observed samples. That way, the transmitted symbols can always be retrieved regardless of the channel null locations [106]. Note that since the number of padded zeros required to cancel IBI equals the CP length, ZP- and CP-OFDM transmission have the same bandwidth efficiency. For some existing OFDM systems, such as HIPERLAN/2 and DAB physical layer, the length of the CP is chosen to be 1/4 of the block size, which results in a bandwidth efficiency of 80%.

Approaches that have been proposed to increase the bandwidth efficiency in OFDM systems include [103, 104, 111]. In [103], an OFDM system that does not use a guard interval (referred to here as NGI-OFDM) was proposed. Because equalization in such a system may be ill-conditioned, a Moore-Penrose pseudoinverse of the channel matrix has to be performed. A partial response (PR) OFDM transmission scheme has been proposed in [104] that employs a smooth window function. In [111], a vector OFDM scheme was proposed which performs cyclic prefix insertion after blocking of conventional OFDM data blocks, so that the average overhead due to the guard interval is decreased. In wireline applications, channel impulse response shortening techniques have been developed so that the length of the guard interval can be reduced [62]. Application in wireless systems may be difficult/expensive due to the time-varying characteristic of wireless channels.

In this chapter, we propose a new OFDM transmission scheme with adaptive zero-padding (AZP-OFDM). We first examine the redundancy introduced in CP- and ZP-OFDM as well as OFDM without using a guard interval. The reduction of redundancy is then investigated and a new system design criterion based on channel matrix condition is introduced.

Using this criterion, a bandwidth efficient AZP-OFDM scheme is developed. Complexity issues are also addressed in system design, which results in more flexibility in that one can make tradeoffs among performance, efficiency and complexity. Generally multicarrier transmission suffers from problems including high peak-to-average power ratio (PAPR) [71]. By reducing the redundancy, the proposed AZP scheme achieves improved signal-to-noise ratio (SNR) compared to that of ZP-OFDM, which is an added benefit besides increased bandwidth efficiency. In channels with large delay spread, simulation results show that the proposed AZP-OFDM offers better performances than those of both CP- and ZP-OFDM with fixed guard interval lengths.

This chapter is organized as follows: a brief description of CP- and ZP-OFDM as well as OFDM transmission without using a guard interval are provided in Section 3.2. Section 3.3 addresses redundancy issues in these schemes. In Section 3.4, we first propose a system design criterion based on channel matrix condition. The application to OFDM to trade off bandwidth efficiency and performance leads to our proposed AZP-OFDM scheme. A modification to lower equalization complexity is also discussed, along with an algorithm for choosing the key parameter. Simulation results and some further discussions in the context of HIPERLAN/2 channel models as well as channels with exponential power delay profiles are provided in Section 3.5.

3.2 System Model

3.2.1 CP-OFDM

A baseband discrete-time equivalent model of a CP-OFDM transmitter is shown in Fig. 3.1. A serial stream of information bits, b_n, is first passed through an error-control encoder, then serial-to-parallel (S/P) converted into data blocks of size N, $\boldsymbol{u} \stackrel{\text{def}}{=} [u_0, u_1, \cdots, u_{N-1}]^T$.

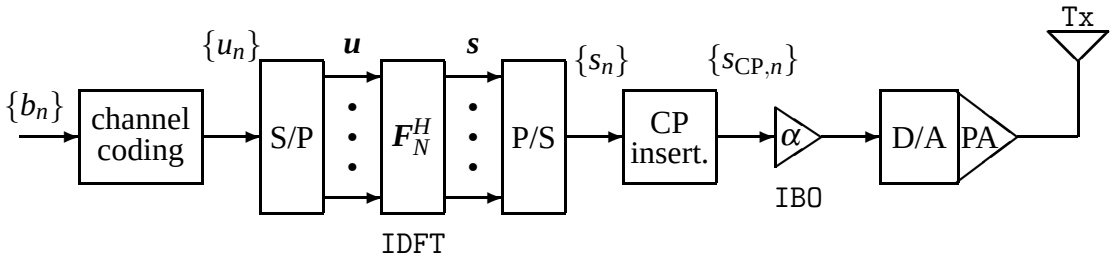

Figure 3.1. Block diagram of CP-OFDM transmitter.

Performing multicarrier modulation via inverse Discrete Fourier Transform (IDFT), we obtain

$$\boldsymbol{s} = \boldsymbol{F}_N^H \boldsymbol{u}.$$

A length G CP is then inserted between each block, and the resulting redundant block $\{\boldsymbol{s}_{\mathrm{CP}}\}$ of length $M = N + G$ is parallel-to-serial (P/S) converted into time-domain samples $\{s_{\mathrm{CP},n}\}$ and sent sequentially through the channel. The input back-off (IBO) and nonlinear distortion introduced by the power amplifier (PA) will be discussed in Section 3.5. The multipath propagation channel can be modelled as a finite impulse response (FIR) filter with tap vector $\boldsymbol{h} \stackrel{\text{def}}{=} [h_0, h_1, \cdots, h_L, 0, \cdots, 0]^T$ and additive white Gaussian noise (AWGN) $\eta_n \sim N(0, \sigma^2)$. This baseband discrete-time equivalent model combines effects of the spectral-shaping, sampling the continuous-time channel, and the receive-filter.

We assume perfect symbol and block synchronization. If the length of the CP, G, is no less than the channel model order, L, after discarding the first G entries corresponding to the CP, we obtain[1]

$$\boldsymbol{r}_{\mathrm{CP}} = \boldsymbol{H}_{\mathrm{CP}} \boldsymbol{s} + \boldsymbol{\eta}_N, \tag{3.1}$$

where $\boldsymbol{H}_{\mathrm{CP}}$ is the $N \times N$ circulant matrix [41] with first column $[h_0, \cdots, h_L, 0, \cdots, 0]^T$; and

[1]Note that if $G < L$, (3.1) is not valid due to residual IBI. For a general signal model with IBI, see [54].

$\boldsymbol{\eta}_N$ is an $N \times 1$ AWGN vector. After demodulation by DFT, we obtain

$$\begin{aligned} \boldsymbol{r}_{\mathrm{CP}}^{f} &= \boldsymbol{F}_N \boldsymbol{H}_{\mathrm{CP}} \boldsymbol{F}_N^H \boldsymbol{u} + \boldsymbol{F}_N \boldsymbol{\eta}_N \\ &= \boldsymbol{D}_h \boldsymbol{u} + \boldsymbol{\eta}^f, \end{aligned} \tag{3.2}$$

where the superscript ^{f} denotes a frequency-domain variable, $\boldsymbol{D}_h = \mathrm{diag}\{H_0, H_1, \cdots, H_{N-1}\}$ with $H_k = \sum_{l=0}^{L} h_l e^{-j2\pi kl/N}$ denoting the channel frequency response on the k-th subcarrier, and $\boldsymbol{\eta}^f = \boldsymbol{F}_N \boldsymbol{\eta}_N$ is the DFT-processed noise vector.

3.2.2 ZP-OFDM

ZP-OFDM [91] differs from CP-OFDM only in that instead of CP insertion, a guard interval of G zeros is padded at the end of each block. Assuming $G \geq L$, the received block is now given by

$$\boldsymbol{r}_{\mathrm{ZP}} = \boldsymbol{H}_{\mathrm{ZP}} \boldsymbol{s} + \boldsymbol{\eta}_M \tag{3.3}$$

where $\boldsymbol{H}_{\mathrm{ZP}}$ is a $M \times N$ tall Toeplitz matrix with first column $[h_0, h_1, \cdots, h_L, 0, \cdots, 0]^T$. Zero-forcing (ZF) or minimum mean squared error (MMSE) equalization can be performed at the receiver [106]. However, direct ZF or MMSE equalization requires the inversion of a $M \times M$ or $N \times N$ matrix, respectively. The computation can be lowered with fast algorithms based on the Fast Fourier Transform (FFT) [67].

3.2.3 NGI-OFDM

An OFDM transmission scheme without using guard intervals, which we refer to as NGI-OFDM, for frequency-selective channels was proposed in [103] to achieve maximal bandwidth efficiency. NGI-OFDM has the same transmitter structure as CP-OFDM except that there is no guard interval inserted and removed. The IBI due to time dispersion of the

channel is combated by interference cancellation as in [54]. After IBI cancellation, the "IBI-free" received block symbol is given by

$$\boldsymbol{r}_{\mathrm{NGI}} = \boldsymbol{H}_{\mathrm{NGI}}\boldsymbol{s} + \boldsymbol{\eta}_N \tag{3.4}$$

where $\boldsymbol{H}_{\mathrm{NGI}}$ is an $N \times N$ lower triangular Toeplitz matrix with first column $[h_0, h_1, \cdots, h_L, 0, \cdots, 0]^T$, which is not circulant and cannot be diagonalized with DFT and IDFT matrices. Therefore, inter-carrier interference (ICI) has been introduced and must be mitigated for symbol detection by solving (3.4). To avoid stability problems with matrix inversion for a probably ill-conditioned channel matrix, Moore-Penrose pseudo inversion [41] is employed in [103]. However, the ICI cancellation algorithm in [103] does not take advantage of the lower triangular Toeplitz structure of the channel matrix $\boldsymbol{H}_{\mathrm{NGI}}$. Furthermore, from our analysis (Section 3.3) and simulations (Section 3.5) in the context of standard HIPERLAN/2 channel models, the system performance of NGI-OFDM over hostile wireless propagation channels is not acceptable.

3.3 Redundancy Issues in OFDM Transmission

Note that the length of the guard interval in ZP-OFDM is the same as that in CP-OFDM. Both have the same bandwidth efficiency $N/(N+G)$. Typically, $G = N/4$, (e.g., in DAB and HIPERLAN/2), which results in a bandwidth efficiency of 80%. The insertion of CP or ZP introduces redundancy in OFDM transmission and decreases the system throughput, which is unattractive for wideband communications. We now discuss whether such redundancy is necessary for OFDM systems.

3.3.1 CP- and ZP-OFDM

As described above, CP-OFDM uses redundancy in the cyclic prefix to cancel IBI and transform the linear convolutional channel into a circular one (cf. (3.1)), which makes simple one-tap equalization possible (cf. (3.2)). One main problem in CP-OFDM is that the transmitted symbols cannot be recovered when some subcarriers encounter channel nulls even in the absence of noise [106]. Moreover, if a channel null is located close to the DFT grid ($|H(k_0)| \ll 1$ for some $k_0 \in [0, N-1]$), then equalization will suffer from a "noise-enhancement" problem. Therefore, *CP-OFDM offers simple equalization without guaranteed symbol recovery*.

In ZP-OFDM, redundancy is introduced in terms of G trailing zeros, which not only cancels IBI but also guarantees symbol recovery. This can be shown as follows. Consider the noise-free received block in (3.3). Taking $\mathscr{Z}$-transform

$$R_{\mathrm{ZP}}(z) = H_{\mathrm{ZP}}(z)S(z). \tag{3.5}$$

ZF equalization for ZP-OFDM turns out to be a deconvolution procedure. The DFT of $\boldsymbol{r}_{\mathrm{ZP}}(i)$ is obtained by sampling its Fourier transform

$$R_{\mathrm{ZP}}(e^{j\omega}) = R_{\mathrm{ZP}}(z)|_{z=e^{j\omega}} = H_{\mathrm{ZP}}(e^{j\omega})S(e^{j\omega}). \tag{3.6}$$

To avoid aliasing, at least $M(\geq N+L)$ samples should be evaluated [48][2]

$$R_{\mathrm{ZP}}\left(e^{j2k\pi/M}\right) = H_{\mathrm{ZP}}\left(e^{j2k\pi/M}\right) S\left(e^{j2k\pi/M}\right), \quad k = 0, 1, \cdots, M-1, \tag{3.7}$$

i.e., there are M virtual subcarriers compared to CP-OFDM where the number of subcarriers is N. Heuristically, more virtual subcarriers offer diversity and immunity to channel nulls. In other words, robustness to channel nulls in ZP-OFDM is achieved by means of using M virtual subcarriers. The price paid for this benefit is increased equalization complexity [67]. Therefore, *ZP-OFDM guarantees symbol recovery with increased complexity.*

[2]Note that this has also been used in [67] for fast ZF and MMSE equalization of ZP-OFDM.

3.3.2 NGI-OFDM

Equalization in NGI-OFDM is achieved by solving the linear systems of equations in (3.4). The perturbation analysis of direct methods for solving such linear equations (see, e.g., [25, 27]) is summarized in the following theorem[3].

Theorem 1 *([25, Theorem 7.7.4]) Consider the linear system $\boldsymbol{A}\boldsymbol{x} = \boldsymbol{b}$, where the matrix $\boldsymbol{A} \in \boldsymbol{R}^{n\times n}$ is nonsingular. Let $(\boldsymbol{A}+\delta\boldsymbol{A})(\boldsymbol{x}+\delta\boldsymbol{x}) = \boldsymbol{b}+\delta\boldsymbol{b}$, be a perturbed system, and assume that*

$$\varepsilon \stackrel{\text{def}}{=} \|\boldsymbol{A}^{-1}\| \cdot \|\delta\boldsymbol{A}\| = \kappa(\boldsymbol{A})\frac{\|\delta\boldsymbol{A}\|}{\|\boldsymbol{A}\|} < 1. \tag{3.8}$$

Then $(\boldsymbol{A}+\delta\boldsymbol{A})$ is nonsingular and the norm of the perturbation $\delta\boldsymbol{x}$ is bounded by

$$\frac{\|\delta\boldsymbol{x}\|}{\|\boldsymbol{x}\|} \leq \frac{\kappa(\boldsymbol{A})}{1-\varepsilon}\left(\frac{\|\delta\boldsymbol{A}\|}{\|\boldsymbol{A}\|} + \frac{\|\delta\boldsymbol{b}\|}{\|\boldsymbol{b}\|}\right), \tag{3.9}$$

where $\kappa(\boldsymbol{A}) \stackrel{\text{def}}{=} \|\boldsymbol{A}\| \cdot \|\boldsymbol{A}^{-1}\|$ is the condition number with respect to the problem of matrix inversion.

■

We note that $\kappa(\boldsymbol{A})$ depends on the choice of matrix norm, e.g., if the 2-norm is chosen, $\kappa_2(\boldsymbol{A}) = \sigma_{\max}/\sigma_{\min}$ with $\sigma_{\max}$ and $\sigma_{\min}$ denote, respectively, the maximum and minimum singular values of $\boldsymbol{A}$ [25]. Consider the equalization problem of NGI-OFDM in (3.4). For simplicity of notation, we drop the indices and subscripts,

$$\boldsymbol{r} = \boldsymbol{H}\boldsymbol{s} + \boldsymbol{\eta}.$$

Assuming no channel mismatch i.e., $\delta\boldsymbol{H} = 0$, the condition in (3.8) is satisfied since $\varepsilon = \|\boldsymbol{H}^{-1}\| \cdot \|\delta\boldsymbol{H}\| = 0$. Define the signal-to-noise ratio (SNR) at the input and output of the

[3]Note that this theorem holds for any consistent vector and matrix norms, and is not restricted to the 2-norm [25].

equalizer as, respectively,

$$\gamma_{in} \stackrel{\text{def}}{=} \frac{\|\boldsymbol{Hs}\|^2}{\|\boldsymbol{\eta}\|^2}, \qquad \gamma_{out} \stackrel{\text{def}}{=} \frac{\|\boldsymbol{s}\|^2}{\|\hat{\boldsymbol{s}}-\boldsymbol{s}\|^2} \equiv \frac{\|\boldsymbol{s}\|^2}{\|\boldsymbol{H}^\dagger\boldsymbol{r}-\boldsymbol{s}\|^2}, \tag{3.10}$$

where $\hat{\boldsymbol{s}} = \boldsymbol{H}^\dagger\boldsymbol{r}$ is the output of the equalizer. We have the following corollary.

Corollary 1 *The relative estimation error and the SNR at the output of equalizer of NGI-OFDM are bounded by, respectively,*

$$\frac{\|\hat{\boldsymbol{s}}-\boldsymbol{s}\|}{\|\boldsymbol{s}\|} \leq \kappa(\boldsymbol{H})\frac{\|\boldsymbol{\eta}\|}{\|\boldsymbol{Hs}\|}, \tag{3.11}$$

$$\gamma_{out} \geq \frac{\gamma_{in}}{\kappa^2(\boldsymbol{H})}. \tag{3.12}$$

■

Since multicarrier demodulation using DFT is a unitary transform, the SNR remains the same at the input of decision devices, which determines system performance. For example, for QPSK modulation, the symbol error rate (SER) is given by [84]

$$P_s = 2Q\left(\sqrt{\gamma_{out}}\right)\left(1-\tfrac{1}{2}Q\left(\sqrt{\gamma_{out}}\right)\right). \tag{3.13}$$

An example of the equalizer output SNR, γ_{out}, with ZF equalization in HIPERLAN/2 channel A [31] and the bound from Corollary 1 is shown in Fig. 3.2. Table 3.1 summarizes the channel models that were standardized for HIPERLAN/2. We can see from Fig. 3.2 that the bound is not tight. However, from Fig. 3.2, we can see that this bound is proportional to the mean square estimation error (MSEE). Therefore the lower bound in (3.12) may serve as a predictor for γ_{out}. Fig. 3.3 shows an example of the condition number of NGI-OFDM channel matrix varying with time in HIPERLAN/2 channel A with a terminal speed $v = 3(m/s)$. As a comparison, those of CP- and ZP-OFDM are also shown. From Fig. 3.3 we can see that the condition number of NGI-OFDM is usually very large, which

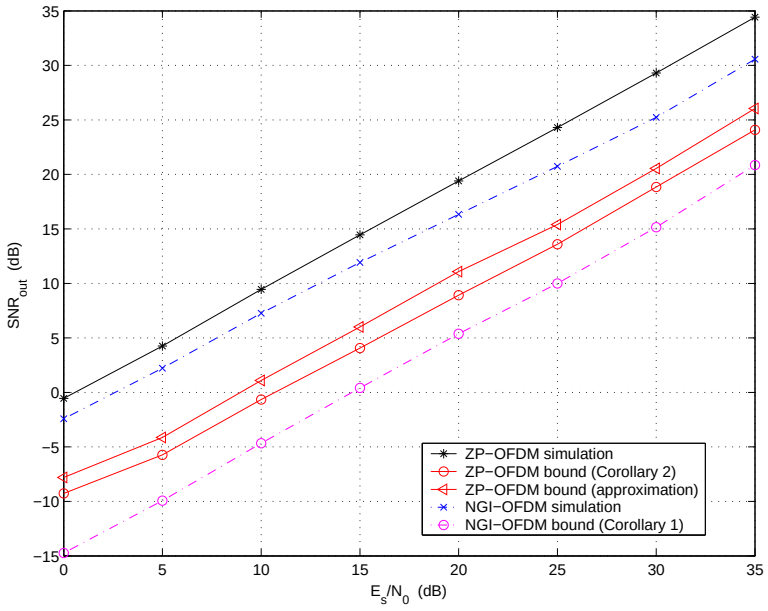

Figure 3.2. Equalizer output SNR and bounds for ZF equalization in HIPERLAN/2 channel A.

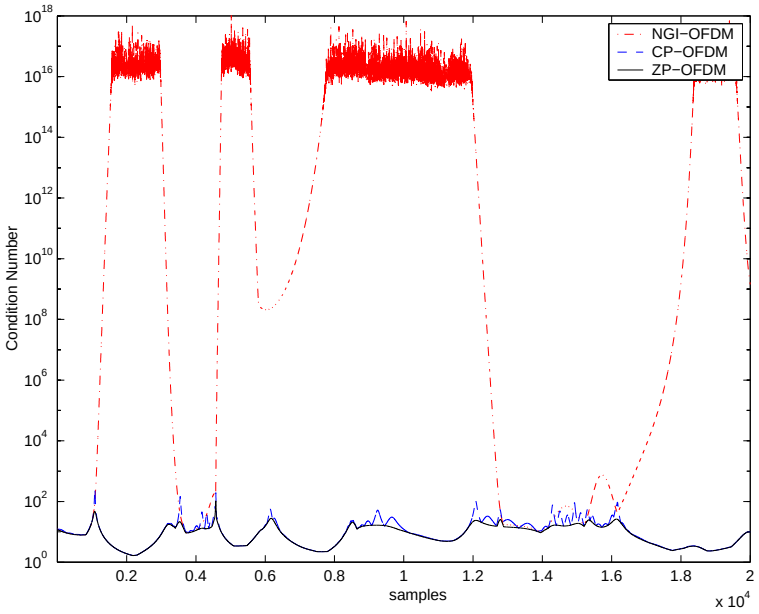

Figure 3.3. Condition number of NGI-OFDM channel matrix variation with time in HIPERLAN/2 channel A with terminal speed $v = 3(m/s)$.

Table 3.1. Channel Models for HIPERLAN/2

Channel Model	RMS delay spread	Ricean factor
A	50 ns	-
B	100 ns	-
C	150 ns	-
D	140 ns	10 dB
E	250 ns	-

makes equalization in (3.4) an ill-conditioned problem, and moreover causes unacceptable performance in NGI-OFDM, as will be shown in Section 3.5.

We note that equalization in CP-OFDM also requires solving linear equations (3.1). So the above perturbation analysis for NGI-OFDM applies. For ZP-OFDM, the system is overdetermined and the above analysis has to be modified, as detailed in Section 3.4. From Fig. 3.3, we see that the condition number of the CP-OFDM channel matrix is usually much smaller compared to that of NGI-OFDM, which explains why CP-OFDM offers better performance than NGI-OFDM. This can also been shown from a signals-and-systems viewpoint. From the received signal models in (3.3) and (3.4), we know that the NGI signal is a length-N rectangularly windowed version of ZP-OFDM, which suffers from *Gibbs Phenomenon* [63]. In the $\mathscr{Z}$-transform domain, $R_{\rm NGI}(z)$ is obtained by discarding those items with power less than $1-N$. Consider the system identification problem to find an equivalent convolutional channel for NGI-OFDM, i.e., to find $\hat{H}_{\rm NGI}(z)$ such that

$$R_{\rm NGI}(z) = \hat{H}_{\rm NGI}(z)S(z)$$

Since $S(z)$ divides $R_{\rm ZP}(z)$, it cannot divide $R_{\rm NGI}(z)$. Therefore the effective channel impulse response, $\hat{h}_{\rm NGI}(l) = \mathscr{Z}^{-1}\{\hat{H}_{\rm NGI}(z)\}$, is lengthened. Fig. 3.4 shows an example of the

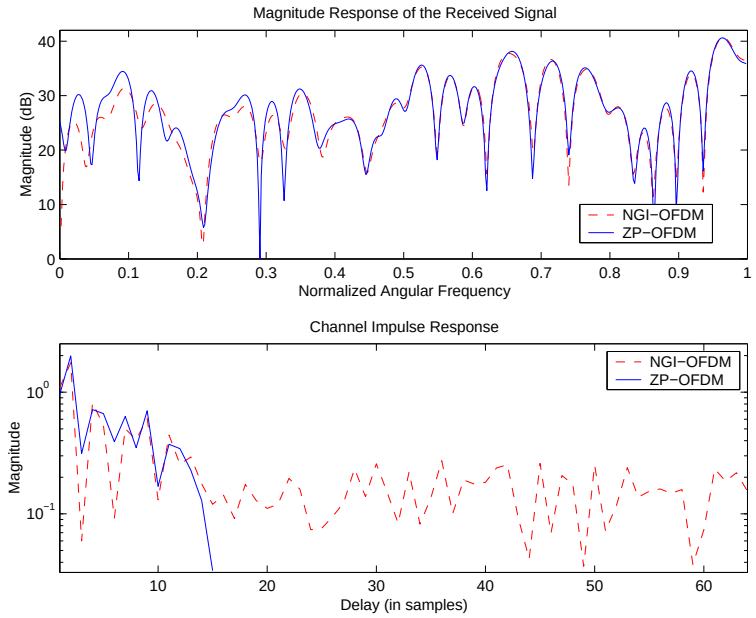

Figure 3.4. The Gibbs Phenomenon and channel impulse response lengthening effect in NGI-OFDM ($N = 64, L = 14$).

channel impulse response lengthening effect in NGI-OFDM systems. Now that the effective channel order is larger than the original one, L, there are more channel nulls and the possibility for subcarriers encounter channel nulls is also increased.

Compared with CP- and ZP- based schemes, NGI-OFDM offers high bandwidth efficiency, but suffers from inferior performance and high complexity, as will be discussed. We conclude that redundancy is required for OFDM transmission over wireless channels. Therefore it is meaningful to investigate introducing redundancy in a "better" way, or, in other words, to find better tradeoffs among efficiency, performance and complexity.

3.4 Proposed Adaptive Zero-Padding (AZP) OFDM

To increase the bandwidth efficiency of ZP-OFDM systems, redundancy introduced in transmission must be reduced. In fact, from the guaranteed symbol recovery property of ZP-OFDM discussed in the previous section, we find that the necessary amount of redundancy is L. Padding more zeros does not affect the system performance and only results in lower bandwidth efficiency. On the other hand, if we loosen the constraint on symbol recovery slightly by padding fewer zeros, higher bandwidth efficiency may be achieved. This does not mean a loss of symbol recovery capability, but a tradeoff between efficiency and performance, as will be made clear in Section 3.4.1. Tradeoffs in complexity will be discussed in Section 3.4.2.

3.4.1 AZP-OFDM Scheme

Consider the signal model in ZP-OFDM. Rewrite (3.3) as

$$\boldsymbol{r} = \boldsymbol{H}\boldsymbol{s} + \boldsymbol{\eta} \tag{3.14}$$

Equalization in ZP-OFDM requires solving an overdetermined system, which can be easily treated as full rank least squares (LS) problem [25, 27, 41]. The sensitivity of the LS problem is characterized by the condition of channel matrix $\boldsymbol{H}$ with respect to the 2-norm, $\kappa_2(\boldsymbol{H}) \stackrel{\text{def}}{=} \sigma_1/\sigma_N$, where σ_1 and σ_N denote, respectively, the maximum and minimum singular values of $\boldsymbol{H}$.

Theorem 2 *([27, Theorem 3.4]) Suppose that $\boldsymbol{A}$ is m-by-n with $m \geq n$ and has full rank. Suppose that $\boldsymbol{x}$ minimizes $\|\boldsymbol{A}\boldsymbol{x} - \boldsymbol{b}\|$. Let $\boldsymbol{\xi} = \boldsymbol{A}\boldsymbol{x} - \boldsymbol{b}$ be the residual. Let $\hat{\boldsymbol{x}}$ minimize $\|(\boldsymbol{A} + \delta\boldsymbol{A})\hat{\boldsymbol{x}} - (\boldsymbol{b} + \delta\boldsymbol{b})\|$. Assume*

$$\varepsilon \stackrel{\text{def}}{=} \max\left(\frac{\|\delta\boldsymbol{A}\|}{\|\boldsymbol{A}\|}, \frac{\|\delta\boldsymbol{b}\|}{\|\boldsymbol{b}\|}\right) < \frac{1}{\kappa_2(\boldsymbol{A})} \equiv \frac{\sigma_n}{\sigma_1} \tag{3.15}$$

Then

$$\frac{\|\hat{\boldsymbol{x}}-\boldsymbol{x}\|}{\|\boldsymbol{x}\|} \leq \varepsilon \cdot \left(\frac{2\kappa_2(\boldsymbol{A})}{\cos(\theta)} + \tan(\theta)\left(\kappa_2(\boldsymbol{A})\right)^2 \right) + \mathscr{O}\left(\varepsilon^2\right) \equiv \varepsilon \cdot \kappa_{LS} + \mathscr{O}\left(\varepsilon^2\right). \tag{3.16}$$

where θ *is defined by* $\sin(\theta) \stackrel{\text{def}}{=} \frac{\|\boldsymbol{\xi}\|}{\|\boldsymbol{b}\|}$*, i.e.,* θ *is the angle between the vectors* $\boldsymbol{b}$ *and* $\boldsymbol{Ax}$ *and measures whether the residual norm* $\|\boldsymbol{\xi}\|$ *is large (near* $\|\boldsymbol{b}\|$*) or small (near 0).* κ_{LS} *is the condition number of the LS problem.*

■

Note that the assumption $\varepsilon \cdot \kappa_2(\boldsymbol{A}) < 1$ guarantees that $\boldsymbol{A}+\delta\boldsymbol{A}$ has full rank so that $\hat{\boldsymbol{x}}$ is uniquely determined. This bound can be interpreted as [27]: if θ is 0 or very small, then the residual is small and the effective condition number is about $2\kappa_2(\boldsymbol{A})$, much like ordinary linear equation solving; if θ is not small but not close to $\pi/2$, the residual is moderately large, and then the effective condition number can be much larger (on the order of $\kappa_2^2(\boldsymbol{A})$); if θ is close to $\pi/2$, the true solution is nearly zero, then the effective condition number becomes unbounded even if $\kappa_2(\boldsymbol{A})$ is small.

For our equalization problem in (3.14), if we assume no channel mismatch, i.e., $\delta\boldsymbol{H} = 0$; then the residual $\boldsymbol{\xi} \stackrel{\text{def}}{=} \boldsymbol{Hs} - (\boldsymbol{r}-\boldsymbol{\eta}) = 0$, so $\sin(\theta) = 0, \tan(\theta) = 0$. Define $\varepsilon \stackrel{\text{def}}{=} \frac{\|\boldsymbol{\eta}\|}{\|\boldsymbol{Hs}\|}$, and the SNR at the input of the equalizer $\gamma_{in} \stackrel{\text{def}}{=} \frac{\|\boldsymbol{r}\|^2}{\|\boldsymbol{\eta}\|^2} = \frac{1}{\varepsilon^2}$. The condition (3.15) is equivalent to

$$\gamma_{in} > \kappa_2^2(\boldsymbol{H}), \tag{3.17}$$

which may be violated, but (3.16) still holds except that the bound is loosened in this case, because $\boldsymbol{H}$ always has full rank and $\hat{\boldsymbol{s}} = \boldsymbol{H}^{\dagger}\boldsymbol{r}$ is uniquely determined, as required by the condition in (3.15). Therefore, we have the following corollary.

Corollary 2 *The relative estimation error of equalization in ZP-OFDM is bounded by*

$$\frac{\|\hat{\boldsymbol{s}}-\boldsymbol{s}\|}{\|\boldsymbol{s}\|} \equiv \frac{\|\boldsymbol{H}^{\dagger}\boldsymbol{r}-\boldsymbol{s}\|}{\|\boldsymbol{s}\|} \leq \frac{2\kappa_2(\boldsymbol{H})}{\sqrt{\gamma_{in}}} + \mathscr{O}\left(\frac{1}{\gamma_{in}}\right). \tag{3.18}$$

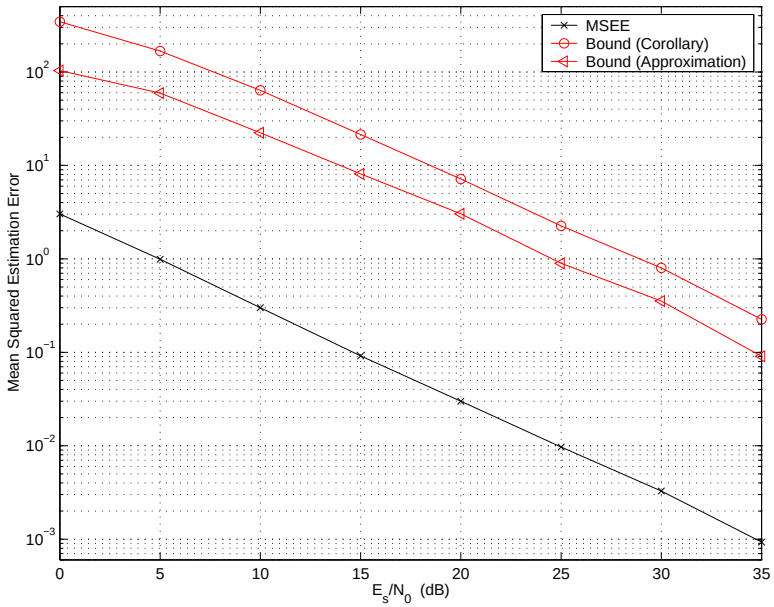

Figure 3.5. Mean squared estimation error (MSEE) and bounds for ZF equalization in HIPERLAN/2 channel A.

■

Fig. 3.5 shows the MSEE of ZF equalization in HIPERLAN/2 channel A and the upper bound from Corollary 2. We can see that the upper bound is not tight. This is due to a probable violation of the condition in (3.17). However, from Fig. 3.5 we can see that this bound is proportional to the MSEE. Therefore the bound acts as a prediction for the MSEE. We note that γ_{in} may range from 0 to 20 dB in wireless communications and usually $\kappa_2(\boldsymbol{H}) \gg 1$. Therefore $\mathscr{O}\left(\frac{1}{\gamma_{in}}\right)$ is usually negligible in (3.18). If we define the SNR at the output of the equalizer $\gamma_{out} \stackrel{\text{def}}{=} \frac{\|\boldsymbol{s}\|^2}{\|\hat{\boldsymbol{s}}-\boldsymbol{s}\|^2} \equiv \frac{\|\boldsymbol{s}\|^2}{\|\boldsymbol{H}^{\dagger}\boldsymbol{s}-\boldsymbol{s}\|^2}$ as in (3.10), we obtain approximately

$$\gamma_{out} \geq \frac{\gamma_{in}}{4\kappa_2^2(\boldsymbol{H})} \tag{3.19}$$

An example of the output SNR, γ_{out}, for ZF equalization in HIPERLAN/2 channel A is also shown in Fig. 3.2 together with the bound from Corollary 2. Again, the bound gives a

good prediction of γ_{out}.

Since system performance is determined by the SNR at the equalizer output, γ_{out}, which can be predicted by $\kappa_2(\boldsymbol{H})$ together with γ_{in}, we may use $\kappa_2(\boldsymbol{H})$ as a system design criterion. To be specific, redundancy introduced by zero-padding can be reduced by means of inserting fewer zeros at the end of each block, which is referred to as adaptive ZP-OFDM (AZP-OFDM), while keeping $\kappa_2(\boldsymbol{H})$ relatively low. Assume K zeros are padded, with $0 \leq K \leq L$, the new signal model is given by

$$\boldsymbol{r}' = \boldsymbol{H}'\boldsymbol{s} + \boldsymbol{\eta}' \tag{3.20}$$

where $\boldsymbol{r}'$ and $\boldsymbol{\eta}'$ are $(N+K)$-vectors and $\boldsymbol{H}'$ is a $(N+K) \times N$ matrix, respectively. Note that the received signal in AZP-OFDM (3.20) is just a "truncated" version of ZP-OFDM. The corresponding channel matrix $\boldsymbol{H}'$ is a submatrix of the ZP-OFDM channel matrix $\boldsymbol{H}$ constructed by deleting its last $M-N-K$ rows. Let $\{\sigma_i\}_{i=1}^{N}$ denote the singular values of $\boldsymbol{H}$ and $\{\sigma_i'\}_{i=1}^{N}$ denote the singular values of $\boldsymbol{H}'$, both arranged in nonincreasing order. From the interlacing property of singular values [45], we know $\sigma_1 \geq \sigma_1' \geq \sigma_2 \geq \sigma_2' \geq \cdots \geq \sigma_N \geq \sigma_N' \geq 0$. Usually $\sigma_1 \gg \sigma_N$. Heuristically, σ_N is more sensitive to perturbation. Therefore deleting some of the last rows of $\boldsymbol{H}$, or in other words, padding with fewer zeros in ZP-OFDM, increases $\kappa_2(\boldsymbol{H})$, as is confirmed by simulations. This is the price paid for increased bandwidth efficiency.

Of course, in so doing, the received signal will experience IBI, which can be canceled via decision feedback. Note that in AZP-OFDM, redundancy is reduced but still exists, which makes robust symbol recovery possible. Either ZF or MMSE equalization can be employed. Similar to ZP-OFDM, equalization in AZP-OFDM requires the solution of an overdetermined system of equations. The fast equalization algorithms developed in [67] cannot be applied due to their different required channel matrix structure. Therefore, AZP-OFDM trades off efficiency and performance, with the price of increased complexity.

3.4.2 Modification for Low Complexity Equalization

Alternatively, by taking advantage of the band-Toeplitz structure of the channel matrix, we propose a modification to the AZP-OFDM scheme. To be specific, if we discard K initial observations, we obtain a system with the same number of observations as unknowns, i.e.,

$$\boldsymbol{r}'' = \boldsymbol{H}''\boldsymbol{s} + \boldsymbol{\eta}'' \tag{3.21}$$

where $\boldsymbol{r}''$ and $\boldsymbol{\eta}''$ are N-vectors and $\boldsymbol{H}''$ is an $N \times N$ Toeplitz matrix. We note that the received signal in (3.21) is a "windowed" version of that in ZP-OFDM (see (3.3)), with window width N and delay K. As a result, ZF equalization is transformed into solving a band-Toeplitz system (with band width L), for which there are efficient solvers [18].

We note that the modified scheme differs from AZP-OFDM in the number of trailing zeros, K, (as will be discussed in Section 3.4.3) and in equalization at the receiver. Both the NGI and the proposed methods are windowed versions of ZP-OFDM with the same window width, but in the modified AZP scheme, the window is shifted to a "best" position to capture more of the transmitted energy in the received signal, while in NGI-OFDM, the window is always fixed at the head part of the received block; in other words, the modified AZP system itself is nearly as overdetermined as in ZP-OFDM (therefore, redundancy-based), but transformed for simpler equalization, while NGI-OFDM does not introduce redundancy. Of course, by discarding some observations, we lose part of the redundancy in the received signal. As a result, the system performance will be slightly worse. However, due to the choice of AZP length (as will be clear in Section 3.4.3), the resulting system is still well-conditioned, as has been confirmed by simulations.

3.4.3 Choice of ZP Length

From the previous discussion, the condition number of the channel matrix can be used as a system design criterion. However, the calculation of the condition number of a matrix is computationally complex. Since $\kappa_2(\boldsymbol{H}) = \sigma_1/\sigma_N$ and σ_N is more sensitive to perturbation, $\kappa_2(\boldsymbol{H})$ depends mainly on σ_N. Hence, instead of using condition number, we consider the smallest singular value of the channel matrix, σ_N, as a criterion. In (3.18), if we substitute $\kappa_2(\boldsymbol{H})$ by $\frac{1}{\sigma_N}$, we obtain an approximation bound for MSEE and γ_{out} as, respectively,

$$\frac{\|\hat{\boldsymbol{s}} - \boldsymbol{s}\|}{\|\boldsymbol{s}\|} \lesssim \frac{2}{\sigma_N \sqrt{\gamma_{in}}} + \mathcal{O}\left(\frac{1}{\gamma_{in}}\right) \tag{3.22}$$

$$\gamma_{out} \gtrsim \frac{1}{4}\gamma_{in}\sigma_N^2 \tag{3.23}$$

To gain more insight into the criteria for choice of ZP length, we consider a special case of a two-tap channel, i.e., $\boldsymbol{h} = [h_0, h_1, 0, \cdots, 0]^T$. For this channel, the ZP length $K \in \{0, 1\}$. It can be shown that singular values of channel matrices (of both $K = 0$ and 1) depend only on $|h_0|$ and $|h_1|$. Fig. 3.6 compares two criteria for choice of ZP length in all possible two-tap channels. We see that $1/\sigma_N$ offers a close approximation to $\kappa_2(\boldsymbol{H})$, up to a scaling factor. An example of the approximate bound for the MSEE is also shown in Fig. 3.5. From Fig. 3.5, we see that (3.22) can also be used to predict the MSEE.

Fortunately, some efficient algorithms have been developed for calculating the smallest singular value of a matrix [27]. Here we adopt the power method, which can find the largest magnitude eigenvalue of a matrix $\boldsymbol{A}$ and the corresponding eigenvector. To find the other eigen pairs, the power method can be applied to $(\boldsymbol{A} - \sigma\boldsymbol{I})^{-1}$ for some *shift* σ, and it will converge to the eigenvalue with magnitude closest to σ. By choosing σ close to a desired eigenvalue, convergence of the algorithm can be accelerated [27]. Table 3.2 details the algorithm. For a complete treatment of the power method and its variations, see [25, 27].

To estimate the smallest singular value of $\boldsymbol{H}$, the power method can be applied to

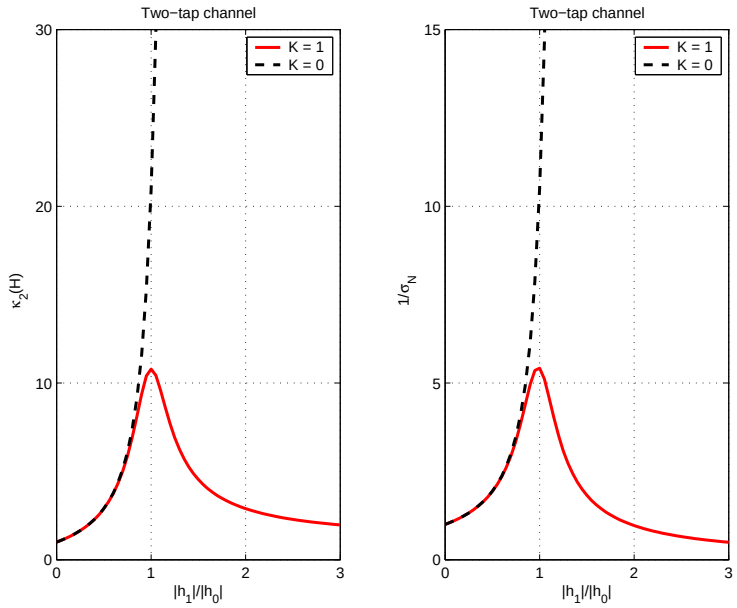

Figure 3.6. Criteria for choice of ZF length: $\kappa_2(\boldsymbol{H})$ versus σ_N in two-tap channel.

Table 3.2. Inverse Iteration of Power Method

Initialization choose $\boldsymbol{x}_0$; $i = 0$.
Iteration until convergence
$\boldsymbol{y}_{i+1} = (\boldsymbol{A} - \sigma \boldsymbol{I})^{-1} \boldsymbol{x}_i$
$\boldsymbol{x}_{i+1} = \boldsymbol{y}_{i+1} / \|\boldsymbol{y}_{i+1}\|_2$ (approximate eigenvector)
$\lambda_{i+1} = \boldsymbol{x}_{i+1}^H \boldsymbol{A} \boldsymbol{x}_{i+1}$ (approximate eigenvalue)
$i \leftarrow i+1$

$(\boldsymbol{H}^H \boldsymbol{H} - \sigma^2 \boldsymbol{I})^{-1}$ with an initial shift σ equal to 0. The initial guess of the singular value can be chosen to be previous estimate as well, due to the slow changing property of the channel matrix spectra as will be discussed in Section 3.5. Specifically, for the modified AZP-OFDM, to take the advantage of the channel matrix structure, we set $\sigma = 0$ so that in every iteration, the computational cost is mainly in solving two band-Toeplitz systems,

i.e., $(\boldsymbol{H}^H\boldsymbol{H})^{-1} = \boldsymbol{H}^{-1}\boldsymbol{H}^{-H}$. The convergence criterion for the power method used in our proposed method can be set quite loose because we are not required to estimate the singular value accurately.

Remark: We note that the choice of the number of padding zeros of modified AZP-OFDM may be different from that of the original AZP-OFDM. For the original AZP scheme, the condition number of the channel matrix will decrease with an increase of AZP length. Therefore the singular value finding algorithm may stop whenever the smallest singular value is large enough to guarantee symbol recovery. Beyond that, increasing AZP length will improve system performance, but the bandwidth efficiency will decrease, and therefore its choice may depend on the system requirements. On the other hand, in the modified scheme, there exists some optimal choice of AZP length. Heuristically, if we slide a window over the received block, there exists an optimal shift for the windowed sequence to capture most of the energy in the original sequence. This can be achieved by a simple search procedure.

3.5 Simulation Results and Discussions

3.5.1 Statistics of AZP Length

Standard HIPERLAN/2 channel models [31] are used. The OFDM block size of 64 and a terminal speed of $3m/s$ are assumed. The expected bandwidth efficiency for different channel models ranges from 93%–100%, while employing CP- or ZP-OFDM, bandwidth efficiency is fixed at 80%. The variation of AZP length depends on the velocity of the mobile terminal. An example of the variation of the channel matrix condition number with different numbers of padding zeros as well as variation of the estimated K with time is shown in Fig. 3.7 for HIPERLAN/2 channel A with a terminal speed of $3m/s$.

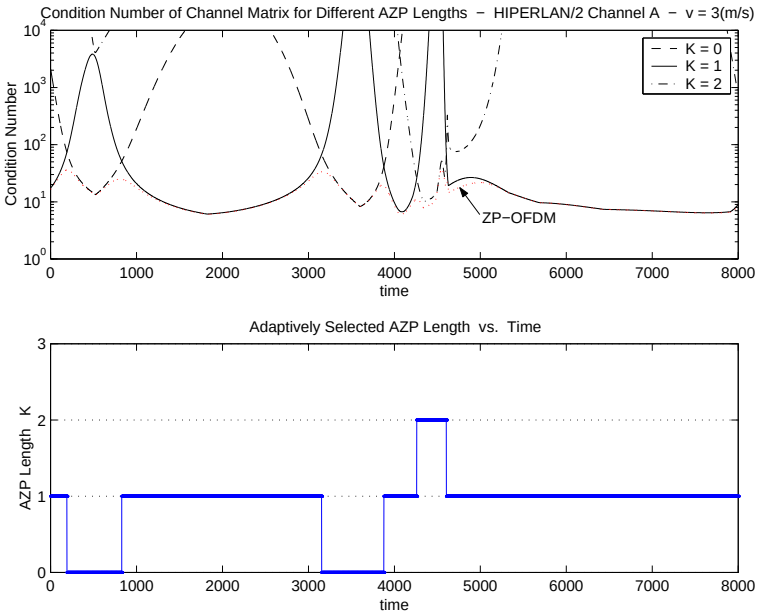

Figure 3.7. Variation of AZP length with time for HIPERLAN/2 channel model A with terminal speed $v = 3(m/s)$.

We see that for a terminal speed of $3m/s$, the AZP length varies very slowly and it most likely changes among neighboring values. This is due to small changes in the channel only resulting in small variations of the spectra of the channel matrix [45].

3.5.2 Complexity Issues

The AZP length results lead to further reductions in implementation complexity in that the AZP length need not be updated very frequently. The search algorithm can be simplified, examining several neighboring values, instead of performing exhaustive search over the set of all possible values. Moreover, since in the proposed schemes, accurate estimate of the smallest singular value is not required, the convergence criterion in applying the power method can be very loose, which will reduce the number of iterations significantly.

Equalization in (3.20) is a band Toeplitz LS problem, for which special methods

have been devised of complexity $O((N+K)N)$. Some "super-fast" methods require only $O((N+K)\log N)$ operations [12]. For modified AZP-OFDM, in each iteration for choosing AZP length and in the processing of each data block, the main cost is for solving band Toeplitz equations. Usually the system design results in a narrow band matrix. As a result the computational cost can be significantly reduced [25]. The complexity of CP-OFDM is $O(N\log N)$, while using ZP-OFDM with fast equalization algorithms [67], the complexity is $O(M\log M)$. In our simulations under the context of HIPERLAN/2 channel models, we estimate AZP length every 20 blocks and the power method usually converges in several iterations. In summary, the proposed scheme has almost the same complexity as ZP-OFDM, both of which are slightly higher than that of CP-OFDM.

3.5.3 Clipping Effects

As is well-known, one of the major drawbacks of OFDM is the high peak-to-average power ratio (PAPR) of the signal to be transmitted. As a result, OFDM signals cause serious problems such as distortion of the transmitted signal due to the PA nonlinearity. We consider the simplified PA model shown in Fig.3.8, with both input and output normalized, as in [67]. According to [67], by defining the *clipping ratio*, $\mathscr{C}$, as the number of clipped symbols over the total number of symbols, and the IBO as the ratio of the mean power at PA input to the input saturation power, (which is a function of $\mathscr{C}$), the transmitter output SNR difference between CP- and ZP-OFDM is given by [67]

$$\Delta_{\mathrm{ZP}}(\mathscr{C}) = 10\log\left(\frac{P}{N}\right) + IBO_{\mathrm{ZP}}(\mathscr{C}) - IBO_{\mathrm{CP}}(\mathscr{C})$$

Therefore, such SNR loss will be smaller with a shorter guard interval, as is the case in our proposed AZP-OFDM. Since the length of AZP, K, is not fixed, we can estimate the

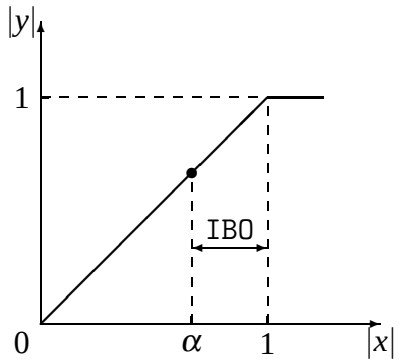

Figure 3.8. A simplified power amplifier model.

expected SNR loss compared with CP-OFDM as

$$\overline{\Delta_{\mathrm{AZP}}}(\mathscr{C}) = E_K\left[10\log\frac{N+K}{N} + IBO_{\mathrm{AZP}}(\mathscr{C}) - IBO_{\mathrm{CP}}(\mathscr{C})\right] \tag{3.24}$$

For HIPERLAN/2 transmission, Fig. 3.9 shows the simulated SNR loss for ZP- and AZP-OFDM with respect to CP-OFDM. The clipping effect alone requires reducing the transmit-power by less than 0.3 dB compared to CP-OFDM in order to guarantee the same amount of out-of-band radiation, while the reduction for ZP-OFDM is about 0.9 dB [67].

3.5.4 Uncoded BER performance

Example 1: (uncoded BER in HL/2 channel A) Fig. 3.10 shows the uncoded BER performances of NGI-, CP-, ZP- and the proposed modified AZP-OFDM scheme in channel A. The AZP length, K, is updated every 20 blocks. NGI-OFDM experiences serious error floors. AZP-OFDM has similar performance to CP-OFDM at low SNR, and both are slightly worse than that of ZP-OFDM. This is due to the guaranteed symbol recovery capability in ZP-OFDM, whereas for AZP-OFDM, this property has been sacrificed to achieve higher bandwidth efficiency and lower complexity.

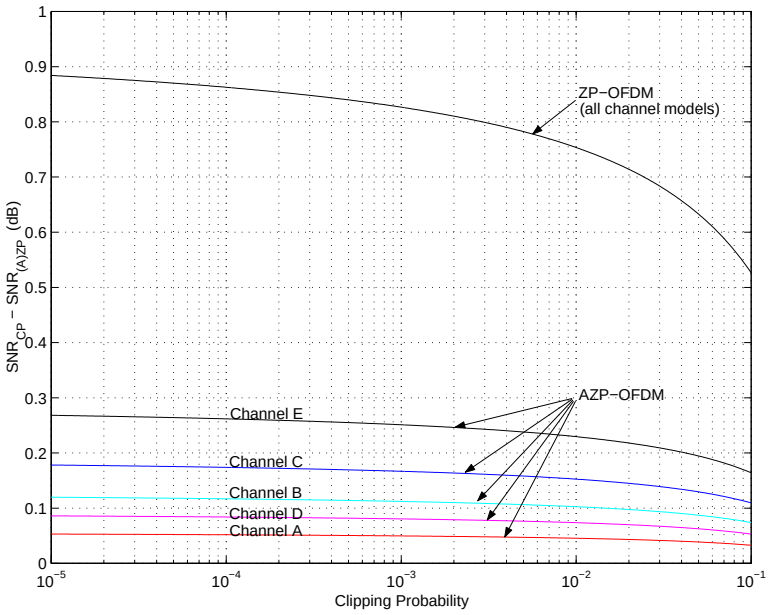

Figure 3.9. SNR difference between CP and (A)ZP induced by clipping effects.

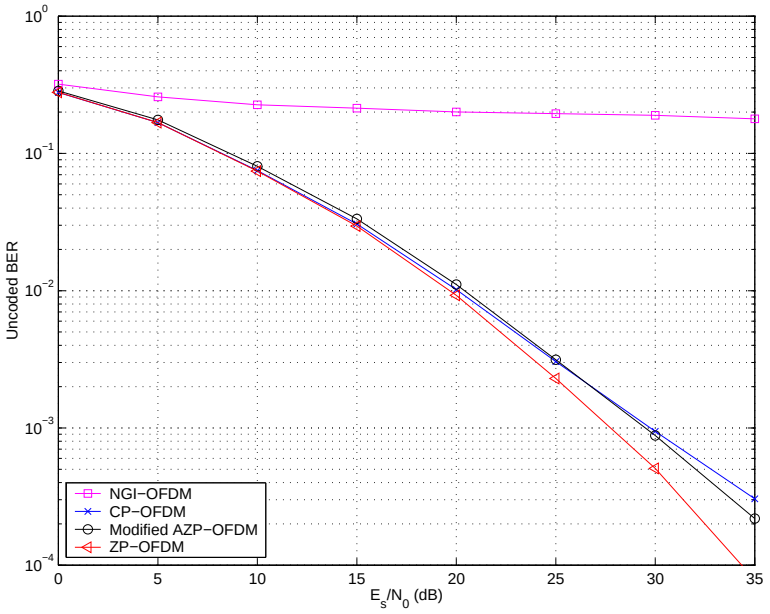

Figure 3.10. Uncoded BER in HIPERLAN/2 channel A for QPSK.

Example 2: (uncoded BER in channels with exponential power delay profile) We assume channel model order $L = N$, and channel tap powers $\rho_l^2 = \beta e^{-\alpha l}$, for $l = 0, 1, \cdots, N-1$, with β chosen to normalize the total channel power, i.e., $\beta = \frac{1}{\sum_{l=0}^{N-1} e^{-\alpha l}}$ and $\sum_{l=0}^{N-1} \rho_l^2 = 1$. Obviously, small α corresponds to large rms delay spread. Fig. 3.11 shows the uncoded BER performance of CP-OFDM, ZP-OFDM and AZP-OFDM in a system with block size $N = 32$ and guard length $G = 4$. We see that for small α, both CP- and ZP-OFDM, with fixed guard length, experience serious error floors. Using AZP-OFDM, since the guard length is adaptive, the system is more robust to channels with large delay spread. The expected bandwidth efficiencies of AZP-OFDM for different α are, respectively, $71.35\%(\alpha = 0.05)$, $77.20\%(\alpha = 0.1)$, and $90.27\%(\alpha = 0.5)$, compared with fixed bandwidth efficiencies in CP- and ZP-OFDM, 88.89%. In other words, when the delay spread is low, AZP-OFDM has performance slightly below that of CP- and ZP-OFDM, while if the delay spread is large, performance can be maintained at the expense of bandwidth efficiency.

3.6 Conclusion

This chapter has shown how to optimize the transmit redundancy for OFDM transmission over wireless channels to tradeoff performance, complexity and bandwidth efficiency. A new bandwidth efficient zero-padding scheme, AZP-OFDM, was proposed based on the channel matrix condition, which is flexible for system design compared with the standard CP-/ZP-OFDM. The new AZP-OFDM transmission method offers robust performance over a large range of time dispersion (delay spread) while keeping implementation complexity low.

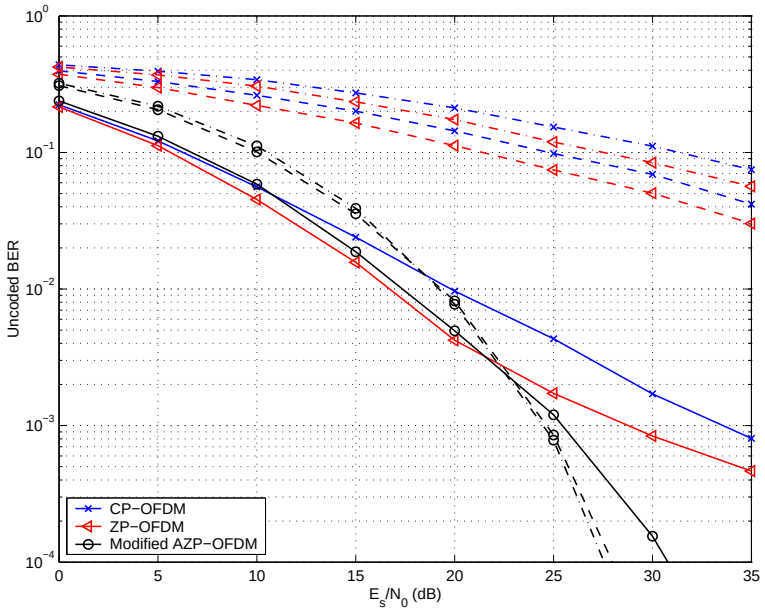

Figure 3.11. Uncoded BER in channels with exponential power delay profiles for QPSK, $N = 32$, $G = 4$, (solid line: $\alpha = 0.5$, dashed line: $\alpha = 0.1$, dash-dot line: $\alpha = 0.05$).

Chapter 4

Minimum BER Power Allocation Schemes for Multicarrier Wireless Transmission

4.1 Introduction

Wideband wireless communication signals suffer from serious inter-symbol interference (ISI) due to frequency-selective channels. Multicarrier (MC) modulation, especially Orthogonal Frequency Division Multiplexing (OFDM) using a cyclic prefix (CP) has been receiving growing interest in recent years as countermeasures of frequency selectivity of wireless channels due to simplified frequency-domain equalization (FDE) [106]. Time-domain equalization (TDE) of conventional single-carrier (SC) transmission usually has much higher complexity, especially when the channel delay spread is large.

Comparison between MC and SC has been investigated over the years. Simulations [90] have shown that the *uncoded* performance of SC transmission with FDE substantially outperforms that of CP-OFDM. It was also suggested [90] for CP-OFDM to use powerful channel coding and frequency-domain interleaving to combat performance degradation from channel nulls. Recently, it has been shown that block SC transmission with similar block structure and FDE to CP-OFDM, has similar equalization complexity and

coded performance as OFDM [34]. Single-carrier employing a decision feedback equalizer (DFE) was proposed [8] and shown to have similar capacity and complexity compared with OFDM. In this chapter, we present a framework for analytical comparison among CP-based MC and SC block transmission schemes. From our analysis in Section 4.4, uncoded CP-OFDM is shown to be inferior to CP-SC block transmission with the same processing complexity, which motivates optimization of MC transmission by utilizing channel state information (CSI) — we term this as *power allocation*.

Joint power and bit allocation has been widely studied in Discrete Multitone (DMT) — a multicarrier scheme in wire-line applications, where the channel is regarded as static [10]. Adaptive modulation for OFDM over wideband wireless channels has been studied in [24]. Wireless systems, however, are time-varying. For simplicity of implementation, power allocation alone may be employed as an alternative to joint power and bit allocation. A minimum *aggregate* error rate power allocation algorithm was proposed in [40], which minimizes the block error rate. In this chapter, we propose a minimum *average* bit error rate (BER) power allocation algorithm for multicarrier wireless communications, which we denote as MBER. Due to the nonlinear nature of the MBER power allocation problem, there is no closed-form solution, with high implementation complexity. To lower complexity, we propose a simpler approximate MBER algorithm with closed-form optimum solution and small performance loss. Power allocation using equal gain (EG) and minimum mean squared error (MMSE) criteria are also considered. Analytical performance comparison among SC and a variety of MC schemes are presented. Simulations are provided and compared to our analyses.

Conventional OFDM without power and bit allocation is an open-loop scheme, which assumes no CSI knowledge at the transmitter. On the other hand, OFDM with power allocation, is a closed-loop scheme, requiring CSI. In time-division duplex (TDD), due to the

reciprocity of the uplink and downlink channels, CSI can be obtained from uplink measurements using pilot and/or data symbols. For frequency-division duplex (FDD) systems, CSI estimates require a feedback channel. Uncertain CSI arises due to [114]: 1) outdated estimates due to feedback delay; 2) channel estimation error; 3) quantization error; 4) errors introduced by feedback channel. This motivates analysis of the performance of closed-loop MC transmission under CSI uncertainty.

The rest of this chapter is organized as follows. Section 4.2 describes system models for CP-OFDM and CP-SC, and analyzes their error rate performance with linear equalization. Power allocation algorithms for CP-OFDM with perfect CSI are developed in Section 4.3. In Section 4.4, we compare CP-SC to a variety of MC schemes, and demonstrate performance improvements of the closed-loop transmission schemes studied in Section 4.3. Section 4.5 is devoted to the study of power allocation with imperfect CSI. Section 4.6 presents numerical results which are compared to our analyses.

4.2 Background

As described in Chapter 2, a serial stream of data, u_n, is serial-to-parallel (S/P) converted into data blocks of size N, $\boldsymbol{u} \stackrel{\text{def}}{=} [u_0, u_1, \cdots, u_{N-1}]^T$. For MC transmission, MC modulation is performed via IDFT to obtain the time-domain signal block, $\boldsymbol{F}^H \boldsymbol{u}$, where $\boldsymbol{F}$ is the N-point DFT matrix. For SC systems, no MC modulation is performed. A guard interval in terms of CP of length G is then inserted between each block, and the resulting cyclic-prefixed block is parallel-to-serial (P/S) converted and sent sequentially through the channel. A multipath propagation channel can be modelled as a finite impulse response (FIR) filter with tap vector $[h_0, h_1, \cdots, h_L]^T$ and AWGN $\eta_n \sim \mathcal{N}(0, N_0)$. At the receiver, the first G entries corresponding to the CP are removed. For simplicity of analysis purposes, we assume that

both input and noise are white, and the length of the CP, G, is no less than the channel model order, L.

4.2.1 CP-OFDM

In CP-OFDM, the received block can be written as (after CP removal)

$$\boldsymbol{r}_{\mathrm{MC}} = \boldsymbol{H}\boldsymbol{F}^{H}\boldsymbol{u} + \boldsymbol{\eta}, \tag{4.1}$$

where $\boldsymbol{H}$ is an $N \times N$ circulant channel matrix with first column $\boldsymbol{h} \stackrel{\text{def}}{=} [h_0, \cdots, h_L, 0, \cdots, 0]^T$ and $\boldsymbol{\eta}$ is the $N \times 1$ AWGN vector. By assumption, $\boldsymbol{R}_{uu} \stackrel{\text{def}}{=} \mathbb{E}\{\boldsymbol{u}\boldsymbol{u}^H\} = E_s\boldsymbol{I}$ and $\boldsymbol{R}_{\eta\eta} \stackrel{\text{def}}{=} \mathbb{E}\{\boldsymbol{\eta}\boldsymbol{\eta}^H\} = N_0\boldsymbol{I}$. Performing MC demodulation via DFT, we obtain the frequency-domain received block

$$\boldsymbol{r}^{f}_{\mathrm{MC}} \stackrel{\text{def}}{=} \boldsymbol{F}\boldsymbol{r}_{\mathrm{MC}} = \boldsymbol{D}\boldsymbol{u} + \boldsymbol{\eta}^{f}, \tag{4.2}$$

where $\boldsymbol{D} \stackrel{\text{def}}{=} \mathrm{diag}(\boldsymbol{F}\boldsymbol{h})$, and the superscript ^{f} denotes the frequency-domain variable. The frequency-domain zero-forcing (ZF) and MMSE equalizers are given by, respectively [106],

$$\boldsymbol{G}^{\mathrm{MC}}_{\mathrm{ZF}} = \boldsymbol{D}^{\dagger}, \qquad \boldsymbol{G}^{\mathrm{MC}}_{\mathrm{MMSE}} = \boldsymbol{D}^{H}\left(\frac{1}{\gamma_s}\boldsymbol{I} + \boldsymbol{D}\boldsymbol{D}^{H}\right)^{-1}. \tag{4.3}$$

where $\gamma_s \stackrel{\text{def}}{=} E_s/N_0$. Since both frequency-domain equalizers are diagonal matrices, matrix inversion is trivial, also know as one-tap equalization.

4.2.2 Single-Carrier with CP (CP-SC)

After CP removal at the CP-SC receiver, the received block can be written as

$$\boldsymbol{r}_{\mathrm{SC}} = \boldsymbol{H}\boldsymbol{u} + \boldsymbol{\eta}, \tag{4.4}$$

The ZF and MMSE time-domain equalizers are given by circulant matrices, respectively [106],

$$\boldsymbol{G}_{\mathrm{ZF}}^{\mathrm{SC}} = \boldsymbol{H}^{\dagger}, \qquad \boldsymbol{G}_{\mathrm{MMSE}}^{\mathrm{SC}} = \boldsymbol{H}^{H}\left(\frac{1}{\gamma_s}\boldsymbol{I} + \boldsymbol{H}\boldsymbol{H}^{H}\right)^{-1}, \tag{4.5}$$

for which there exist FFT-based implementations, also known as FDE [34]. To be specific, the received block is first transformed to the frequency domain, i.e.,

$$\boldsymbol{r}_{\mathrm{SC}}^{f} \stackrel{\mathrm{def}}{=} \boldsymbol{F}\boldsymbol{r}_{\mathrm{SC}} = \boldsymbol{D}\boldsymbol{F}\boldsymbol{u} + \boldsymbol{\eta}^{f}. \tag{4.6}$$

Equalization is then performed in the frequency domain with either ZF or MMSE criterion, as in CP-OFDM (see (4.3)). Finally, the equalized block is transformed back to the time domain (via IFFT) to obtain the estimate of transmitted block.

4.2.3 Instantaneous BER Performance

For simplicity of analysis, we consider BPSK modulation. The instantaneous BER is defined as the BER for a fixed channel realization.

In CP-OFDM, the one-tap equalizer outputs are given by, respectively, (for $k = 0, 1, \cdots, N-1$)

$$\left[\hat{\boldsymbol{u}}_{\mathrm{ZF}}^{\mathrm{MC}}\right]_k = u_k + H_k^{-1}[\boldsymbol{\eta}^{f}]_k, \tag{4.7}$$

$$\left[\hat{\boldsymbol{u}}_{\mathrm{MMSE}}^{\mathrm{MC}}\right]_k = \frac{|H_k|^2}{\gamma_s^{-1} + |H_k|^2}u_k + \frac{H_k^{*}}{\gamma_s^{-1} + |H_k|^2}[\boldsymbol{\eta}^{f}]_k, \tag{4.8}$$

where $H_k \stackrel{\mathrm{def}}{=} [\boldsymbol{F}\boldsymbol{h}]_k = \frac{1}{\sqrt{N}}\sum_{l=0}^{L} h_l e^{-j\frac{2\pi kl}{N}}$ is the channel frequency response of the k-th subcarrier. Since $\frac{|H_k|^2}{\gamma_s^{-1}+|H_k|^2} \neq 1$ for $\gamma_s < \infty$, we see that the MMSE equalization output $\hat{\boldsymbol{u}}_{\mathrm{MMSE}}^{\mathrm{MC}}$ in (4.8) is a biased estimate of the transmitted signal $\boldsymbol{s}$. Furthermore, from (4.7) and (4.8), we have

$$\left[\hat{\boldsymbol{u}}_{\mathrm{MMSE}}^{\mathrm{MC}}\right]_k = \frac{|H_k|^2}{\gamma_s^{-1} + |H_k|^2}\left[\hat{\boldsymbol{u}}_{\mathrm{ZF}}^{\mathrm{MC}}\right]_k,$$

i.e., the MMSE estimate is actually a scaled version of the ZF estimate. The corresponding decision-point SNR's are given by, respectively (for $k = 0, 1, \cdots, N-1$),

$$\gamma_{\mathrm{ZF},k}^{\mathrm{MC}} = \frac{\mathbb{E}\left\{|u_k|^2\right\}}{\mathbb{E}\left\{\left|H_k^{-1}[\boldsymbol{\eta}^f]_k\right|^2\right\}} = \gamma_s|H_k|^2, \tag{4.9}$$

$$\gamma_{\mathrm{MMSE},k}^{\mathrm{MC}} = \frac{\mathbb{E}\left\{|u_k|^2\right\}}{\mathbb{E}\left\{\left|u_k - [\hat{\boldsymbol{u}}_{\mathrm{MMSE}}^{\mathrm{MC}}]_k\right|^2\right\}} = 1 + \gamma_s|H_k|^2. \tag{4.10}$$

The above SNR's of MMSE equalization do not take into account the bias in the decision variable, and the increased SNR is an artifact of the SNR definition [22]. Since there is no inter-carrier interference (ICI), it is shown in Appendix A that the error rate performance can be approximately determined by the unbiased SNR [22][1]. By scaling (4.8) to remove the bias, we calculate the unbiased SNR for MMSE equalization $\gamma_{\mathrm{MMSE\text{-}U},k}^{\mathrm{MC}} = \gamma_s|H_k|^2$, which is exactly the same as that of ZF equalization. Therefore, from here on, only ZF equalization is considered in CP-OFDM. The average instantaneous BER is given by

$$P^{\mathrm{MC}}(\boldsymbol{h}) = \frac{1}{N}\sum_{k=0}^{N-1} Q\left(\sqrt{2\gamma_s|H_k|^2}\right), \tag{4.11}$$

where $Q(x) \stackrel{\mathrm{def}}{=} \frac{1}{\sqrt{2\pi}}\int_x^\infty e^{-y^2/2}dy$.

For CP-SC, the ZF equalization output is

$$\hat{\boldsymbol{u}}_{\mathrm{ZF}}^{\mathrm{SC}} = \boldsymbol{u} + \boldsymbol{H}^\dagger\boldsymbol{\eta}. \tag{4.12}$$

Clearly, (4.12) is an unbiased estimate, and there is no ISI. The error rate performance is determined by the decision-point SNR,

$$\begin{aligned}\gamma_{\mathrm{ZF},k}^{\mathrm{SC}} &= \frac{E_s}{N_0[(\boldsymbol{H}^H\boldsymbol{H})^\dagger]_{k,k}} \\ &= \frac{\gamma_s}{\frac{1}{N}\sum_{l=0}^{N-1}|H_l|^{-2}}, \quad \forall k.\end{aligned} \tag{4.13}$$

[1]The noise term in the decision variable is generally not AWGN. Assuming AWGN gives a good approximation to the BER performance.

Using (4.13), the average instantaneous BER is given by

$$P_{\mathrm{ZF}}^{\mathrm{SC}}(\boldsymbol{h}) = Q\left(\sqrt{\frac{2\gamma_s}{\frac{1}{N}\sum_{l=0}^{N-1}|H_l|^{-2}}}\right). \tag{4.14}$$

For MMSE-equalized CP-SC, the decision variable is

$$\hat{\boldsymbol{u}}_{\mathrm{MMSE}}^{\mathrm{SC}} = \boldsymbol{B}\boldsymbol{u} + \boldsymbol{G}_{\mathrm{MMSE}}^{\mathrm{SC}}\boldsymbol{\eta}, \tag{4.15}$$

where $\boldsymbol{B} \overset{\text{def}}{=} \boldsymbol{G}_{\mathrm{MMSE}}^{\mathrm{SC}}\boldsymbol{H} = \boldsymbol{H}^H\left(\gamma_s^{-1}\boldsymbol{I} + \boldsymbol{H}\boldsymbol{H}^H\right)^{-1}\boldsymbol{H}$ is generally not diagonal, and (4.15) experiences ISI. In this case, the decision-point SNR cannot be used to calculate BER because the ISI term cannot be approximated as Gaussian according to our simulations. Since both $\boldsymbol{G}_{\mathrm{MMSE}}^{\mathrm{SC}}$ and $\boldsymbol{H}$ are circulant, $\boldsymbol{B}$ is also circulant. The coefficients of the desired and interfering terms are the same for all symbols in the block, which can be calculated efficiently using an FFT. Denoting, respectively,

$$\begin{aligned}
\Theta_k &\overset{\text{def}}{=} \frac{|H_k|^2}{\gamma_s^{-1} + |H_k|^2}, \\
\underline{\Theta} &\overset{\text{def}}{=} [\Theta_0, \cdots, \Theta_{N-1}]^T, \\
\underline{\theta} &\overset{\text{def}}{=} \boldsymbol{F}_N^H\underline{\Theta} = [\theta_0, \cdots, \theta_{N-1}]^T,
\end{aligned}$$

we have

$$\begin{aligned}
\boldsymbol{B} &= \boldsymbol{H}^H\left(\gamma_s^{-1}\boldsymbol{I} + \boldsymbol{H}\boldsymbol{H}^H\right)^{-1}\boldsymbol{H} \\
&= \boldsymbol{F}_N^H \underbrace{\boldsymbol{D}^H\left(\gamma_s^{-1}\boldsymbol{I} + \boldsymbol{D}\boldsymbol{D}^H\right)^{-1}\boldsymbol{D}}_{\mathrm{diag}\{\underline{\Theta}\}}\boldsymbol{F}_N \\
&= \mathrm{circulant}\{\underline{\theta}\},
\end{aligned} \tag{4.16}$$

where circulant($\underline{x}$) denotes a circulant matrix with first column $\underline{x}$. Therefore, θ_0 is the coefficient of the desired signal, and $\{\theta_k\}_{k=1}^{N-1}$ represent ISI coefficients. The noise variance in (4.15) is given by

$$\sigma_k^2 = N_0\left[\boldsymbol{G}_{\mathrm{MMSE}}^{\mathrm{SC}}\left(\boldsymbol{G}_{\mathrm{MMSE}}^{\mathrm{SC}}\right)^H\right]_{k,k}$$

$$= N_0 \cdot \frac{1}{N} \sum_{l=0}^{N-1} \frac{|H_l|^2}{(\gamma_s^{-1} + |H_l|^2)^2}$$
$$\stackrel{\text{def}}{=} \sigma^2, \tag{4.17}$$

which is independent of k. Using Beaulieu series [7], we calculate

$$P_{\text{MMSE}}^{\text{SC}}(\boldsymbol{h}) \approx \frac{1}{2} - \frac{2}{\pi} \sum_{\substack{m=1 \\ m \text{ odd}}}^{M} \frac{1}{m} e^{-\frac{m^2\omega^2}{2}} \sin\left(\frac{m\omega\theta_0}{\sigma}\right) \prod_{k=1}^{N-1} \cos\left(\frac{m\omega\theta_k}{\sigma}\right),$$

where the choice of parameters M and ω is described in [7].

4.3 Power Allocation for CP-OFDM with Perfect CSI

We now consider CP-OFDM transmission utilizing perfect CSI at the transmitter. A general power allocation method is briefly introduced and a variety of new schemes are then proposed. Power allocation algorithms adjust the transmitted signal power across subcarriers under the constraint of constant power per block. Denote p_k^2 as the transmitted power of the k-th subcarrier ($k = 0, 1, \cdots, N-1$), and define the power allocation matrix $\boldsymbol{P} = \text{diag}\{p_0, p_1, \cdots, p_{N-1}\}$. The block power constraint can be normalized as

$$\text{trace}\{\boldsymbol{P}^2\} = \sum_{k=0}^{N-1} p_k^2 = N. \tag{4.18}$$

From (4.2), the received frequency-domain block is given by $\boldsymbol{r}_{\text{PMC}}^f = \boldsymbol{DPu} + \boldsymbol{\eta}^f$, where the subscript $_{\text{PMC}}$ denotes MC with power allocation. With one-tap equalization, we obtain,

$$\hat{\boldsymbol{u}}_{\text{PMC}} = \boldsymbol{u} + (\boldsymbol{DP})^{\dagger} \boldsymbol{\eta}^f. \tag{4.19}$$

Using (4.9), the decision-point SNR of the k-th subcarrier is given by $\gamma_k^{\text{PMC}} = \gamma_s |H_k|^2 p_k^2$, and the average instantaneous BER[2]

$$P(\boldsymbol{h}, \boldsymbol{P}) = \frac{1}{N} \sum_{k=0}^{N-1} Q\left(\sqrt{2\gamma_s |H_k|^2 p_k^2}\right). \tag{4.20}$$

Note that CP-OFDM without power allocation is a special case of $\boldsymbol{P} = \boldsymbol{I}$.

[2]For simplicity of notation, we drop super- and subscripts.

4.3.1 MBER Power Allocation

By differentiating (4.20), we note that $\nabla^2_{p_k^2} P(\boldsymbol{h},\boldsymbol{P}) > 0$, the Hessian matrix is diagonal with positive diagonal entries, and, therefore, positive definite. Hence, $P(\boldsymbol{h},\boldsymbol{P})$ is a convex function of $\{p_k^2\}_{k=0}^{N-1}$. Also, it is readily verified that the block power constraint (4.18) defines a convex feasible region. Therefore, power-constrained MBER power allocation

$$\begin{cases} \min P(\boldsymbol{h},\boldsymbol{P}) = \frac{1}{N}\sum_{k=0}^{N-1} Q\left(\sqrt{2\gamma_s|H_k|^2 p_k^2}\right) \\ \text{subject to} \quad \sum_{k=0}^{N-1} p_k^2 = N \end{cases}, \tag{4.21}$$

is a convex programming problem, for which there exists a unique global minimum [60]. Due to the high nonlinearity of the objective function, there is no closed-form solution to this problem. A solution of this "water-filling"-like problem is given in Appendix B. The solution $\{p^2_{\mathrm{MBER},k}\}_{k=0}^{N-1}$ is unique and satisfies

$$\sqrt{\frac{\gamma_s|H_k|^2}{p_k^2}} e^{-\gamma_s|H_k|^2 p_k^2} = \mu, \quad (k = 0,1,\cdots,N-1), \tag{4.22}$$

which can be solved numerically. The parameter μ is chosen numerically according to the total power constraint (4.18). To be specific, we can bound the parameter μ as follows: since $\sum_{k=0}^{N-1} p_k^2 = N$, we have $\min_k p_k^2 \le 1 \le \max_k p_k^2$. Furthermore, since $\sqrt{\frac{\gamma_s|H_k|^2}{p_k^2}} e^{-\gamma_s|H_k|^2 p_k^2}$ is monotone decreasing in p_k^2, we have

$$\underbrace{\min_k \sqrt{\gamma_s|H_k|^2} e^{-\gamma_s|H_k|^2}}_{\mu_{\min}} \le \mu \le \underbrace{\max_k \sqrt{\gamma_s|H_k|^2} e^{-\gamma_s|H_k|^2}}_{\mu_{\max}}.$$

An algorithm for MBER power allocation is summarized in Table 4.1. This algorithm requires an iterative procedure to obtain the optimum solution and N nonlinear equations must be solved numerically in each iteration. Therefore MBER suffers from slow convergence and high computational complexity, which motivates the approximate MBER algorithm discussed next.

Table 4.1. MBER Power Allocation Algorithm

Initialization	$\mu_0 \leftarrow \mu_{\min},\ \mu_1 \leftarrow \mu_{\max}$;
	$p_k^2 \leftarrow 1$ for $k = 0, 1, \cdots, N-1$;
	`choose error tolerance` ε.
Iteration	`do` $\{$
	$\mu \leftarrow \frac{\mu_0+\mu_1}{2}$
	`solve` (4.22) `for` $k = 0, 1, \cdots, N-1$
	`if` $(\sum_k p_k^2 < N), \quad \mu_1 \leftarrow \mu$
	`else` $\quad \mu_0 \leftarrow \mu$
	$\}$ `until` $\quad \lvert\sum_k p_k^2 - N\rvert \le \varepsilon$

4.3.2 Approximate MBER (AMBER) Power Allocation

Instead of solving (4.21) directly, we approximate the objective function to find a suboptimal solution. An expression for the approximate BER is given by [116]

$$P_b \approx \frac{1}{5} e^{-c\gamma_s}, \tag{4.23}$$

where c is a constellation-specific constant, e.g., for BPSK, $c_{\text{BPSK}} = 1$. Accordingly, we formulate the AMBER power allocation problem as

$$\begin{cases} \min \frac{1}{5N} \sum_{k=0}^{N-1} \exp(-\gamma_s |H_k|^2 p_k^2) \\ \text{subject to } \sum_{k=0}^{N-1} p_k^2 = N \end{cases}, \tag{4.24}$$

which is also a convex programming problem. Using Lagrange multipliers, we obtain the closed-form solution,

$$p_{\text{AMBER},k}^2 = \frac{\ln |H_k|^2 + \nu}{\gamma_s |H_k|^2}, \qquad \nu \overset{\text{def}}{=} \frac{\gamma_s - \frac{1}{N}\sum_{l=0}^{N-1} |H_l|^{-2} \ln |H_l|^2}{\frac{1}{N}\sum_{l=0}^{N-1} |H_l|^{-2}}. \tag{4.25}$$

However, the above solution does *not* take into account the inherent inequality constraints, $p_k^2 \geq 0, \forall k$, which are satisfied only if

$$\nu \geq \max_k \left\{ -\ln |H_k|^2 \right\}. \tag{4.26}$$

Otherwise, according to Appendix B, the solution should be modified as[3]

$$p_{\text{AMBER},k}^2 = \left(\frac{\ln |H_k|^2 + \nu}{\gamma_s |H_k|^2} \right)_+, \tag{4.27}$$

where $(x)_+ \stackrel{\text{def}}{=} \max\{0, x\}$, and ν is chosen to satisfy the block power constraint (4.18). Note that the block power $\sum_k p_k^2(\nu) = \sum_k \left(\frac{\ln |H_k|^2 + \nu}{\gamma_s |H_k|^2} \right)_+$ is a piecewise-linear increasing function of ν, with breakpoints at $-\ln |H_k|^2$. Therefore ν is unique and can be readily determined. Table 4.2 summarizes an algorithm for AMBER power allocation. Compared to the MBER power allocation algorithm in Table 4.1, the AMBER algorithm includes a sorting procedure, but no numerical solution of nonlinear equations. The AMBER algorithm requires at most N recursions.

4.3.3 Equal-Gain (EG) Power Allocation

Since the $Q(\cdot)$ function decreases very rapidly in its argument, the BER (4.20) is usually dominated by a few terms with smallest $|H_k|$'s. Power allocation algorithms try to pre-equalize the gains of subcarriers, $|H_k| p_k$. One empirical solution is to allocate the transmitted power so that all gains are equal[4], i.e.,

$$\begin{cases} |H_k|^2 p_k^2 &= C, \quad (k = 0, 1, \cdots, N-1) \\ \sum_{k=0}^{N-1} p_k^2 &= N \end{cases}, \tag{4.28}$$

where C is a constant independent of k. From the first equation in (4.28), we have $p_k^2 = C|H_k|^{-2}$. Substituting p_k^2 into the second equation in (4.28), we obtain $C =$

[3] An equivalent solution is obtained in [49] by minimizing the Chernoff upper bound of BER.

[4] This scheme was also addressed in [10] as an approximate of power allocation at high SNR.

Table 4.2. AMBER Power Allocation Algorithm

Initialization	sort $\{|H_k|^2\}_{k=0}^{N-1}$ in decreasing order $\Rightarrow \{d_k\}_{k=0}^{N-1}$;
	if (4.26) holds, go to Solution;
	$k=0$, $P_0=0$.
Recursion	if $(P_k < N)$, do {
	$k \leftarrow k+1$
	$P_k = P_{k-1} + (\ln d_{k-1} - \ln d_k)\sum_{l=0}^{k-1} \frac{1}{\gamma_s d_l}$
	}
	$\nu = \gamma_s(N-P_{k-1})\left(\sum_{l=0}^{k-1} d_l^{-1}\right)^{-1} - \ln d_{k-1}$
Solution	$p^2_{\mathrm{AMBER},k} = \left(\frac{\ln\|H_k\|^2+\nu}{\gamma_s\|H_k\|^2}\right)_+$, for $k=0,1,\cdots,N-1$

$\left(\frac{1}{N}\sum_{l=0}^{N-1}|H_l|^{-2}\right)^{-1}$. Therefore, the EG solution is given by

$$p^2_{\mathrm{EG},k} = \frac{|H_k|^{-2}}{\frac{1}{N}\sum_{l=0}^{N-1}|H_l|^{-2}}, \quad (k=0,\cdots,N-1). \tag{4.29}$$

4.3.4 MMSE Power Allocation

From (4.19), we obtain the mean squared-error (MSE) for CP-OFDM equalization with power allocation as

$$\begin{aligned} \mathrm{MSE} &= \mathrm{E}\left\{\| \hat{\boldsymbol{u}}_{\mathrm{PMC}} - \boldsymbol{u} \|^2\right\} \\ &= \mathrm{trace}\left\{(\boldsymbol{DP})^{\dagger}\mathbb{E}\left\{\boldsymbol{\eta}\boldsymbol{\eta}^H\right\}[(\boldsymbol{DP})^{\dagger}]^H\right\} \\ &= N_0\sum_{k=0}^{N-1} p_k^{-2}|H_k|^{-2}. \end{aligned} \tag{4.30}$$

Using Lagrange multipliers, the MMSE power allocation solution under the block power constraint (4.18) can be found as

$$p^2_{\mathrm{MMSE},k} = \frac{|H_k|^{-1}}{\frac{1}{N}\sum_{l=0}^{N-1}|H_l|^{-1}}, \quad (k=0,\cdots,N-1). \tag{4.31}$$

Comparing (4.31) to (4.29), we note that

$$\frac{p_{\mathrm{EG},k}^2}{p_{\mathrm{MMSE},k}^2} = \frac{1}{|H_k|} \cdot \underbrace{\frac{\sum_{l=0}^{N-1} |H_l|^{-1}}{\sum_{m=0}^{N-1} |H_m|^{-2}}}_{\text{constant}} \tag{4.32}$$

i.e., the EG solution allocates more power to weaker subcarriers.

4.4 Comparison of CP-OFDM and CP-SC

From the previous sections (4.2.3 and 4.3), we note that since closed-form decision-point SNR and instantaneous BER performance are available, an analytical performance comparison is possible. We compare the instantaneous BER of ZF-equalized CP-SC and several CP-OFDM schemes.

4.4.1 CP-SC versus CP-OFDM without Power Allocation

From (4.11) and (4.14), the average instantaneous BER expressions can be unified as

$$P(\{\xi_k\}_{k=0}^{N-1}) = \frac{1}{N} \sum_{k=0}^{N-1} Q\left(\sqrt{\frac{2\gamma_s}{\xi_k}}\right), \tag{4.33}$$

where ξ_k's for OFDM and SC are given by, respectively,

$$\xi_k^{\mathrm{MC}} = |H_k|^{-2}, \quad \xi_k^{\mathrm{SC}} = \frac{1}{N} \sum_{l=0}^{N-1} |H_l|^{-2} \stackrel{\mathrm{def}}{=} \xi^{\mathrm{SC}}. \tag{4.34}$$

From the second derivatives of (4.33),

$$\frac{d^2P}{d\xi_k^2} = \frac{1}{2N} \sqrt{\frac{\gamma_s}{\pi \xi_k^5}} \left(\frac{\gamma_s}{\xi_k} - \frac{3}{2}\right) e^{-\frac{\gamma_s}{\xi_k}}, \tag{4.35}$$

we know that the Hessian matrix is positive definite, as long as the decision-point SNR $\gamma_k = \frac{\gamma_s}{\xi_k} > \frac{3}{2}$ (1.76 dB). This condition holds asymptotically when γ_s is large. Under this condition, $P(\{\xi_k\}_{k=0}^{N-1})$ is a convex function of ξ_k's. From (4.34), we know $\xi^{\mathrm{SC}} = \frac{1}{N} \sum_{k=0}^{N-1} \xi_k^{\mathrm{MC}}$. By Jensen's inequality, we conclude that

$$P_{\mathrm{ZF}}^{\mathrm{SC}}(\boldsymbol{h}) \leq P^{\mathrm{MC}}(\boldsymbol{h}). \tag{4.36}$$

4.4.2 CP-SC versus CP-OFDM with EG Power Allocation

For CP-OFDM with EG power allocation, we calculate the decision-point SNR (cf. (4.29))

$$\gamma_{\mathrm{EG},k}^{\mathrm{PMC}} = \frac{\gamma_s}{\frac{1}{N}\sum_{l=0}^{N-1}|H_l|^{-2}} \equiv \gamma_k^{\mathrm{SC}}. \tag{4.37}$$

Therefore, CP-OFDM with EG power allocation has the same performance as ZF-equalized CP-SC.

4.4.3 CP-SC versus CP-OFDM with MMSE Power Allocation

From (4.20), (4.33) and (4.31), we have

$$\xi_{\mathrm{MMSE},k}^{\mathrm{PMC}} = \frac{1}{|H_k|}\cdot\frac{1}{N}\sum_{l=0}^{N-1}\frac{1}{|H_l|}.$$

When $\gamma_s \gg 1$, by Taylor series expansion of $P(\{\xi_{\mathrm{MMSE},k}^{\mathrm{PMC}}\})$ at ξ^{SC}, we can write $P_{\mathrm{MMSE}}^{\mathrm{PMC}}(\boldsymbol{h})$ as

$$\begin{aligned} P_{\mathrm{MMSE}}^{\mathrm{PMC}}(\boldsymbol{h}) &= P(\xi^{\mathrm{SC}}) + \left(\frac{1}{N}\sum_{k=0}^{N-1}\xi_{\mathrm{MMSE},k}^{\mathrm{PMC}} - \xi^{\mathrm{SC}}\right)\frac{dP(\xi^{\mathrm{SC}})}{d\xi} \\ &\quad + \frac{1}{2N}\sum_{k=0}^{N-1}\left(\xi_{\mathrm{MMSE},k}^{\mathrm{PMC}} - \xi^{\mathrm{SC}}\right)^2\frac{d^2P(\xi^{\mathrm{SC}})}{d\xi^2} + \cdots. \end{aligned} \tag{4.38}$$

We note that in the above series expansion,

$$\frac{1}{N}\sum_{k=0}^{N-1}\xi_{\mathrm{MMSE},k}^{\mathrm{PMC}} - \xi^{\mathrm{SC}} = \left(\frac{1}{N}\sum_{l=0}^{N-1}\frac{1}{|H_l|}\right)^2 - \frac{1}{N}\sum_{l=0}^{N-1}\frac{1}{|H_l|^2} \le 0,$$

while

$$\sum_{k=0}^{N-1}\left(\xi_{\mathrm{MMSE},k}^{\mathrm{PMC}} - \xi^{\mathrm{SC}}\right)^2 \ge 0.$$

However, from the first and second derivatives of $P(\xi)$, we obtain $\frac{d^2P/d\xi^2}{dP/d\xi} = \frac{1}{\xi}\left(\frac{\gamma_s}{\xi} - \frac{3}{2}\right)$. When $\gamma_s \gg 1$, we have $\frac{d^2P}{d\xi^2} \gg \frac{dP}{d\xi}$, and, accordingly, from (4.38),

$$P^{\mathrm{SC}}(\boldsymbol{h}) \le P_{\mathrm{MMSE}}^{\mathrm{PMC}}(\boldsymbol{h}). \tag{4.39}$$

4.4.4 CP-SC versus CP-OFDM with AMBER Power Allocation

Note that in (4.25), at high SNR, the condition $\nu \geq \max_k \left\{ -\ln |H_k|^2 \right\}$ holds, and the AMBER power allocation can be obtained as

$$p_k^2 = \frac{\ln |H_k|^2 + \nu}{\gamma_s |H_k|^2}, \quad \nu \stackrel{\text{def}}{=} \frac{\gamma_s - \frac{1}{N} \sum_{l=0}^{N-1} |H_l|^{-2} \ln |H_l|^2}{\frac{1}{N} \sum_{l=0}^{N-1} |H_l|^{-2}}. \tag{4.40}$$

From (4.20), (4.33) and (4.27), we obtain, for AMBER power-allocated CP-OFDM,

$$\xi_{\text{AMBER},k}^{\text{PMC}} = \frac{\frac{1}{N} \sum_{l=0}^{N-1} |H_l|^{-2}}{1 + \frac{1}{\gamma_s} \cdot \frac{1}{N} \sum_{l=0}^{N-1} |H_l|^{-2} \left(\ln |H_k|^2 - \ln |H_l|^2 \right)}. \tag{4.41}$$

At moderate to high SNR, $\gamma_s \gg 1$, and we can approximate

$$\xi_{\text{AMBER},k}^{\text{PMC}} \approx \xi^{\text{SC}} \left(1 - \frac{1}{\gamma_s} \cdot \frac{1}{N} \sum_{l=0}^{N-1} \frac{\ln |H_k|^2 - \ln |H_l|^2}{|H_l|^2} \right). \tag{4.42}$$

From Taylor's series expansion of $P_{\text{AMBER}}^{\text{PMC}}(\boldsymbol{h})$ at ξ^{SC}, we have

$$\begin{aligned} P_{\text{AMBER}}^{\text{PMC}}(\boldsymbol{h}) &\approx P(\xi^{\text{SC}}) - \frac{\xi^{\text{SC}}}{\gamma_s} \frac{dP(\xi_{\text{ZF}}^{\text{SC}})}{d\xi} \times \underbrace{\left(\frac{1}{N} \sum_{l=0}^{N-1} \ln |H_l|^2 \cdot \frac{1}{N} \sum_{l=0}^{N-1} \frac{1}{|H_l|^2} - \frac{1}{N} \sum_{l=0}^{N-1} \frac{\ln |H_l|^2}{|H_l|^2} \right)}_{\geq 0} \\ &\leq P(\xi^{\text{SC}}) = P^{\text{SC}}(\boldsymbol{h}). \end{aligned}$$

4.5 Power Allocation with Imperfect CSI

Let $\hat{\boldsymbol{h}} \stackrel{\text{def}}{=} [\hat{h}_0, \cdots, \hat{h}_L, 0, \cdots, 0]^T$, where $\{\hat{h}_l\}_{l=0}^L$ denotes an estimate of $\{h_l\}_{l=0}^L$ available at the transmitter. Assume $\{\hat{h}_l\}_{l=0}^L$ and $\{h_l\}_{l=0}^L$ are jointly complex Gaussian. The statistics of the partial CSI and its relation to the true channel are described by the mean vector $\boldsymbol{m}_{\hat{h}}$, covariance matrix $\boldsymbol{R}_{hh}$, and cross-covariance matrix $\boldsymbol{R}_{h\hat{h}}$ [53].

4.5.1 Analysis of Power Allocation with Imperfect CSI

Since only the estimated CSI, $\hat{\boldsymbol{h}}$, is available at the transmitter, the allocated power is a function of $\hat{\boldsymbol{h}}$, i.e., $\{p_k^2(\hat{\boldsymbol{h}})\}_{k=0}^{N-1}$. Accordingly, the instantaneous BER is given by

$$P(\boldsymbol{h},\hat{\boldsymbol{h}},\boldsymbol{P}) = \frac{1}{N}\sum_{k=0}^{N-1} Q\left(\sqrt{2\gamma_s|H_k|^2 p_k^2(\hat{\boldsymbol{h}})}\right). \tag{4.43}$$

Using the approximation given in [116], we have the approximate instantaneous BER,

$$\tilde{P}(\boldsymbol{h},\hat{\boldsymbol{h}},\boldsymbol{P}) = \frac{1}{5N}\sum_{k=0}^{N-1} \exp\{-\gamma_s|H_k|^2 p_k^2(\hat{\boldsymbol{h}})\}. \tag{4.44}$$

Applying the analysis in [53], we obtain the closed-form approximate BER as[5]

$$\tilde{P}(\hat{\boldsymbol{h}},\boldsymbol{P}) = \frac{1}{5N}\sum_{k=0}^{N-1} \frac{\exp\{\boldsymbol{m}^H\boldsymbol{R}^{-1}(\boldsymbol{\Psi}_k^{-1}-\boldsymbol{R})\boldsymbol{R}^{-1}\boldsymbol{m}\}}{\det(\boldsymbol{R}\boldsymbol{\Psi}_k)} \stackrel{\text{def}}{=} \tilde{P}_b. \tag{4.45}$$

where $\boldsymbol{\Psi}_k \stackrel{\text{def}}{=} \gamma_s p_k^2 \boldsymbol{f}_k\boldsymbol{f}_k^H + \boldsymbol{R}^{-1}$, and $\boldsymbol{f}_k$ denotes the k-th column of $\boldsymbol{F}^H$. By using the matrix inversion lemma[6], we have

$$\boldsymbol{\Psi}_k^{-1} - \boldsymbol{R} = -\frac{\gamma_s p_k^2 \boldsymbol{R}\boldsymbol{f}_k\boldsymbol{f}_k^H\boldsymbol{R}}{1+\gamma_s p_k^2 \boldsymbol{f}_k^H\boldsymbol{R}\boldsymbol{f}_k},$$

and (4.45) can be simplified to

$$\tilde{P}_b = \frac{1}{5N}\sum_{k=0}^{N-1} \frac{1}{1+\gamma_s p_k^2 \boldsymbol{f}_k^H\boldsymbol{R}\boldsymbol{f}_k} \exp\left\{-\frac{\gamma_s p_k^2|\boldsymbol{f}_k^H\boldsymbol{m}|^2}{1+\gamma_s p_k^2 \boldsymbol{f}_k^H\boldsymbol{R}\boldsymbol{f}_k}\right\}, \tag{4.46}$$

where the fact $\det(\boldsymbol{R}\boldsymbol{\Psi}_k) = \det(\boldsymbol{I}+\gamma_s p_k^2\boldsymbol{R}\boldsymbol{f}_k\boldsymbol{f}_k^H) = 1+\gamma_s p_k^2\boldsymbol{f}_k^H\boldsymbol{R}\boldsymbol{f}_k$ has been used.

4.5.2 Special Cases

Three cases of partial CSI are investigated: *delayed CSI*, *noisy CSI* and *covariance feedback* [114].

[5] We drop the subscripts of $\boldsymbol{m}$ and $\boldsymbol{R}$ for simplicity of notation.

[6] $\boldsymbol{A} = \boldsymbol{B}^{-1} + \boldsymbol{C}\boldsymbol{D}^{-1}\boldsymbol{C}^H$, $\boldsymbol{A}^{-1} = \boldsymbol{B} - \boldsymbol{B}\boldsymbol{C}(\boldsymbol{D}+\boldsymbol{C}^H\boldsymbol{B}\boldsymbol{C})^{-1}\boldsymbol{C}^H\boldsymbol{B}$

4.5.2.1 Delayed CSI

We assume that the channel is time-varying with a delay of D blocks in CSI feedback information, a symbol duration T_s, and a fading channel using Jakes' model and Doppler frequency f_D. In order to investigate the effect of channel variation independent of channel estimation schemes, it is further assumed that the CSI at the transmitter is perfect but outdated, i.e., $\hat{\boldsymbol{h}}(t) = \boldsymbol{h}(t - DNT_s)$. The cross-covariance matrix of $\boldsymbol{h}$ and $\hat{\boldsymbol{h}}$ is given by $\boldsymbol{R}_{h\hat{h}} = \rho \boldsymbol{D}_h$, where $\rho \stackrel{\text{def}}{=} J_0(2\pi f_D DNT_s)$ is the correlation coefficient, and $\boldsymbol{D}_h \stackrel{\text{def}}{=} \mathrm{E}\{\boldsymbol{h}\boldsymbol{h}^H\} = \mathrm{E}\{\hat{\boldsymbol{h}}\hat{\boldsymbol{h}}^H\} = \mathrm{diag}\{\sigma_0^2, \sigma_1^2, \cdots, \sigma_L^2, 0, \cdots, 0\}$ with $\sigma_l^2 = \mathrm{E}\{|h_l|^2\}$. Note that ρ is a measure of the quality of the partial CSI: $\rho = 1$ corresponds to perfect CSI while $\rho = 0$ corresponds to no CSI. Since $\boldsymbol{h}$ and $\hat{\boldsymbol{h}}$ are jointly complex Gaussian, we have the conditional mean and covariance of $\boldsymbol{h}$ given $\hat{\boldsymbol{h}}$, respectively, $\boldsymbol{m} = E[\boldsymbol{h}|\hat{\boldsymbol{h}}] = \rho\hat{\boldsymbol{h}}, \quad \boldsymbol{R} = (1-\rho^2)\boldsymbol{D}_h$.

Without loss of generality, we assume normalized total channel tap power $\mathrm{trace}\{\boldsymbol{D}_h\} = \sum_l \sigma_l^2 = 1$. The approximate BER (4.46) can be simplified as

$$\tilde{P}_b' = \frac{1}{5N} \sum_{k=0}^{N-1} \frac{1}{1 + \gamma_s p_k^2 (1-\rho^2)/N} \exp\left\{ -\frac{\gamma_s p_k^2 |\hat{H}_k|^2 \rho^2}{1 + \gamma_s p_k^2 (1-\rho^2)/N} \right\}, \tag{4.47}$$

where $\hat{H}_k \stackrel{\text{def}}{=} \boldsymbol{f}_k^H \hat{\boldsymbol{h}}$, and the fact $\boldsymbol{f}_k^H \boldsymbol{D}_h \boldsymbol{f}_k = 1/N$ has been used.

We now consider the special cases of perfect and no CSI.

- Perfect CSI ($\rho = 1$): The above analysis does not apply because $\boldsymbol{R} = \boldsymbol{0}$. However, as ρ approaches 1, we have

  $$\lim_{\rho \to 1} \tilde{P}_b' = \frac{1}{5N} \sum_{k=0}^{N-1} \exp\{-\gamma_s p_k^2 |H_k|^2\},$$

  which reduces to the case analyzed in previous sections. Therefore, (4.47) includes the perfect CSI scenario as a special case.

- No CSI ($\rho = 0$): Eq. (4.47) reduces to

  $$\tilde{P}_b' = \frac{1}{5N} \sum_{k=0}^{N-1} \frac{1}{1 + \gamma_s p_k^2 |\hat{H}_k|^2 / N}.$$

Using Lagrange multipliers, it is easy to verify that the optimal power allocation solution under the total power constraints is $\boldsymbol{P} = \boldsymbol{I}$. In other words, when no CSI available at the transmitter, OFDM without power allocation is optimum in the sense of minimum BER.

4.5.2.2 Noisy CSI

We assume the CSI available at the transmitter is modelled as $\boldsymbol{h} = \hat{\boldsymbol{h}} + \boldsymbol{e}$, where $\boldsymbol{e} \sim \mathcal{N}(\boldsymbol{0}, \sigma_e^2 \boldsymbol{I})$ denotes noise in CSI, due to quantization error, estimation error, or feedback channel error [114]. Here, $\boldsymbol{m} = E[\boldsymbol{h}|\hat{\boldsymbol{h}}] = \hat{\boldsymbol{h}}$, $\boldsymbol{R} = \sigma_e^2 \boldsymbol{I}$, and (4.46) can be simplified as

$$\tilde{P}_b'' = \frac{1}{5N} \sum_{k=0}^{N-1} \frac{1}{1 + \gamma_s p_k^2 \sigma_e^2 / N} \exp\left\{ - \frac{\gamma_s p_k^2 |\hat{H}_k|^2}{1 + \gamma_s p_k^2 \sigma_e^2 / N} \right\}. \tag{4.48}$$

We note that taking $\lim_{\sigma_e^2 \to 0} \tilde{P}_b''$, (4.48) reduces to the case of power allocation with perfect CSI.

4.5.2.3 Covariance Feedback

Assuming knowledge of channel covariance, while the mean is set to zero, i.e., $\hat{\boldsymbol{h}} \sim N(\boldsymbol{0}, \boldsymbol{D}_h)$[7], (4.46) simplifies to

$$\tilde{P}_b''' = \frac{1}{5N} \sum_{k=0}^{N-1} \frac{1}{1 + \gamma_s p_k^2 |\hat{H}_k|^2 / N}. \tag{4.49}$$

As in the case of no CSI, the optimal constrained power allocation solution is $\boldsymbol{P} = \boldsymbol{I}$.

Remark: When the conditional CSI statistics $\boldsymbol{m}$ and $\boldsymbol{R}$ are available at the transmitter, such information can be used in the design of power allocation schemes that are robust to CSI uncertainty [49]. The MBER power allocation algorithm in Table 4.1 applies straightforwardly.

[7] This is a valid assumption when channel varies too fast for transmitter to estimate its local mean [114].

4.6 Numerical Results and Discussions

We now compare our analytical results in the previous sections to simulations.

4.6.1 Power Allocation with Perfect CSI

4.6.1.1 Illustration of MBER and AMBER Power Allocation

We verify the minimum BER property of the MBER power allocation algorithm, as well as the approximating ability of the AMBER scheme. For convenience of illustration, we consider the block size $N = 2$ system over the two-tap channel $h_0^2 = 0.8, h_1^2 = 0.2$, with $\gamma_s = 20$ (13 dB). In this case, the power allocation solution can be normalized as

$$\boldsymbol{P}(\theta) = \sqrt{2} \begin{pmatrix} \cos\theta & 0 \\ 0 & \sin\theta \end{pmatrix},$$

where θ is a function of the power allocation scheme. For CP-OFDM without power allocation, $\theta = \pi/4$, corresponding to $\boldsymbol{P} = \boldsymbol{I}$. Fig. 4.1 illustrates a polar plot of $-\log_{10}(P(\boldsymbol{h}, \theta))$ versus θ. As we can see, the MBER solution points in the minimum BER direction, and the AMBER solution offers a close approximation. Both of them offer improved performance over CP-OFDM without power allocation.

4.6.1.2 Instantaneous BER Performance

For analytical comparisons of asymptotic performances in Section 4.4, it is of interest to compare them to simulations of finite SNR's. The channel is randomly generated, with frequency response shown in the upper part of Fig. 4.2. The power allocation coefficients of EG, MMSE, AMBER and MBER schemes are also shown in the lower part of Fig. 4.2. We can see that AMBER solution is very close to that of MBER. The instantaneous BER performance of this channel is plotted in Fig. 4.3. At all SNR's shown, CP-OFDM with

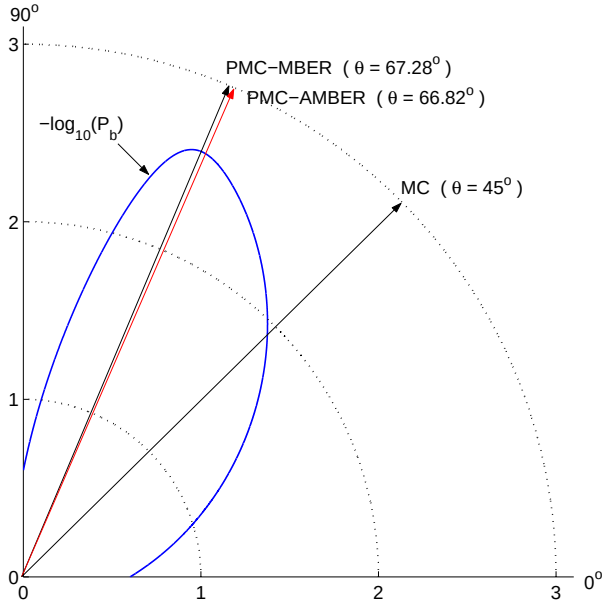

Figure 4.1. A polar plot of $-\log_{10} P(\boldsymbol{h}, \theta)$ vs. θ.

MBER and AMBER power allocation outperforms ZF-equalized SC (or OFDM with EG power allocation) and conventional CP-OFDM without power allocation.

4.6.1.3 BER Performance in Fading Channels

We compare the BER performance of CP-SC and a variety of CP-OFDM schemes in fading channels. The channel models in [54] are used. Channel 1 with tap powers $[0.15, 0.65, 0.15, 0.05]$ has moderate nulls, while channel 2 with tap powers $[0.39, 0.16, 0.26, 0.19]$ has severe nulls, as shown in Fig. 4.4. From Figs. 4.5 and 4.6, we see that CP-OFDM with AMBER power allocation offers performance very close to that of the MBER scheme in fading channels. Both algorithms outperform ZF-equalized SC (or, equivalently, CP-OFDM with EG power allocation) and conventional CP-OFDM without power allocation. At a BER of 10^{-3}, CP-OFDM with MBER or AMBER power allocation has a gain of around 7.5 dB as compared to EG power allocation as well as scheme without

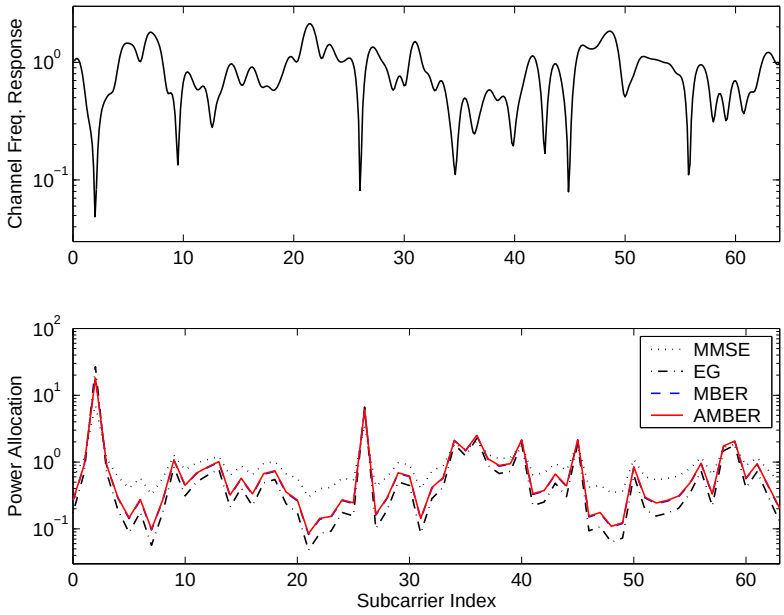

Figure 4.2. Channel frequency response and corresponding power allocation coefficients at $\gamma_s = 20$ (dB) ($N = 64$).

power allocation. We also note from these figures that CP-OFDM with EG (equivalently, CP-SC with ZF equalization) and MMSE power allocation has poor BER performance in fading channels at all SNR shown. It is expected, however, when the input SNR is high enough, power allocation will outperform no-power-allocation.

Remark 1: In MC systems, each symbol occupies a narrow spectral band and a long time duration, which increases resistance to frequency-selective (multipath) fading. In SC systems, block equalization can be viewed as a form of diversity combining, which offers multipath diversity gain. For MC schemes, the equivalent channel is decoupled in the frequency domain. Multipath signals are non-resolvable in the frequency domain which results in a loss of multipath diversity gain in MC systems.

Remark 2: Recall from Section 4.3 that the power allocation matrix $\boldsymbol{P}$ is constrained to be diagonal, in order not to introduce ICI. However, if we allow ICI in power allocation,

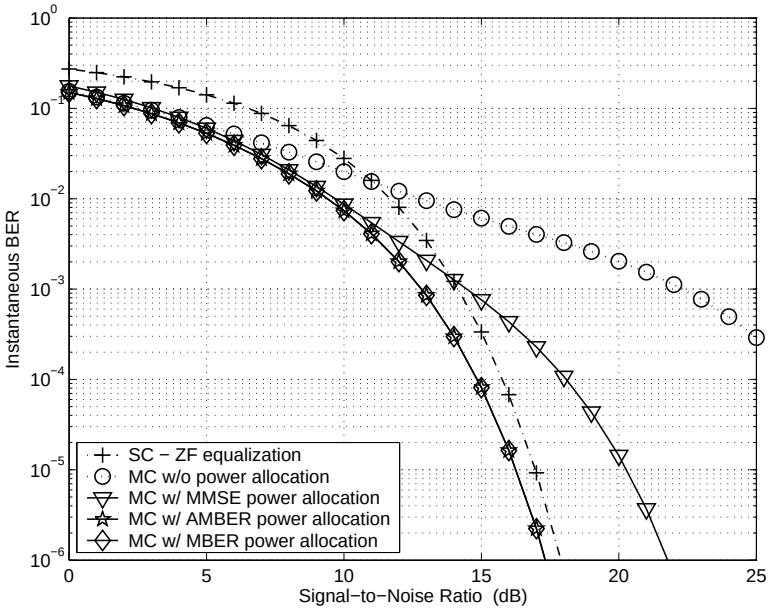

Figure 4.3. Instantaneous BER comparison of single and multicarrier ($N = 64$).

improvements from precoding are possible [91], at the cost of higher processing complexity[8].

4.6.2 Power Allocation with Imperfect CSI

An example of the approximate instantaneous BER as a function of the normalized Doppler frequency $f_D DNT_s$ is shown in Fig. 4.7. We see that for this channel realization, the performance of all power allocation schemes approach their optimum when the normalized Doppler frequency $f_D DNT_s$ is less than 10^{-2}. When $f_D DNT_s > 0.1$, the performances of power-loaded schemes drop rapidly as $f_D DNT_s$ increases. As an example, we consider the system parameters chosen in wireless LAN standards. For the terminal velocity $v = 108$

[8]We note that the optimal precoder and decoder for MC and SC systems will converge since they solve the same problem in different domains: the IFFT and FFT operation will be absorbed in the precoder and decoder of the SC system.

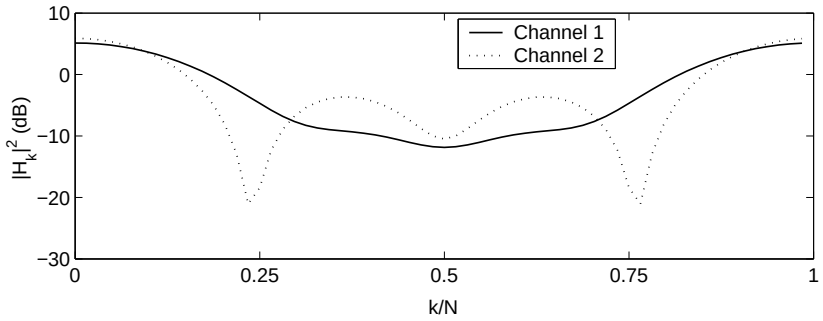

Figure 4.4. Magnitude spectrum of ISI channel ($N = 64$).

km/hour, the Doppler frequency is $f_D = 500$ Hz. If we choose the feedback delay $D = 5$ blocks, we have the normalized Doppler frequency $f_D DNT_s = 10^{-2}$, i.e., the power allocation performance will not be affected significantly by the feedback delay. However, if the feedback delay $D > 50$ blocks, power allocation schemes will not perform well.

4.7 Conclusion

Cyclic-Prefix-based single-carrier (SC) and OFDM multicarrier schemes are compared in this chapter. It has been shown that uncoded CP-OFDM is inferior to CP-SC in frequency-selective channels. Power allocation algorithms are proposed for CP-OFDM. Analytical performance comparison and simulation results show that CP-OFDM with either MBER or AMBER power allocation offer superior performance to CP-SC with ZF equalization. Power allocation with imperfect channel knowledge is also analyzed.

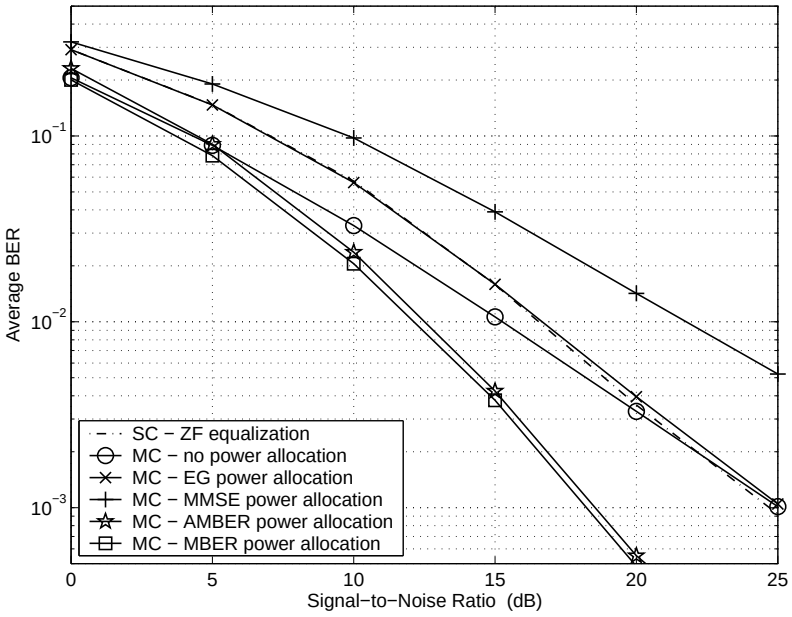

Figure 4.5. BER comparison in fading channel 1 ($N = 16$).

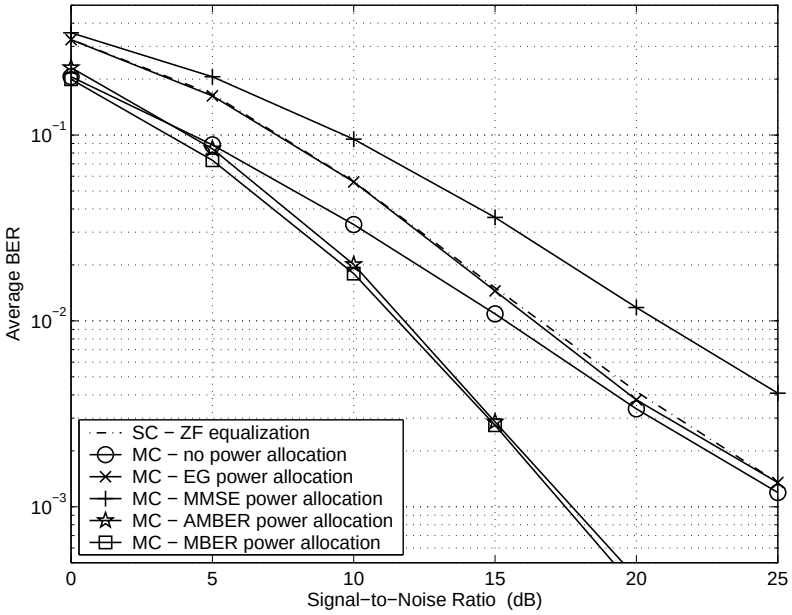

Figure 4.6. BER comparison in fading channel 2 ($N = 16$).

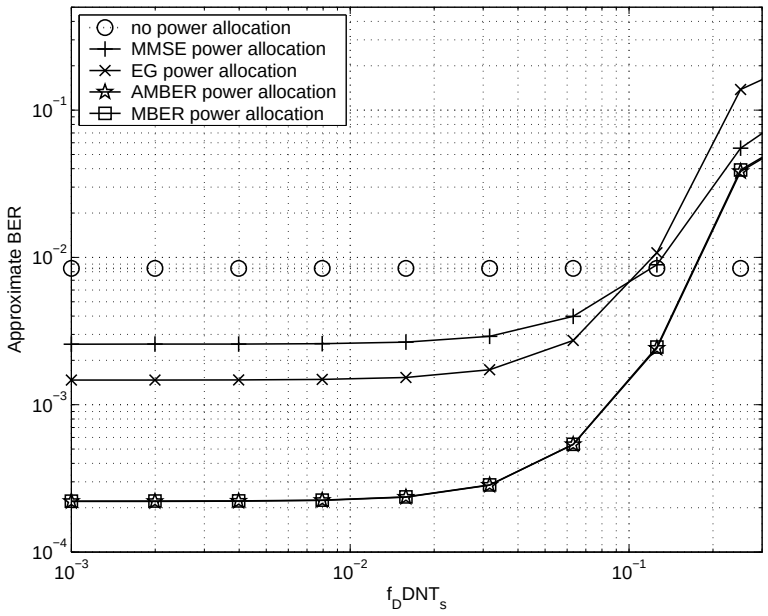

Figure 4.7. An example of the approximate instantaneous BER as a function of the normalized Doppler frequency for various power allocation schemes ($N = 64$, $\gamma_s = 20$ dB).

Chapter 5

Minimum BER Power Allocation for MIMO Spatial Multiplexing Systems

5.1 Introduction

The capacity of wireless communications systems can be increased substantially by using multiple transmit and receive antennas, known as multiple-input multiple-output (MIMO) systems, provided that multipath scattering effects have been exploited appropriately [37]. MIMO communications offers key advantages over single-input single-output (SISO) communications, such as diversity gain and spatial multiplexing gain [80]. Diversity gain improves link reliability, while spatial multiplexing gain increases the transmission rate. Our goal of this chapter is to investigate transmit optimization for MIMO spatial multiplexing, which is receiver-dependent. Signal reception for MIMO spatial multiplexing can employ criteria such as zero-forcing (ZF), minimum mean-squared error (MMSE), maximum likelihood (ML), successive interference cancellation (SIC), or ordered SIC (OSIC) as, for example, in the case of the Vertical Bell Laboratories Layered Space-Time (V-BLAST) architecture [37, 109]. Among these schemes, ZF has both lowest computational complexity and performance, while ML has highest complexity and performance.

In order to achieve high MIMO diversity and/or spatial multiplexing gains, appropriate transceiver designs are necessary. Efforts to optimize MIMO transceiver structures have involved joint transmit-receive optimization and linear precoding for specific receivers. Joint precoding/decoding optimization under MMSE criterion is investigated in [92], and [76] presents a unified framework for joint transmit-receive design using convex optimization. Minimum bit error rate (MBER) precoding for ZF equalization of block transmission [28] is readily applicable to MIMO systems, as well as precoding for multicarrier MIMO using ML receiver and pairwise error probability as criterion [86]. These designs generally require high complexity processing at both the transmitter and the receiver as well as high feedback overhead. Precoded MIMO transmission with reduced feedback has been recently proposed, based on quantized channel state information (CSI) feedback and limited feedback signal design. For example, quantized CSI feedback has been incorporated into transmitter optimization [52, 69]. Limited feedback signal design also occurs at the receiver [44, 55, 59]. However, existing precoding schemes with reduced feedback generally also require high processing complexity, e.g., diagonalization of the channel matrix and/or precoding codebook design.

In this chapter, we consider simultaneous reduction of complexity and feedback overhead by constraining precoding to transmit power allocation, i.e., we optimize only the transmit power of signal streams, but apply a more suitable criterion[1]. As opposed to MMSE precoding/decoding [92], we consider MBER as the optimization criterion. Compared to MBER precoding for ZF receivers, we apply MBER power allocation to SIC and OSIC as well. General power allocation by minimizing error rate does *not* have a closed-form solution, and has high computational complexity. An approximate solution

[1]Power allocation for multicarrier MIMO systems was considered in [78], where MIMO was operated in a diversity mode and the transmit power was allocated across the frequency dimension (subcarriers).

can be found instead, which was originally given in [74], and applied to power allocation for multicarrier systems [49, 78, 105]. The approximate MBER (AMBER) solution offers performance close to that of the exact solution with low computational complexity [105]. Recently, it has come to our attention that a similar AMBER power allocation for V-BLAST was proposed independently [68], which is a special case of our proposed solution for well-conditioned channels, as shown in Section 5.3. Simulation results show that in generally correlated fading channels [1], our proposed AMBER power allocation together with SIC or OSIC (V-BLAST) reception offers superior performance over existing precoding schemes with closed-form solutions.

Transmitter-side power allocation ideally requires CSI or allocated power to be available at the transmitter. In some cases, CSI can be made available at the transmitter, e.g., in time-division duplex (TDD) systems, due to the reciprocity of the uplink and downlink channels. In this case, all existing limited feedback schemes do *not* possess any advantages since feedback overhead is not a concern. However, power allocation is still attractive due to the significant reduction in processing complexity. On the other hand, in channels that lack reciprocity in uplink and downlink, e.g., frequency-division duplex (FDD), complete CSI is not available at the transmitter, and CSI or power information has to be fed back. Regardless of availability, CSI or power feedback is imperfect in practice due to channel estimation, quantization, feedback delay, and/or errors introduced by feedback channel [115]. This motivates performance analysis of power allocation under uncertain feedback. While a general analysis is difficult, we analyze the special cases of noisy CSI and power feedback. Based on this analysis, we propose an AMBER power allocation algorithm that takes statistical knowledge of noisy feedback into account. Furthermore, as a byproduct, a modified algorithm for perfect CSI which takes into account error propagation effects in SIC and OSIC receivers is devised.

The rest of this chapter is organized as follows: MIMO signal reception and performance are introduced in Section 5.2. Section 5.3 investigates power allocation for MIMO with ZF, SIC and OSIC receivers and their performances. In Section 5.4, performance degradation and power allocation under imperfect feedback are studied. Section 5.5 presents numerical results in general correlated fading channels.

5.2 MIMO Signal Reception and Performance

Consider a MIMO spatial multiplexing communication system with N_t transmit and N_r receive antennas where $N_r \geq N_t$. The received signal can be modelled as

$$\boldsymbol{r} = \boldsymbol{H}\boldsymbol{s} + \boldsymbol{\eta}, \tag{5.1}$$

where $\boldsymbol{s}$ is the $N_t \times 1$ transmitted signal vector; $\boldsymbol{H}$ is the $N_r \times N_t$ channel matrix, which is assumed to be generally correlated Ricean fading as in Section 2.1.2; and $\boldsymbol{\eta}$ is the $N_r \times 1$ additive Gaussian noise vector. For simplification of analysis, we assume white noise and input, i.e., $\mathbb{E}[\boldsymbol{s}\boldsymbol{s}^H] = E_s\boldsymbol{I}_{N_t}$ and $\mathbb{E}[\boldsymbol{\eta}\boldsymbol{\eta}^H] = N_0\boldsymbol{I}_{N_r}$, and define the input signal-to-noise ratio (SNR) $\gamma_s \stackrel{\text{def}}{=} E_s/N_0$. Binary phase shift keying (BPSK) modulation is assumed without loss of generality (as will be made clear in Section 5.3.2).

5.2.1 ZF Receiver

With ZF equalization, the estimate of the transmitted signal $\boldsymbol{s}$ is given by

$$\hat{\boldsymbol{s}} = \boldsymbol{H}^{\dagger}\boldsymbol{r} = \boldsymbol{s} + \boldsymbol{H}^{\dagger}\boldsymbol{\eta}. \tag{5.2}$$

The decision-point SNR of the k-th signal stream, i.e., the signal from the k-th transmit antenna, $1 \leq k \leq N_t$, is obtained as

$$\gamma_{Z,k} = \gamma_s \left[\left(\boldsymbol{H}^H \boldsymbol{H} \right)^{-1} \right]^{-1}_{k,k} \stackrel{\text{def}}{=} \gamma_s g^2_{Z,k}, \tag{5.3}$$

where $g_{Z,k}^2 \stackrel{\text{def}}{=} \left[\left(\boldsymbol{H}^H\boldsymbol{H}\right)^{-1}\right]_{k,k}^{-1}$ denotes the power gain of the k-th stream using ZF equalization.

5.2.2 SIC Receiver

Without loss of generality, we assume stream $k=1$ is detected first. The interference due to the first stream is then regenerated and subtracted before stream $k=2$ is detected. This procedure is repeated successively until all streams are detected. We ignore error propagation from early stages, which is a valid assumption at moderate-to-high SNR. Assuming ZF equalization is employed at each stage, the decision-point SNR of the k-th stream at the k-th stage is given by

$$\gamma_{S,k} = \gamma_s \left[\left(\boldsymbol{H}_{(k)}^H\boldsymbol{H}_{(k)}\right)^{\dagger}\right]_{k,k}^{-1} \stackrel{\text{def}}{=} \gamma_s g_{S,k}^2, \tag{5.4}$$

where $\boldsymbol{H}_{(k)}$ is generated in a recursive fashion by nulling the $(k-1)$-st column of $\boldsymbol{H}_{(k-1)}$ for $k=2,\cdots,N_t$, and $\boldsymbol{H}_{(1)} \stackrel{\text{def}}{=} \boldsymbol{H}$ (cf. Section 2.3.1.3).

5.2.3 OSIC Receiver

To improve SIC performance, the streams can be reordered based on SNR at each stage. This receiver differs from SIC receiver only in the detection ordering. An SNR-based ordering scheme that maximizes minimum SNR appears in [37, 109], and is reproduced in Table 2.1. The decision-point SNR of the k-th stream at the k-th stage is given by

$$\gamma_{O,k} = \gamma_s \left[\left((\boldsymbol{H}_{(k)}^O)^H\boldsymbol{H}_{(k)}^O\right)^{\dagger}\right]_{k,k}^{-1} \stackrel{\text{def}}{=} \gamma_s g_{O,k}^2, \tag{5.5}$$

where $\boldsymbol{H}^O$ denotes the reordered channel matrix as in Table 2.1.

The average BER of the above receivers can be calculated as [84][2]

$$\bar{P}(\gamma_s;\{g_k^2\}) = \frac{1}{N_t}\sum_{k=1}^{N_t} Q\left(\sqrt{2\gamma_s g_k^2}\right), \tag{5.6}$$

where $Q(x) \stackrel{\text{def}}{=} \frac{1}{\sqrt{2\pi}}\int_x^\infty e^{-y^2/2}dy$; the gain g_k^2 depends on the receiver structure and is given in (5.3), (5.4) and (5.5).

5.3 AMBER Power Allocation with Perfect Feedback

5.3.1 MIMO with Power Allocation

Denote the power allocated to the k-th stream as p_k^2. The received signal can be written as

$$\boldsymbol{r} = \boldsymbol{HPs} + \boldsymbol{\eta}, \tag{5.7}$$

where $\boldsymbol{P} \stackrel{\text{def}}{=} \text{diag}\{p_1,\cdots,p_k\}$ denotes the power allocation matrix. We assume the total transmit power is constrained via

$$\text{tr}(\boldsymbol{PP}^T) = \sum_{k=1}^{N_t} p_k^2 = N_t. \tag{5.8}$$

Compared with general precoding, power allocation constrains the precoder to a diagonal matrix.

5.3.2 AMBER Power Allocation Algorithm

The average BER of MIMO spatial multiplexing in (5.6) can be straightforwardly generalized to

$$\bar{P}\left(\gamma_s;\{p_k^2\};\{g_k^2\}\right) = \frac{1}{N_t}\sum_{k=1}^{N_t} Q\left(\sqrt{2\gamma_s g_k^2 p_k^2}\right), \tag{5.9}$$

[2]This is a lower bound for SIC and OSIC due to the neglecting of error propagation, which is also an accurate approximate at moderate-to-high SNR's.

which is the same as the MBER power allocation problem for CP-OFDM in Chapter 4. Therefore, the results in Section 4.3 can be applied directly. For general constellations, the BER can be approximated as $P_b(\gamma) \approx \frac{1}{5}\exp\{-c\gamma\}$, where c is a constellation-specific constant [116]. For BPSK modulation, $c = 1$, and the average BER in (5.9) can be approximated as

$$\bar{P}\left(\gamma_s;\{p_k^2\};\{g_k^2\}\right) \approx \frac{1}{5N_t}\sum_{k=1}^{N_t}\exp\{-\gamma_s p_k^2 g_k^2\} \stackrel{\text{def}}{=} \tilde{P}\left(\gamma_s;\{p_k^2\};\{g_k^2\}\right). \tag{5.10}$$

Minimization of (5.10) under power constraint (5.8) results in the power allocation [105][3]

$$p_k^2 = \gamma_s^{-1} g_k^{-2}\left(\ln g_k^2 + \nu\right)_+, \quad 1 \le k \le N_t, \tag{5.11}$$

where $(x)_+ \stackrel{\text{def}}{=} \max\{0, x\}$, and ν is chosen to satisfy the power constraint (5.8). Note that the total power $\sum_k p_k^2(\nu) = \sum_k \gamma_s^{-1} g_k^{-2}\left(\ln g_k^2 + \nu\right)_+$ is a piecewise-linear increasing function of ν, with breakpoints at $-\ln g_k^2$'s. Therefore ν is unique and can be readily determined. A recursive algorithm is given in Table 4.2, which requires at most N_t recursions. Extension of the results to other constellations is straightforward.

5.3.3 Remarks on Performance, Complexity and Overhead

5.3.3.1 AMBER Power Allocation versus General Precoding

While other precoding schemes either apply an MBER criterion to ZF equalization [28], or use an MMSE criterion [92], the proposed power allocation enables SIC and OSIC under an MBER criterion.

[3] As shown in [49, 74], an equivalent solution can be obtained by minimizing a Chernoff upper bound of the BER [84].

5.3.3.2 Asymptotic Performance

By substituting (5.11) into (5.9), we obtain the average BER of power allocation as

$$\bar{P}_{pa}\left(\gamma_s;\{g_k^2\}\right)=\frac{1}{N_t}\sum_{k=1}^{N_t}Q\left(\sqrt{2\left(\ln g_k^2+\nu\right)_+}\right), \tag{5.12}$$

which makes performance comparison difficult due to the nonlinear operator $(\cdot)_+$. However, at moderate-to-high SNR, it is possible to proceed. When the condition

$$\nu\geq\max_k\left\{-\ln g_k^2\right\} \tag{5.13}$$

is valid, the power allocation in (5.11) simplifies to

$$p_k^2=\gamma_s^{-1}g_k^{-2}(\ln g_k^2+\nu), \tag{5.14}$$

and ν is obtained in closed-form as

$$\nu=\frac{\gamma_s-\frac{1}{N_t}\sum_{l=1}^{N_t}\frac{\ln g_l^2}{g_l^2}}{\frac{1}{N_t}\sum_{l=1}^{N_t}\frac{1}{g_l^2}}\stackrel{\text{def}}{=}\nu_a. \tag{5.15}$$

From (5.13) and (5.15), we observe that the simplified power allocation (5.14) is valid at moderate-to-high SNR regimes ($\gamma_s\gg 1$), and/or when the channel is well-conditioned (when the gains g_k's are less spread)[4]. Furthermore, if (5.13) holds, the average BER of the power allocation in (5.12) can be approximated by

$$\bar{P}_{pa}(\gamma_s;\{g_k^2\}) = \frac{1}{N_t}\sum_{k=1}^{N_t}Q\left(\sqrt{2\left(\ln g_k^2+\nu_a\right)}\right) \tag{5.16}$$

$$\approx \frac{1}{5N_t}e^{-\nu_a}\sum_{k=1}^{N_t}g_k^{-2}\stackrel{\text{def}}{=}\tilde{P}_{pa}(\gamma_s;\{g_k^2\}). \tag{5.17}$$

[4]We note that power allocation proposed in [68] is equivalent to (5.14) and (5.15), representing a special case of the general solution (5.11).

5.3.3.3 Asymptotic Optimality of AMBER Solution

The exact MBER solution satisfies

$$\sqrt{\frac{\gamma_s g_k^2}{p_k^2}} e^{-\gamma_s g_k^2 p_k^2} = \zeta, \quad \forall k \in [1, N_t],$$

where ζ is chosen to satisfy the power constraint (5.8) [74]. Therefore, we have

$$g_k^2 p_k^2 - g_m^2 p_m^2 = \frac{\ln p_m^2 g_k^2 - \ln p_k^2 g_m^2}{2\gamma_s}, \quad \forall k, m \in [1, N_t],$$

which implies $g_k^2 p_k^2 \overset{(\gamma_s \to \infty)}{=} g_m^2 p_m^2$. We obtain

$$\lim_{\gamma_s \to \infty} p_{\mathrm{MBER},k}^2 = \frac{g_k^{-2}}{\frac{1}{N_t} \sum_{l=1}^{N_t} g_l^{-2}}.$$

On the other hand, from (5.14) and (5.15), we have

$$\lim_{\gamma_s \to \infty} p_{\mathrm{AMBER},k}^2 = \frac{g_k^{-2}}{\frac{1}{N_t} \sum_{l=1}^{N_t} g_l^{-2}},$$

i.e., the AMBER solution asymptotically converges to the exact MBER solution.

5.3.3.4 AMBER Power Allocation versus No Power Allocation

A comparison between asymptotic performances of schemes with and without power allocation follows Section 4.4. Generally, power allocation improves error rate performance at moderate-to-high SNR.

5.3.3.5 ZF versus SIC

For MIMO without power allocation, it has been shown in [109] that SIC receiver offers better performance than that of ZF receiver. We now compare the performances of ZF and SIC under power allocation. From (5.3) and (5.4), it is easily seen that $g_{Z,1}^2 = g_{S,1}^2$.

Consider $k = 2, \cdots, N_t$. Denote $\boldsymbol{h}_k$ as the k-th column of matrix $\boldsymbol{H}$, and $\boldsymbol{H}_{\bar{k}}$ as the sub-matrix consisting of all but the k-th column of $\boldsymbol{H}$. We have

$$g_{Z,k}^2 = [(\boldsymbol{H}^H\boldsymbol{H})^{-1}]_{k,k}^{-1} = \frac{\det(\boldsymbol{H}^H\boldsymbol{H})}{\det(\boldsymbol{H}_{\bar{k}}^H\boldsymbol{H}_{\bar{k}})} = \left\|\boldsymbol{\Upsilon}_{\boldsymbol{H}_{\bar{k}}}^{\perp}\boldsymbol{h}_k\right\|^2, \tag{5.18}$$

where $\boldsymbol{\Upsilon}_{\boldsymbol{X}}^{\perp} \stackrel{\text{def}}{=} \boldsymbol{I} - \boldsymbol{X}(\boldsymbol{X}^H\boldsymbol{X})^{-1}\boldsymbol{X}^H$, is the orthogonal projection matrix. Similarly,

$$g_{S,k}^2 = \left\|\boldsymbol{\Upsilon}_{\boldsymbol{H}_{(k+1)}}^{\perp}\boldsymbol{h}_k\right\|^2. \tag{5.19}$$

Since $\boldsymbol{H}_{\bar{k}} = [\,\boldsymbol{h}_1 \vdots \cdots \vdots \boldsymbol{h}_{k-1} \vdots \boldsymbol{H}_{(k+1)}]$, we have $g_{Z,k}^2 \leq g_{S,k}^2$ for $k = 2, \cdots, N_t$. From (5.17), we observe that $\tilde{P}_{pa}(\gamma_s; \{g_k\})$ is a monotone decreasing function in g_k^2. Therefore, we conclude that

$$\tilde{P}_{pa}(\gamma_s; \{g_{S,k}^2\}) \leq \tilde{P}_{pa}(\gamma_s; \{g_{Z,k}^2\}), \tag{5.20}$$

i.e., with power allocation, SIC outperforms ZF as well.

5.3.3.6 SIC versus OSIC

Comparison between SIC and OSIC involves examining whether the SNR-based ordering is still optimal under power allocation. While a generally strict analysis is difficult, we provide a few observations as a heuristic solution. At moderate-to-high SNR ($\gamma_s \gg 1$), ν_a in (5.15) can be approximated as

$$\nu_a \approx \frac{\gamma_s}{\frac{1}{N_t}\sum_{k=1}^{N_t}\frac{1}{g_k^2}}.$$

We can further approximate the average BER of power allocation schemes (5.17) as

$$\tilde{P}_{pa}(\gamma_s; \{g_k^2\}) \approx \frac{1}{5}\left(\frac{1}{N_t}\sum_{k=1}^{N_t}\frac{1}{g_k^2}\right)\exp\left\{-\frac{\gamma_s}{\left(\frac{1}{N_t}\sum_{k=1}^{N_t}\frac{1}{g_k^2}\right)}\right\} \stackrel{\text{def}}{=} \tilde{P}'_{pa}\left(\gamma_s; \frac{1}{N_t}\sum_{k=1}^{N_t}\frac{1}{g_k^2}\right). \tag{5.21}$$

From (5.21), $\tilde{P}'_{pa}\left(\gamma_s; \frac{1}{N_t}\sum_{k=1}^{N_t}\frac{1}{g_k^2}\right)$ is a monotone increasing function in $\frac{1}{N_t}\sum_{k=1}^{N_t}\frac{1}{g_k^2}$, and is dominated by small g_k^2's. SNR-based ordering maximizes $\min_k\{g_k^2\}$. Therefore, heuristically, SNR-based ordering is expected to offer improved performance in power allocation

schemes. We will verify this by simulation in Section 5.5.

5.3.3.7 Feedback Overhead

In channels that lack reciprocity between uplink and downlink, MIMO with general precoding requires either $N_t \times N_r$ complex channel coefficients or precoding matrix feedback. On the other hand, if the proposed power allocation scheme is employed, only N_t real coefficients are required at the transmitter, a factor of $\frac{1}{2N_r}$ savings.

5.3.3.8 Complexity

Precoding schemes require diagonalization of a channel matrix as well as matrix transformations [28, 92]. Using power allocation, operations performed at the transmitter are trivial.

5.3.3.9 Simplified Scenarios

Some aspects of power allocation for general MIMO spatial multiplexing are open problems, as shown in the above. However, for a special case of two-input multiple-output (TIMO) system, closed-form analytical results can usually be obtained, as shown in Chapter 6.

5.4 AMBER Power Allocation with Imperfect Feedback

Here we assume that perfect CSI is available at the receiver, while noisy feedback of CSI or allocated power is available at the transmitter. Noisy feedback is modelled as a zero-mean Gaussian random variable as in [49]. Such a noisy CSI model arises in, e.g., ML channel estimation [78]. An SIC receiver is considered. For an OSIC receiver, the analysis applies

directly after ordering. Extension to ZF receiver is also straightforward.

5.4.1 Power Allocation with Noisy CSI Feedback

Since only the CSI feedback, $\hat{\boldsymbol{H}}$, is available at the transmitter, the allocated power is a function of $\hat{\boldsymbol{H}}$, i.e., $\{p_k^2(\hat{\boldsymbol{H}})\}_{k=1}^{N_t}$; while the power gains are functions of perfect CSI at the receiver, i.e., $\{g_k^2(\boldsymbol{H})\}_{k=1}^{N_t}$. From (5.9), the conditional approximate average BER is obtained as

$$\tilde{P}(\gamma_s;\boldsymbol{H};\hat{\boldsymbol{H}}) = \frac{1}{5N_t}\sum_{k=1}^{N_t}\exp\{-\gamma_s p_k^2(\hat{\boldsymbol{H}})g_k^2(\boldsymbol{H})\}. \tag{5.22}$$

By averaging both sides of (5.22) over the Gaussian conditional distribution $f_{\boldsymbol{H}|\hat{\boldsymbol{H}}}\left(\boldsymbol{H}|\hat{\boldsymbol{H}}\right)$ as in [53], we obtain the approximate BER

$$\tilde{P}(\gamma_s;\hat{\boldsymbol{H}}) = \frac{1}{5N_t}\sum_{k=1}^{N_t}\int\exp\{-\gamma_s p_k^2(\hat{\boldsymbol{H}})g_k^2(\boldsymbol{H})\}\, f_{\boldsymbol{H}|\hat{\boldsymbol{H}}}\left(\boldsymbol{H}|\hat{\boldsymbol{H}}\right)d\hat{\boldsymbol{H}}. \tag{5.23}$$

Generally, it is difficult to find a closed-form expression for (5.23), due to nonlinearity of $g_k^2(\boldsymbol{H})$. In what follows, we study a special case when CSI at the transmitter is noisy, and obtain a closed-form error rate by using approximation techniques.

Noisy CSI is modelled by $[\boldsymbol{H}]_{m,n} = [\hat{\boldsymbol{H}}]_{m,n} + \varepsilon_{m,n}^h$, for $1 \le m \le N_r, 1 \le n \le N_t$, where $\varepsilon_{m,n}^h$ denotes a zero-mean complex Gaussian CSI feedback noise with variance σ_h^2. From Section 5.3, power gains of SIC can be expressed as

$$g_k^2 = \left[\left(\boldsymbol{H}_{(k)}^H\boldsymbol{H}_{(k)}\right)^\dagger\right]_{k,k}^{-1} = \left\|\boldsymbol{\Upsilon}_{\boldsymbol{H}_{(k+1)}}^{\perp}\boldsymbol{h}_k\right\|^2, \quad (1 \le k \le N_t). \tag{5.24}$$

Conditioned on $\hat{\boldsymbol{H}}$, $\boldsymbol{H}_{(k)}^H\boldsymbol{H}_{(k)}$ is distributed as complex noncentral Wishart [51]. While it is difficult to obtain a closed-form density function of g_k^2, which is the Schur complement of the (k,k)-th entry of a noncentral Wishart matrix [66], we approximate the density function. In (5.24), we note that conditioned on $\hat{\boldsymbol{H}}$, both $\boldsymbol{\Upsilon}_{\boldsymbol{H}_{(k+1)}}^{\perp}$ and $\boldsymbol{h}_k$ are random, which makes analysis difficult. We therefore approximate

$$g_k^2 = \left\|\boldsymbol{\Upsilon}_{\boldsymbol{H}_{(k+1)}}^{\perp}\boldsymbol{h}_k\right\|^2 \approx \left\|\boldsymbol{\Upsilon}_{\hat{\boldsymbol{H}}_{(k+1)}}^{\perp}\boldsymbol{h}_k\right\|^2 \stackrel{\text{def}}{=} \tilde{g}_k^2,$$

i.e., we use $\hat{\boldsymbol{H}}_{(k+1)}$ to approximate $\boldsymbol{H}_{(k+1)}$ at stage k.

Claim 5.1 *The approximate power gain $\tilde{g}_k^2$, conditioned on $\hat{\boldsymbol{H}}$ has a noncentral chi-square density function with $2(N_r - N_t + k)$ degrees of freedom and noncentrality parameter $\hat{g}_k^2 \stackrel{\text{def}}{=} \hat{\boldsymbol{h}}_k^H \boldsymbol{\Upsilon}^{\perp}_{\hat{\boldsymbol{H}}_{(k+1)}} \hat{\boldsymbol{h}}_k$.*

A proof is given in Appendix C.

We now use $\tilde{g}_k^2$ to approximate g_k^2 in (5.23), and obtain an approximate BER in closed-form. From the distribution of $\tilde{g}_k^2$ given by Claim 5.1, we obtain its characteristic function as [84]

$$\psi_{\tilde{g}_k^2}(j\omega) \stackrel{\text{def}}{=} \mathbb{E}\left\{e^{j\omega\tilde{g}_k^2}\right\} = (1 - j\omega\sigma_h^2)^{-(N_r - N_t + k)} \exp\left(\frac{j\omega\hat{g}_k^2}{1 - j\omega\sigma_h^2}\right). \tag{5.25}$$

Using the characteristic function in (5.25), we can approximate the average BER (5.23) as

$$\begin{aligned}
\tilde{P}(\gamma_s; \hat{\boldsymbol{H}}; \sigma_h^2) &\approx \frac{1}{5N_t} \sum_{k=1}^{N_t} \int \exp\{-\gamma_s p_k^2 \tilde{g}_k^2\} f_{\tilde{g}_k^2|\hat{\boldsymbol{H}}}\left(\tilde{g}_k^2 | \hat{\boldsymbol{H}}\right) d\hat{\boldsymbol{H}} \\
&= \frac{1}{5N_t} \sum_{k=1}^{N_t} (1 + \gamma_s p_k^2 \sigma_h^2)^{-(N_r - N_t + k)} \exp\left(-\frac{\gamma_s p_k^2 \hat{g}_k^2}{1 + \gamma_s p_k^2 \sigma_h^2}\right) \\
&\stackrel{\text{def}}{=} \tilde{\tilde{P}}(\gamma_s; \hat{\boldsymbol{H}}; \sigma_h^2)
\end{aligned} \tag{5.26}$$

Remarks:

- For perfect CSI at the transmitter, $\hat{\boldsymbol{H}} = \boldsymbol{H}$ and $\sigma_h^2 = 0$, and (5.26) reduces to

  $$\tilde{\tilde{P}}(\gamma_s; \hat{\boldsymbol{H}}; 0) = \frac{1}{5N_t} \sum_{k=1}^{N_t} \exp\left(-\gamma_s p_k^2 \boldsymbol{h}_k^H \boldsymbol{\Upsilon}^{\perp}_{\hat{\boldsymbol{H}}_{(k+1)}} \boldsymbol{h}_k\right) = \frac{1}{5N_t} \sum_{k=1}^{N_t} \exp\left(-\gamma_s p_k^2 g_k^2\right),$$

  which is the approximate BER for power allocation with perfect feedback.

- Since

  $$\lim_{\gamma_s \to \infty} \frac{\tilde{\tilde{P}}(\gamma_s; \hat{\boldsymbol{H}}; \sigma_h^2)}{\gamma_s^{-(N_r - N_t + 1)}} = \frac{1}{5N_t} \frac{\exp\left(-\hat{g}_1^2/\sigma_h^2\right)}{(p_1^2 \sigma_h^2)^{(N_r - N_t + 1)}} \stackrel{\text{def}}{=} c_h,$$

  we have, for $\gamma_s \gg 1$,

  $$\tilde{\tilde{P}}(\gamma_s; \hat{\boldsymbol{H}}; \sigma_h^2) \approx c_h \cdot \gamma_s^{-(N_r - N_t + 1)},$$

decreasing exponentially as $(N_r - N_t + 1)$-th power of γ_s. Therefore, robustness to noisy CSI increases as the number of receive antennas, N_r, is increased relative to the number of transmit antennas, N_t. On the other hand, from (5.6), the BER of MIMO without power allocation can be approximated as

$$\bar{P}\left(\gamma_s; \{g_k^2\}\right) \approx \frac{1}{5N_t} \sum_{k=1}^{N_t} e^{-\gamma_s g_k^2},$$

decreasing exponentially in γ_s. Thus, for sufficiently large γ_s, power allocation schemes with noisy CSI at the transmitter are inferior to MIMO without power allocation, which is not affected by noisy CSI feedback.

5.4.2 Power Allocation with Noisy Power Feedback

Denote $\boldsymbol{p} = [p_1, p_2, \cdots, p_{N_t}]^T$ and $\hat{\boldsymbol{p}} = [\hat{p}_1, \hat{p}_2, \cdots, \hat{p}_{N_t}]^T$, where $\hat{p}_k$ denotes a noisy feedback of power. Noisy power feedback is modelled as $\hat{\boldsymbol{p}} = \boldsymbol{p} + \boldsymbol{\varepsilon}^p$, where $\boldsymbol{\varepsilon}^p$ is a noise vector with distribution $\mathcal{N}(\boldsymbol{0}, \boldsymbol{R})$.

With noisy power, the conditional approximate average BER can be written as

$$\tilde{P}(\gamma_s; \{g_k^2\}; \{\hat{p}_k^2\}) = \frac{1}{5N_t} \sum_{k=1}^{N_t} \exp\left\{-\gamma_s \hat{p}_k^2 g_k^2\right\}. \tag{5.27}$$

By averaging both sides of (5.27) over the distribution of $\boldsymbol{\varepsilon}^p$, the approximate BER is obtained as

$$\begin{aligned}
\tilde{P}(\gamma_s; \{g_k^2\}; \{p_k^2\}) &= \frac{1}{5N_t} \sum_{k=1}^{N_t} \int \exp\{-\gamma_s (p_k + \varepsilon_k^p)^2 g_k^2\} f_{\boldsymbol{\varepsilon}^p}(\boldsymbol{\varepsilon}^p)\, d\boldsymbol{\varepsilon}^p \\
&= \frac{1}{5N_t} \sum_{k=1}^{N_t} \int \frac{\exp\left\{-\gamma_s g_k^2 (\boldsymbol{p} + \boldsymbol{\varepsilon}^p)^T \boldsymbol{e}_k \boldsymbol{e}_k^T (\boldsymbol{p} + \boldsymbol{\varepsilon}^p) - \frac{1}{2} (\boldsymbol{\varepsilon}^p)^T \boldsymbol{R}^{-1} \boldsymbol{\varepsilon}^p\right\}}{(2\pi)^{N_t/2} \left[\det(\boldsymbol{R})\right]^{1/2}} d\boldsymbol{\varepsilon}^p \\
&= \frac{1}{5N_t} \sum_{k=1}^{N_t} (1 + 2\gamma_s g_k^2 [\boldsymbol{R}]_{k,k})^{-1/2} \exp\left\{-\frac{\gamma_s p_k^2 g_k^2}{1 + 2\gamma_s g_k^2 [\boldsymbol{R}]_{k,k}}\right\},
\end{aligned} \tag{5.28}$$

where $\boldsymbol{e}_k$ denotes the k-th column of $\boldsymbol{I}_{N_t}$, and the derivation follows [53]. When the noise

terms ε_k^p's are independent and identically distributed as $\mathcal{N}(0,\sigma_p^2)$, we have

$$\tilde{P}(\gamma_s;\{g_k^2\}) = \frac{1}{5N_t}\sum_{k=1}^{N_t}(1+2\gamma_s g_k^2\sigma_p^2)^{-1/2}\exp\left\{-\frac{\gamma_s p_k^2 g_k^2}{1+2\gamma_s g_k^2\sigma_p^2}\right\} \stackrel{\text{def}}{=} \tilde{\tilde{P}}\left(\gamma_s;\{g_k^2\};\sigma_p^2\right). \tag{5.29}$$

Remarks:

- For perfect power feedback, $\hat{\boldsymbol{p}} = \boldsymbol{p}$ and $\sigma_p^2 = 0$, and the above analysis does not apply because $\boldsymbol{R} = \boldsymbol{0}$. However, from (5.29), we have the limiting case of high quality feedback

  $$\lim_{\sigma_p^2\to 0}\tilde{\tilde{P}}(\gamma_s;\{g_k^2\};\sigma_p^2) = \frac{1}{5N_t}\sum_{k=1}^{N_t}\exp\left(-\gamma_s p_k^2 g_k^2\right),$$

  which reduces to the approximate BER for power allocation with perfect feedback. Therefore, (5.29) includes perfect power feedback as a special case.

- From (5.29), we have

  $$\lim_{\gamma_s\to\infty}\frac{\tilde{\tilde{P}}(\gamma_s;\{g_k\};\sigma_p^2)}{\gamma_s^{-1/2}} = \frac{1}{5N_t}\sum_{k=1}^{N_t}\frac{\exp\left\{-\frac{p_k^2}{2\sigma_p^2}\right\}}{\sqrt{2}g_k\sigma_p} \stackrel{\text{def}}{=} c_p,$$

  i.e., when $\gamma_s \gg 1$,

  $$\tilde{\tilde{P}}(\gamma_s;\{g_k\};\sigma_p^2) \approx c_p\cdot\gamma_s^{-1/2},$$

  decreasing in $\gamma_s^{-1/2}$. Therefore, for sufficiently large γ_s, power allocation schemes with noisy power feedback are inferior to MIMO without power allocation.

5.4.3 Power Allocation Using Feedback Noise Variance

When knowledge of the variance of noisy CSI, σ_h^2, or noisy power feedback, σ_p^2, is available at the transmitter, power allocation can be modified to take feedback noise variance into account as in [49, 86]. To this end, a constrained optimization problem, referred to as

modified AMBER power allocation, can be formulated as

$$\begin{cases} \min \tilde{\tilde{P}} \\ \text{subject to } \sum_{k=1}^{N_t} p_k^2 = N_t \end{cases}, \tag{5.30}$$

where $\tilde{\tilde{P}}$ is the objective function from (5.26) or (5.29). It can be verified that $\frac{d^2\tilde{\tilde{P}}}{d\left(p_k^2\right)^2} > 0$, i.e., $\tilde{\tilde{P}}$ is convex in p_k^2. A solution to the convex optimization problem (5.30) is given by (cf. Appendix B)

$$p_k^2 = (\phi_k)_+ , \tag{5.31}$$

where ϕ_k is the root of the equation $\frac{d\tilde{\tilde{P}}}{d\left(p_k^2\right)} = \mu$, and μ is chosen to satisfy the transmit power constraint. By noting the normalized transmit power constraint $\sum_{k=1}^{N_t} p_k^2 = N_t$, we have $\min_k p_k^2 \leq 1 \leq \max_k p_k^2$, and the parameter μ can be bounded as

$$\underbrace{\min_k \left\{ \left. \frac{d\tilde{\tilde{P}}}{d\left(p_k^2\right)} \right|_{p_k^2=1} \right\}}_{\mu_{\min}} \leq \mu \leq \underbrace{\max_k \left\{ \left. \frac{d\tilde{\tilde{P}}}{d\left(p_k^2\right)} \right|_{p_k^2=1} \right\}}_{\mu_{\max}}$$

The iterative algorithm in Table 4.1 can be used to solve this problem numerically.

Remark: In our analysis above, we have assumed AWGN only in feedback channels. In practice, however, such analysis is a bit optimistic due to fading, delay, noise and errors in feedback channels.

5.5 Numerical Results and Discussions

We compare the performances of a variety of power allocation schemes in fading channels. The channel model in Section 2.1.2 is used in simulations. Performances of transmission methods discussed earlier are simulated, and compared to MBER precoding with ZF equalization [28] as well as optimal MMSE precoding and decoding using trace criterion [92]. In our simulations, we assume linear array geometry and the following parameters are chosen:

$N_t = 4$ transmit and $N_r = 8$ receive antennas; antenna spacings are $d_t = 0.5$ and $d_r = 10$; angles of arrival/departure of deterministic component are $\pi/6$ and 0, respectively; angle spread 10°; $K = 8$ dB for Ricean fading channels; and BPSK modulation is used for the purposes of comparison with [28]. For SIC and OSIC receivers, actual decisions are used for interference cancellation in all simulations.

5.5.1 AMBER Power Allocation with Perfect Feedback

5.5.1.1 Rayleigh Fading

Fig. 5.1 is a plot of the average uncoded BER of different transceivers in an uncorrelated Rayleigh fading channel. We observe that at a BER of 10^{-3}, AMBER power allocation offers 1.2, 1.5 and 0.6 dB SNR gains over ZF, SIC and OSIC receivers, respectively. At all SNR's shown, MMSE precoding/decoding offers performance between that of ZF with and without AMBER power allocation, while MBER precoding for ZF equalization has performance between that of SIC with and without AMBER power allocation.

In Fig. 5.2, average uncoded BER's in a correlated Rayleigh fading channels are illustrated. It is seen that at a BER of 10^{-3}, AMBER power allocation offers 1.9 and 1.0 dB SNR gains over SIC and OSIC, respectively. Comparing to precoding schemes, similar relationship as in uncorrelated Rayleigh fading can be observed.

5.5.1.2 Ricean Fading

In Figs. 5.3 and 5.4, we illustrate average BER's in Ricean uncorrelated and correlated fading channels, respectively. In uncorrelated Ricean fading, SNR gains offered by AMBER power allocation for SIC and OSIC are 2.9 and 1.5 dB, respectively; while the gains increase to 3.1 and 2.0 dB in correlated Ricean fading. We also observe that MMSE precoding/decoding has performance similar to that of SIC without power allocation, while

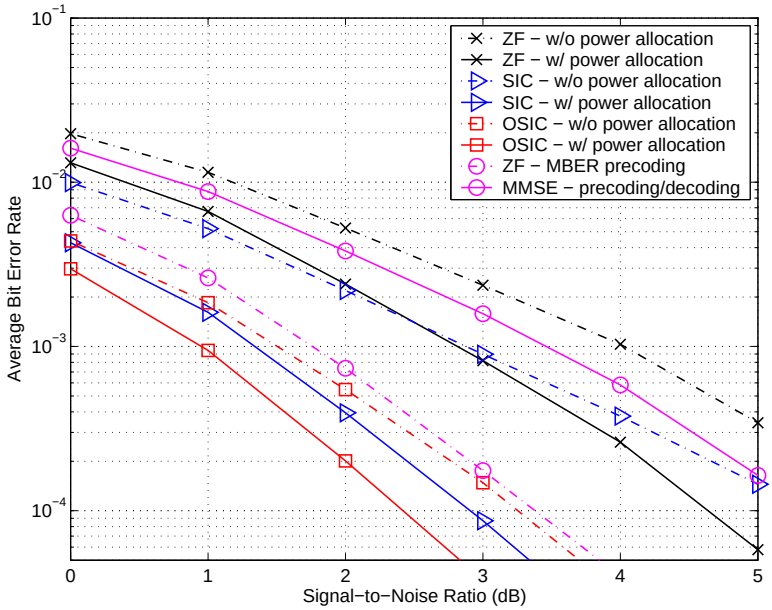

Figure 5.1. Average BER performance in uncorrelated Rayleigh fading MIMO channel ($N_t = 4, N_r = 8$).

performances of MBER precoding for ZF equalization and OSIC without power allocation are nearly identical.

Remarks:

- *Comparison among ZF, SIC and OSIC with AMBER Power Allocation*: For all channels simulated and employing AMBER power allocation, SIC outperforms ZF and OSIC outperforms SIC, which agrees with the heuristic results in Section 5.3.

- *Effects of Spatial Correlation*: With increasing channel spatial correlation, the SNR gains offered by AMBER power allocation increase.

- *Effects of Successive Interference Cancellation and Ordering*: In all simulation results obtained, successive interference cancellation offers greater gains for AMBER power allocation than no-power-allocation, while ordering offers relatively lower

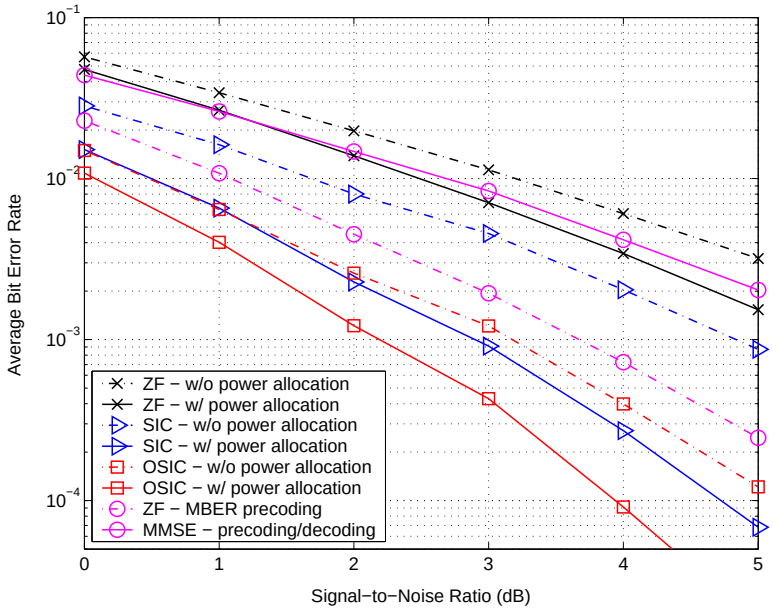

Figure 5.2. Average BER performance in correlated Rayleigh fading MIMO channel ($N_t = 4, N_r = 8$).

gains for AMBER power allocation.

- *AMBER Power Allocation versus Ordering for SIC*: From all simulations, it is also observed that SIC with AMBER power allocation outperforms OSIC without power allocation, i.e., AMBER power allocation outperforms SNR-based ordering for SIC receivers.

- *AMBER Power Allocation versus General Precoding*: In all simulated channels, SIC and OSIC with AMBER power allocation outperform both MMSE precoding/decoding and MBER precoding with ZF equalization. These two precoding schemes are chosen due to existence of closed-form solutions. Their complexity, though higher than that of power allocation, is comparable to power allocation. On

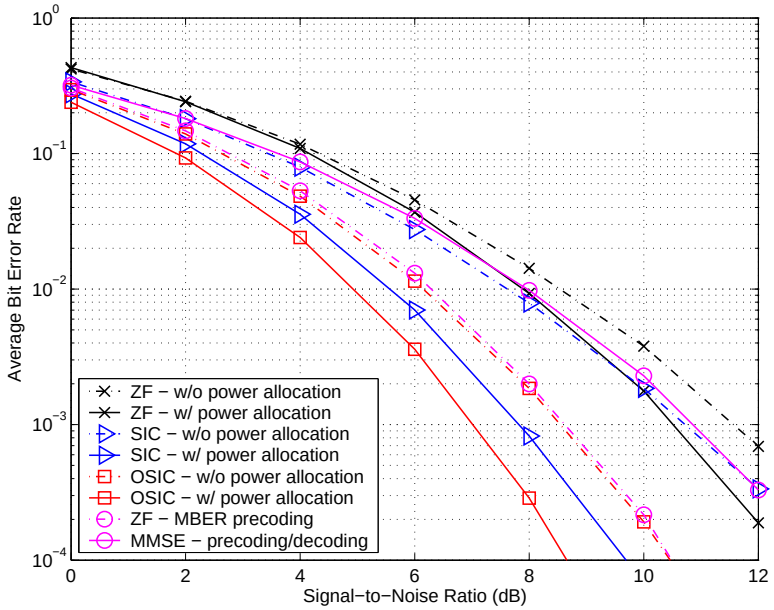

Figure 5.3. Average BER performance in uncorrelated Ricean fading MIMO channel ($N_t = 4, N_r = 8$, $K = 8$ dB).

the other hand, MBER precoding solutions can be found for SIC and OSIC by using numerical methods and/or exhaustive search. While MBER precoding would be expected to outperform power allocation, complexity may be prohibitively high.

- *Effects of Fewer Receive Antennas*: We have simulated BER performances of a MIMO system with 4 transmit and 8 receive antennas. When there are fewer receive antennas, say $N_t = N_r = 4$, error propagation effect might be significant for uncoded systems. Such effects should be considered in future work.

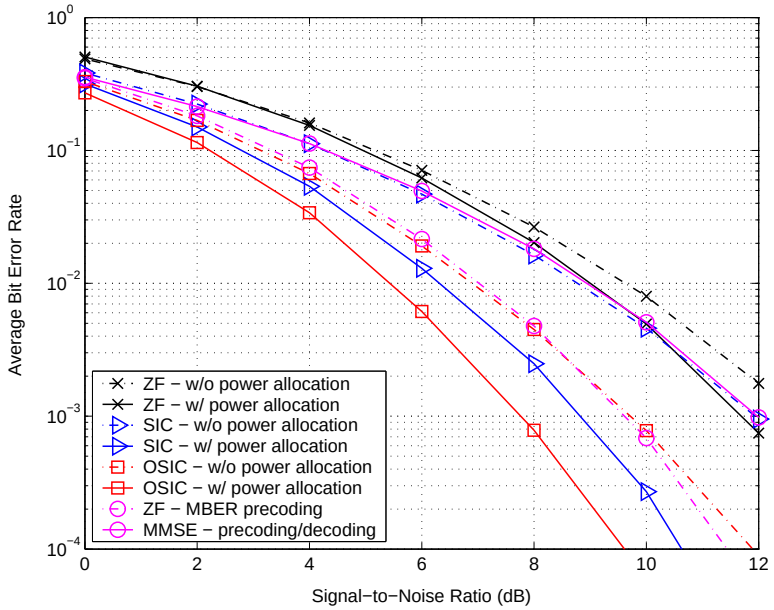

Figure 5.4. Average BER performance in correlated Ricean fading MIMO channel ($N_t = 4, N_r = 8$, $K = 8$ dB).

5.5.2 AMBER Power Allocation with Imperfect Feedback

5.5.2.1 AMBER Power Allocation with Noisy Power Feedback

Fig. 5.5 compares instantaneous approximate BER of OSIC with and without AMBER power allocation as a function of feedback power noise variance. The channel is modelled as Ricean fading with $K = 8$ dB. From Fig. 5.5, when power feedback noise variance σ_p^2 is larger than 0.01, OSIC without power allocation outperforms power allocation, which suggests AMBER power allocation to be quite sensitive to imperfect power feedback.

5.5.2.2 AMBER Power Allocation Using Noisy CSI Variance

Fig. 5.6 depicts average BER performances of OSIC without power allocation, with AMBER power allocation (5.11) and with modified power allocation (5.31), respectively, in

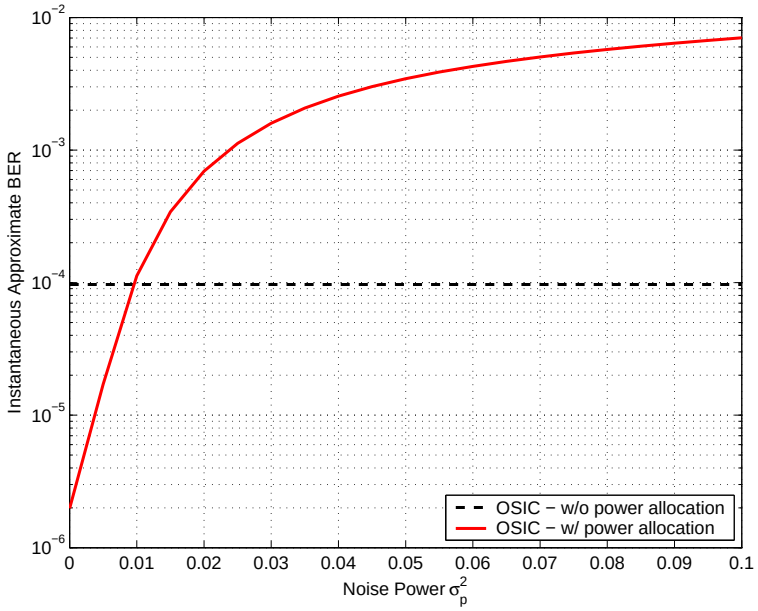

Figure 5.5. An example of approximate BER versus noise variance of power feedback ($N_t = 4, N_r = 8$, $K = 8$ dB, $\gamma_s = 10$ dB).

a correlated Ricean fading channel. Perfect knowledge of noise variance σ_h^2 is assumed. Ordering is conducted at the transmitter based on noisy CSI. We observe that performance of OSIC without power allocation also degrades with an increase of CSI noise power. Also, when the CSI noise variance is larger than 0.6, AMBER power allocation (5.11) has performance inferior to that of no-power-allocation. At all CSI noise variances shown, modified power allocation (5.31) outperforms the other OSIC methods.

Remark: From Fig. 5.6, we also observe that when $\sigma_h^2 = 0$, i.e, perfect CSI case, using (5.31) outperforms (5.11). This can be explained as follows: the modified power allocation solution for perfect CSI is given by $(p_k')^2 = (\phi_k)_+$, where ϕ_k is the solution to $\left.\frac{d\tilde{\bar{P}}(\gamma_s;\hat{\boldsymbol{H}};\sigma_h^2)}{d(p_k'^2)}\right|_{\sigma_h^2=0} = \mu$, which is equivalent to

$$\left(p_k'\right)^2 = \left(\frac{\ln\left[g_k^2 - \gamma_s^{-1}(N_r - N_t + k)\right] + \mu'}{\gamma_s g_k^2}\right)_+, \quad k = 1, 2, \cdots, N_t, \tag{5.32}$$

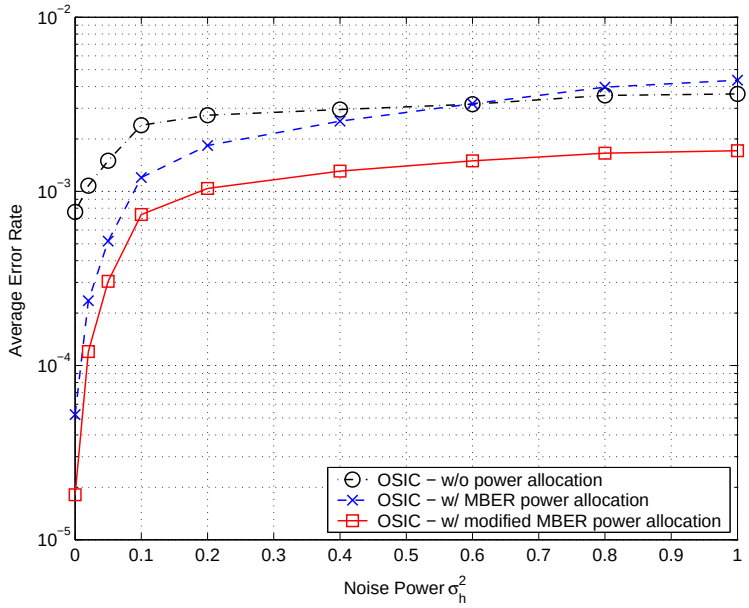

Figure 5.6. Average BER performance versus noisy CSI variance in correlated Ricean fading MIMO channel ($N_t = 4, N_r = 8$, $K = 8$ dB, $\gamma_s = 10$ dB).

where μ and μ' are chosen to satisfy the transmit power constraint. Comparing (5.32) with AMBER power allocation (5.11), it is obvious that in the modified scheme, more power is allocated to earlier successive interference cancellation stages. This change has the benefit of reducing error propagation from earlier stages to later ones, which improves the error rate performance. Note that the power allocation algorithm in Table 4.2 can be easily adapted to solve (5.32) without increasing complexity, resulting in a modified power allocation algorithm that takes error propagation of interference cancellation into account.

5.6 Conclusion

Power allocation using an approximate minimum BER (AMBER) criterion for MIMO spatial multiplexing is studied in this chapter. AMBER power allocation schemes for a variety

of receiver structures have been proposed. Compared with existing precoding schemes, the proposed schemes reduce both complexity and feedback overhead significantly. This method is motivated by an approximate BER analysis, which is also used to develop an AMBER power allocation scheme that uses the variance of the feedback or CSI noise. Simulation results show that the proposed power allocation method improves performance for ZF, SIC and OSIC receivers. Particularly, SIC and OSIC employing AMBER power allocation have the potential to offer superior performances over existing precoding schemes.

Chapter 6

Minimum BER Transmit Power Allocation and Beamforming for TIMO Spatial Multiplexing Systems

6.1 Introduction

As shown in Chapter 5, it is difficult to analyze general multiple-input multiple-output (MIMO) systems. Our goal of this chapter is to investigate transmit optimization for a MIMO spatial multiplexing system with two transmit antennas, known also as two-input multiple-output (TIMO). The study of such a system can be motivated in a number of ways: 1) TIMO systems are important in practical scenarios where there are limitations on cost and/or space to install more antennas; 2) a virtual TIMO channel is created when two single-antenna mobiles operate in cooperative communication mode [93]; 3) when transmit antenna selection is employed in MIMO to achieve diversity with reduced cost of transmit radio frequency chains [42], selecting two out of multiple transmit antennas turns MIMO into TIMO; 4) it is easier to analyze TIMO systems than the more general MIMO systems, and these analyses offer insights into MIMO system design and performance.

When channel state information (CSI) is available at the transmitter, system performance can be improved. The availability of CSI at the transmitter is achievable in time-division duplex (TDD) systems due to the reciprocity of the uplink and downlink channels, or in frequency-division duplex (FDD) systems with a feedback channel. Transmit optimization is receiver-dependent. Signal reception for spatial multiplexing can employ criteria such as zero-forcing (ZF), minimum mean squared-error (MMSE), successive interference cancellation (SIC), or ordered SIC (OSIC) as, for example, in the case of the Vertical Bell Laboratories Layered Space-Time (V-BLAST) [37]. Efforts to optimize MIMO transceiver structures have involved linear MMSE precoding/decoding [92], MBER precoding for ZF equalization [28] and limited feedback precoding schemes [59]. These schemes, however, generally require high feedback overhead and/or high complexity processing, e.g., diagonalization of the channel matrix and/or matrix transformations at both the transmitter and the receiver.

In this chapter, we consider complexity and feedback overhead reduction by introducing structural constraints to precoding. Minimization of bit error rate (MBER) is employed as the optimization criterion while the throughput is fixed. Such a transmission scheme is attractive in delay-sensitive applications, e.g., voice and video communications. We categorize TIMO channels into well- and ill-conditioned cases. Channel condition is determined by a number of factors, such as Ricean factor and/or spatial correlation. For well-conditioned TIMO channels, precoding is constrained to *transmit power allocation*, i.e., we optimize only the transmitted power of signal streams, resulting in reduced processing complexity compared to general precoding. Approximate MBER (AMBER) power allocation is proposed for TIMO spatial multiplexing in well-conditioned channels. In principle, power allocation for general MIMO systems proposed in Chapter 5 can be applied directly to TIMO systems. Nevertheless, useful simplifications and insights can be obtained for

TIMO systems, which are practical in their own right and do not apply to general MIMO systems. An example is the ill-conditioned pinhole channel that can be easily modelled in TIMO systems. When the TIMO channel is ill-conditioned, power allocation is shown to experience error floors. We introduce added degrees of freedom and develop an AMBER *transmit beamforming* scheme, which can eliminate these error floors. Compared to precoding which exploits spatial correlation of transmit antennas [2], the proposed transmit beamforming method utilizes instantaneous CSI and does not depend on the channel model used. It is shown both analytically and by simulation that the proposed transmit optimization schemes offer superior performance compared to existing precoding methods in generally correlated fading channels. As in existing limited feedback schemes, overhead is reduced as the proposed transmit optimization can be conducted at the receiver and fed back to the transmitter.

The rest of this chapter is organized as follows: TIMO signal reception and performance are introduced in Section 6.2, and the ill-conditioned TIMO channel model is defined. Section 6.3 investigates power allocation for MIMO with ZF, SIC and OSIC receivers and their performance. In Section 6.4, an AMBER transmit beamforming scheme is proposed for ill-conditioned TIMO channels. Section 6.5 presents numerical results in generally correlated fading channels.

6.2 TIMO Channel and Signal Reception

Consider a TIMO system with $N_r \geq 2$ receive antennas. The received signal can be modelled as

$$\begin{aligned} \boldsymbol{r} &= \boldsymbol{H}\boldsymbol{s} + \boldsymbol{\eta} \\ &= s_1\boldsymbol{h}_1 + s_2\boldsymbol{h}_2 + \boldsymbol{\eta}, \end{aligned} \tag{6.1}$$

where $\boldsymbol{s} = [s_1, s_2]^T$ denotes a transmitted signal vector, $\boldsymbol{H} = [\boldsymbol{h}_1 \vdots \boldsymbol{h}_2]$ is an $N_r \times 2$ channel matrix, which is assumed to be generally correlated Ricean fading (cf. Section 2.1.2) and $\boldsymbol{\eta}$ is an $N_r \times 1$ additive Gaussian noise vector. For simplicity of analysis purposes, we assume white noise and input, i.e., $\mathbb{E}[\boldsymbol{s}\boldsymbol{s}^H] = E_s \boldsymbol{I}_2$ and $\mathbb{E}[\boldsymbol{\eta}\boldsymbol{\eta}^H] = N_0 \boldsymbol{I}_{N_r}$, and define the input signal-to-noise ratio (SNR) $\gamma_s \stackrel{\text{def}}{=} E_s/N_0$. Binary phase shift keying (BPSK) modulation is assumed at first. Extension to other constellations will be addressed later.

6.2.1 TIMO Signal Reception

6.2.1.1 ZF Receiver

With ZF equalization, the transmitted signal is estimated as

$$\hat{\boldsymbol{s}} = \boldsymbol{H}^{\dagger}\boldsymbol{r} = \boldsymbol{s} + \boldsymbol{H}^{\dagger}\boldsymbol{\eta}, \tag{6.2}$$

where $(\cdot)^{\dagger}$ denotes Moore-Penrose pseudoinverse. The decision-point SNR of the k-th signal stream is obtained as

$$\gamma_{Z,k} = \frac{E_s}{N_0 \left[(\boldsymbol{H}^H\boldsymbol{H})^{-1}\right]_{k,k}} \stackrel{\text{def}}{=} \gamma_s g_{Z,k}^2, \quad k = 1,2, \tag{6.3}$$

where $g_{Z,k}^2 \stackrel{\text{def}}{=} [(\boldsymbol{H}^H\boldsymbol{H})^{-1}]_{k,k}^{-1}$ denotes the power gain of k-th stream using ZF equalization. The power gains can be calculated as

$$g_{Z,1}^2 = \frac{\Delta_{\boldsymbol{H}}}{\|\boldsymbol{h}_2\|^2}, \qquad g_{Z,2}^2 = \frac{\Delta_{\boldsymbol{H}}}{\|\boldsymbol{h}_1\|^2}, \tag{6.4}$$

where $\Delta_{\boldsymbol{H}} \stackrel{\text{def}}{=} \|\boldsymbol{h}_1\|^2\|\boldsymbol{h}_2\|^2 - |\boldsymbol{h}_2^H\boldsymbol{h}_1|^2$.

6.2.1.2 SIC Receiver

Without loss of generality, we assume that stream $k = 1$ is detected first. Assuming ZF equalization is employed, the power gain in detecting s_1 is the same as that of the ZF

receiver, i.e.,

$$g_{S,1}^2 = g_{Z,1}^2 = \frac{\Delta_{\boldsymbol{H}}}{\|\boldsymbol{h}_2\|^2}. \tag{6.5}$$

Assuming that $\hat{s}_1 = s_1$, the interference due to the first stream is then regenerated and subtracted, i.e.,

$$\boldsymbol{r}' = \boldsymbol{r} - \hat{s}_1 \boldsymbol{h}_1 = s_2 \boldsymbol{h}_2 + \boldsymbol{\eta}. \tag{6.6}$$

The detection of s_2 in (6.6) with ZF equalization is given by

$$\hat{s}_2 = \boldsymbol{h}_2^{\dagger} \boldsymbol{r}' = s_2 + \frac{\boldsymbol{h}_2^H \boldsymbol{\eta}}{\|\boldsymbol{h}_2\|^2},$$

which is equivalent to maximal ratio combining (MRC), with power gain

$$g_{S,2}^2 = \|\boldsymbol{h}_2\|^2. \tag{6.7}$$

6.2.1.3 OSIC Receiver

To improve SIC performance, the streams can be reordered based on SNR at each stage. The SNR-based ordering scheme [37] detects the stream with largest decision-point SNR first, or, equivalently, detects the stream with largest power gain first. From (6.3) and (6.4), the stream to be detected first is

$$k_1 = \arg\max_l \gamma_{Z,l} = \arg\max_l g_{Z,l}^2 = \arg\max_l \|\boldsymbol{h}_l\|^2,$$

i.e., SNR-based ordering is equivalent to norm-based ordering in TIMO systems[1]. Therefore, we obtain the power gains as

$$g_{O,1}^2 = \frac{\Delta_{\boldsymbol{H}}}{\min\{\|\boldsymbol{h}_1\|^2, \|\boldsymbol{h}_2\|^2\}}, \quad g_{O,2}^2 = \min\{\|\boldsymbol{h}_1\|^2, \|\boldsymbol{h}_2\|^2\}. \tag{6.8}$$

The average BER of the above receivers can be calculated as [84]

$$\bar{P}(\gamma_s; g_1^2, g_2^2) = \frac{1}{2} Q\left(\sqrt{2\gamma_s g_1^2}\right) + \frac{1}{2} Q\left(\sqrt{2\gamma_s g_2^2}\right), \tag{6.9}$$

[1]We note that this does not apply to general MIMO systems with $N_t \geq 3$.

where the power gains g_1^2 and g_2^2 depend on the receiver structure and are given in (6.4), (6.5), (6.7) and (6.8); $Q(x) \stackrel{\text{def}}{=} \frac{1}{\sqrt{2\pi}} \int_x^\infty e^{-y^2/2} dy$. We note that for SIC and OSIC receivers, (6.9) is only a lower bound due to the neglecting of error propagation. However, at moderate-to-high SNR regimes, this lower bound closely approximates the average BER since error propagation is minimal.

6.2.2 Ill-Conditioned TIMO Channels

Since the $Q(\cdot)$ function decreases rapidly in its argument, the average BER in (6.9) is dominated by the term with smaller power gain. In the extreme case with a vanishing power gain, the system experiences an error floor. We refer to this as an *ill-conditioned* TIMO channel. From gains in (6.4), (6.5), (6.7) and (6.8), the channel is ill-conditioned when either $\Delta_{\boldsymbol{H}} \approx 0$ or $\min\{\|\boldsymbol{h}_1\|^2, \|\boldsymbol{h}_2\|^2\} \approx 0$.

- The condition $\Delta_{\boldsymbol{H}} \approx 0$ is equivalent to $\|\boldsymbol{h}_1\|^2 \cdot \|\boldsymbol{h}_2\|^2 \approx |\boldsymbol{h}_1^H \boldsymbol{h}_2|^2$. We have

$$\frac{|\boldsymbol{h}_1^H \boldsymbol{h}_2|^2}{\|\boldsymbol{h}_2\|^2} = \boldsymbol{h}_1^H \boldsymbol{\Upsilon}_{\boldsymbol{h}_2} \boldsymbol{h}_1 = \|\boldsymbol{\Upsilon}_{\boldsymbol{h}_2} \boldsymbol{h}_1\|^2 \approx \|\boldsymbol{h}_1\|^2,$$

  where $\boldsymbol{\Upsilon}_{\boldsymbol{X}} \stackrel{\text{def}}{=} \boldsymbol{X}(\boldsymbol{X}^H \boldsymbol{X})^{-1} \boldsymbol{X}^H$, is the projection matrix. Therefore, without loss of generality, we can assume $\boldsymbol{h}_2 \approx a \cdot \boldsymbol{h}_1$ with $a \in \mathbb{C}$, and the channel matrix

$$\boldsymbol{H} \approx \boldsymbol{h}_1 [1 \;\; a], \tag{6.10}$$

  which is also an example of a "pinhole" channel [38]. The least-squares (LS) estimate of a can be found to be

$$\hat{a}_{LS} = \boldsymbol{h}_1^\dagger \boldsymbol{h}_2 = \frac{\boldsymbol{h}_1^H \boldsymbol{h}_2}{\|\boldsymbol{h}_1\|^2}. \tag{6.11}$$

- Denote $m = \arg\min_k \{\|\boldsymbol{h}_k\|^2\}$. The condition $\min\{\|\boldsymbol{h}_1\|^2, \|\boldsymbol{h}_2\|^2\} \approx 0$ implies $\boldsymbol{h}_m \approx \boldsymbol{0}$, i.e., the link from the m-th transmit antenna to all receive antennas is blocked. Note that in this case, the model (6.10) is still valid with $a \approx 0$.

6.3 Transmit Power Allocation for TIMO

6.3.1 AMBER Transmit Power Allocation

Denote the power allocated to the k-th stream as p_k^2 ($k = 1,2$). The received signal can be written as

$$\boldsymbol{r} = \boldsymbol{H}\boldsymbol{P}_a\boldsymbol{s} + \boldsymbol{\eta} = p_1 s_1 \boldsymbol{h}_1 + p_2 s_2 \boldsymbol{h}_2 + \boldsymbol{\eta}, \tag{6.12}$$

where $\boldsymbol{P}_a \stackrel{\text{def}}{=} \text{diag}\{p_1, p_2\}$. We assume that the total transmit power is constrained via

$$\text{tr}\left\{\boldsymbol{P}_a^2\right\} = p_1^2 + p_2^2 = 2. \tag{6.13}$$

According to (5.11), the approximate MBER power allocation for TIMO is obtained as

$$p_k^2 = \gamma_s^{-1} g_k^{-2} \left(\ln g_k^2 + \nu\right)_+, \quad (k = 1,2). \tag{6.14}$$

where ν is chosen to satisfy power constraint (6.13). Note the fact that the total transmit power $p_1^2 + p_2^2$ is a piecewise-linear function in ν, with breakpoints at $-\ln g_1^2$ and $-\ln g_2^2$. Without loss of generality, we assume $g_1^2 \geq g_2^2$. We can simplify the solution (6.14) as

$$\begin{cases} p_1^2 = 2,\ p_2^2 = 0 & \text{if } \ln g_1^2 - \ln g_2^2 \geq 2\gamma_s g_1^2 \\ p_1^2 = \frac{\ln g_1^2 + \nu_a}{\gamma_s g_1^2},\ p_2^2 = \frac{\ln g_2^2 + \nu_a}{\gamma_s g_2^2} & \text{otherwise} \end{cases}, \tag{6.15}$$

where $\nu_a = \frac{2\gamma_s g_1^2 g_2^2 - g_1^2 \ln g_2^2 - g_2^2 \ln g_1^2}{g_1^2 + g_2^2}$.

In the first case of (6.15), the solution $p_1^2 = 2$ and $p_2^2 = 0$ implies that the stream with weaker power gain is dropped, and all available power is allocated to the stronger stream. This occurs when $\ln g_1^2 - \ln g_2^2 \geq 2\gamma_s g_1^2$, i.e., either $g_1^2 \gg g_2^2$ or γ_s is small. In this case, if both streams are used for transmission, an error floor is inevitable. To avoid such error floors, only one stream may be transmitted, and power allocation turns out to be *transmit antenna selection* [89]. We note that the condition $\ln g_1^2 - \ln g_2^2 \geq 2\gamma_s g_1^2$ is also a necessary condition of ill-conditioned TIMO channel defined in Section 6.2.2. An alternative scheme to eliminate error floor effects will be addressed in Section 6.4.

6.3.2 Remarks

6.3.2.1 Feedback Overhead and Complexity Issues

As discussed in Chapter 5, the proposed power allocation scheme has less overhead and complexity compared to that of general precoding schemes.

6.3.2.2 Application Scenarios

A TIMO configuration is appropriate for the uplink of a wireless system, where each mobile terminal is equipped with dual transmit antenna while the basestation has more antennas. Equivalently, when transmit antenna selection is employed in a MIMO uplink, selecting two out of multiple transmit antennas creates a TIMO uplink. The downlink, on the other hand, has a multiple-input two-output (MITO) structure. To exploit the inherent transmit diversity in such a MITO system, transmit processing is necessary. For example, linear precoding schemes optimizing system error rate performance [28] or alternatives [92] may be employed, which are beyond the scope of this paper. Alternatively, transmit antenna selection may be employed. We note that selecting two out of multiple transmit antennas results in a two-input two-output system, which belongs to the general TIMO family, and the proposed power allocation applies.

6.3.2.3 Effects of Power Allocation on Detection Ordering

For OSIC, we examine the effect of power allocation on ordering. Without loss of generality, we assume $\|\mathbf{h}_1\| \geq \|\mathbf{h}_2\|$. In norm-based ordering, s_1 is detected first. Denote the corresponding power gains as, respectively, $\alpha_1^2 = \frac{\Delta_{\mathbf{H}}}{\|\mathbf{h}_2\|^2}$, $\alpha_2^2 = \|\mathbf{h}_2\|^2$. Consider the opposite detection ordering. Denote the resulting power gains as, respectively, $\beta_1^2 = \frac{\Delta_{\mathbf{H}}}{\|\mathbf{h}_1\|^2}$, $\beta_2^2 = \|\mathbf{h}_1\|^2$. While a general analysis is difficult, we consider the asymptotic case. Applying similar arguments as in Section 5.3, at moderate-to-high SNR ($\gamma_s \gg 1$), the BER of

power allocation method (6.14) can be approximated as

$$\begin{aligned}\bar{P}\left(\gamma_s; g_1^2, g_2^2\right) &\approx \frac{1}{10} e^{-v_a}\left(g_1^{-2}+g_2^{-2}\right) \\ &\approx \frac{1}{10}\left(g_1^{-2}+g_2^{-2}\right)\exp\left\{-\frac{2\gamma_s}{g_1^{-2}+g_2^{-2}}\right\} \\ &\stackrel{\text{def}}{=} \tilde{P}_a\left(\gamma_s; g_1^2, g_2^2\right). \end{aligned} \tag{6.16}$$

From (6.16), $\tilde{P}_a\left(\gamma_s; g_1^2, g_2^2\right)$ is an monotone increasing function in $g_1^{-2}+g_2^{-2}$. Note that $\alpha_1^2\alpha_2^2 = \beta_1^2\beta_2^2$. By assumption ($\|\boldsymbol{h}_1\| \geq \|\boldsymbol{h}_2\|$), we have $\beta_1^2 \leq \alpha_1^2 \leq \beta_2^2$, and $\beta_1^2 \leq \alpha_2^2 \leq \beta_2^2$. Therefore, $\alpha_1^{-2}+\alpha_2^{-2} \leq \beta_1^{-2}+\beta_2^{-2}$. We conclude

$$\tilde{P}_a(\gamma_s; \alpha_1^2, \alpha_2^2) \leq \tilde{P}_a(\gamma_s; \beta_1^2, \beta_2^2),$$

i.e., for TIMO at moderate-to-high SNR, norm-based ordering (or, equivalently, SNR-based ordering), optimal for TIMO without power allocation as in Section 6.2.1, is also asymptotically optimal for the case of power allocation, in the sense of minimizing average BER.

6.3.2.4 Performance in Ill-Conditioned Channels

Without loss of generality, we assume $|a| \leq 1$ in the ill-conditioned channel (6.10). The power gains of OSIC can be obtained as

$$g_{O,1}^2 \approx 0, \quad g_{O,2}^2 = |a|^2\|\boldsymbol{h}_1\|^2.$$

Applying power allocation in (6.14), we obtain $p_1^2 = 0$, and $p_2^2 = 2$. The average BER of power allocation for ill-conditioned channels can be approximated as

$$\bar{P}(\gamma_s; \boldsymbol{h}_1, a) \approx \frac{1}{10} + \frac{1}{10}\exp\left\{-2\gamma_s|a|^2\|\boldsymbol{h}_1\|^2\right\}, \tag{6.17}$$

which experiences an obvious error floor. This motivates our study of transmit beamforming for ill-conditioned TIMO channels.

6.4 Transmit Beamforming for Ill-Conditioned TIMO Channels

We study the receiver structure for ill-conditioned TIMO channels to observe the error floor effects in performance. A new transmit beamforming method is then proposed in order to mitigate the error floor.

6.4.1 Signal Reception and Performance

Consider the received signal (6.1) in an ill-conditioned TIMO channel (6.10). The ZF equalization output can be obtained as

$$\begin{aligned}\begin{bmatrix} y_1 \\ y_2 \end{bmatrix} &= \boldsymbol{H}^{\dagger}\boldsymbol{r} = \boldsymbol{H}^{\dagger}\boldsymbol{H}\boldsymbol{s}+\boldsymbol{H}^{\dagger}\boldsymbol{\eta} \\ &= \frac{1}{(1+|a|^2)}\begin{bmatrix} s_1+as_2 \\ a^*s_1+|a|^2s_2 \end{bmatrix} + \frac{\boldsymbol{h}_1^H\boldsymbol{\eta}}{(1+|a|^2)\|\boldsymbol{h}_1\|^2}\begin{bmatrix} 1 \\ a^* \end{bmatrix}. \end{aligned} \quad (6.18)$$

From (6.18), we observe that the transmitted signals s_1 and s_2 are coupled in y_1 and y_2, and $y_2 = a^*y_1$. Therefore, it suffices to process one of the estimates, say y_1. Without loss of generality, we assume $\|\boldsymbol{h}_1\| \geq \|\boldsymbol{h}_2\|$, or, equivalently, $|a| \leq 1$. Consider detecting s_1 and s_2 in a SIC fashion. Since the power of s_1 contained in y_1, $\mathbb{E}[|s_1|^2] = E_s$, is larger than that of s_2 contained in y_1, $\mathbb{E}[|as_2|^2] = |a|^2E_s$, the optimal order is chosen to detect s_1 first. The error probability in detection of s_1, regarding s_2 as noise, can be calculated as

$$\Pr(\hat{s}_1 \neq s_1) = \frac{1}{2}Q\left(\sqrt{2\gamma_s\|\boldsymbol{h}_1\|^2[1-\Re(a)]^2}\right) + \frac{1}{2}Q\left(\sqrt{2\gamma_s\|\boldsymbol{h}_1\|^2[1+\Re(a)]^2}\right). \quad (6.19)$$

Assuming s_1 is correctly detected, and performing interference cancellation, s_2 is then detected. The error probability of detecting s_2 can be obtained as

$$\Pr(\hat{s}_2 \neq s_2|\hat{s}_1 = s_1) = Q\left(\sqrt{2\gamma_s\|\boldsymbol{h}_1\|^2[\Re(a)]^2}\right). \quad (6.20)$$

The average BER is given by $\bar{P}(\gamma_s; a, \boldsymbol{h}_1) = \frac{1}{2}\Pr(\hat{s}_1 \neq s_1) + \frac{1}{2}\Pr(\hat{s}_2 \neq s_2)$, which can be approximated as

$$\begin{aligned}\bar{P}(\gamma_s; a, \boldsymbol{h}_1) &\approx \frac{1}{20}\exp\left\{-\gamma_s\|\boldsymbol{h}_1\|^2[1-\Re(a)]^2\right\} + \frac{1}{20}\exp\left\{-\gamma_s\|\boldsymbol{h}_1\|^2[1+\Re(a)]^2\right\} \\ &\quad + \frac{1}{10}\exp\left\{-\gamma_s\|\boldsymbol{h}_1\|^2[\Re(a)]^2\right\}. \end{aligned} \tag{6.21}$$

It is obvious that (6.21) experiences an error floor when either $\Re(a) \approx 0$ or $\Re(a) \approx \pm 1$. This occurs, e.g., when transmit fading coefficients are either in phase or in quadrature, respectively. Furthermore, as shown in Appendix D, power allocation alone cannot eliminate error floors. This motivates our study of a precoding scheme.

6.4.2 Transmit Beamforming Method

Now we consider general precoding for ill-conditioned TIMO channels. Denote the precoding matrix

$$\boldsymbol{P}_b = \begin{bmatrix} p_{11} & p_{12} \\ p_{21} & p_{22} \end{bmatrix}.$$

The normalized transmit power constraint is given by

$$\operatorname{tr}\left(\boldsymbol{P}_b\boldsymbol{P}_b^H\right) = |p_{11}|^2 + |p_{12}|^2 + |p_{21}|^2 + |p_{22}|^2 = 2. \tag{6.22}$$

The received signal is $\boldsymbol{r} = \boldsymbol{H}\boldsymbol{P}_b\boldsymbol{s} + \boldsymbol{\eta}$. With ZF equalization, the estimate of the transmitted signal is given by

$$\begin{bmatrix} z_1 \\ z_2 \end{bmatrix} = \boldsymbol{H}^\dagger\boldsymbol{r} = \frac{1}{1+|a|^2}\left(\begin{bmatrix} 1 & a \\ a^* & |a|^2 \end{bmatrix}\begin{bmatrix} p_{11}s_1 + p_{12}s_2 \\ p_{21}s_1 + p_{22}s_2 \end{bmatrix} + \frac{1}{\|\boldsymbol{h}_1\|^2}\begin{bmatrix} \boldsymbol{h}_1^H\boldsymbol{\eta} \\ a^*\boldsymbol{h}_1^H\boldsymbol{\eta} \end{bmatrix}\right).$$

From (6.23), we know $z_2 = a^* z_1$. Therefore, it suffices to process z_1 only. Consider

$$z_1' \stackrel{\text{def}}{=} (1+|a|^2)z_1 = (p_{11}+ap_{21})s_1 + (p_{12}+ap_{22})s_2 + \frac{\boldsymbol{h}_1^H\boldsymbol{\eta}}{\|\boldsymbol{h}_1\|^2}. \tag{6.23}$$

By symmetry in $\{p_{11}, p_{12}\}$ and $\{p_{21}, p_{22}\}$, we know that the detection order can be determined arbitrarily. Without loss of generality, we assume

$$\begin{cases} \Re(p_{11}+ap_{21}) & \geq & 0, \\ \Re(p_{12}+ap_{22}) & \geq & 0, \\ \Re(p_{11}+ap_{21}) & \geq & \Re(p_{12}+ap_{22}). \end{cases}$$

As a result, s_1 is detected first. Similar to the analysis in Section 6.4.1, we obtain the approximate average BER

$$\begin{aligned} \bar{P}(\gamma_s; \boldsymbol{h}_1, a; \boldsymbol{P}_b) &\approx \frac{1}{20}\exp\left\{-2\gamma_s\|\boldsymbol{h}_1\|^2\left[\Re(p_{11}+ap_{21}-p_{12}-ap_{22})\right]^2\right\} \\ &\quad + \frac{1}{20}\exp\left\{-2\gamma_s\|\boldsymbol{h}_1\|^2\left[\Re(p_{11}+ap_{21}+p_{12}+ap_{22})\right]^2\right\} \\ &\quad + \frac{1}{10}\exp\left\{-2\gamma_s\|\boldsymbol{h}_1\|^2\left[\Re(p_{12}+ap_{22})\right]^2\right\}. \end{aligned} \tag{6.24}$$

At moderate-to-high SNR, $\gamma_s \gg 1$, the second term in (6.24) is relatively small compared to the first term in (6.24). We can approximate

$$\begin{aligned} \bar{P}(\gamma_s; \boldsymbol{h}_1, a; \boldsymbol{P}_b) &\approx \frac{1}{20}\exp\left\{-2\gamma_s\|\boldsymbol{h}_1\|^2\left[\Re(p_{11}+ap_{21}-p_{12}-ap_{22})\right]^2\right\} \\ &\quad + \frac{1}{10}\exp\left\{-2\gamma_s\|\boldsymbol{h}_1\|^2\left[\Re(p_{12}+ap_{22})\right]^2\right\} \\ &\stackrel{\text{def}}{=} \tilde{P}_{IC}. \end{aligned} \tag{6.25}$$

An approximate solution that minimizes (6.25) under the transmit power constraint (6.22) is given in Appendix E. The precoder is found to be

$$\boldsymbol{P}_b = \underbrace{(1+|a|^2)^{-1/2}\begin{bmatrix} 1 \\ a^* \end{bmatrix}}_{\boldsymbol{v}_{\text{BF}}} \times \underbrace{\sqrt{\frac{2}{5}}\begin{bmatrix} 2 & 1 \end{bmatrix}}_{\boldsymbol{v}_{\text{PA}}^T} \stackrel{\text{def}}{=} \boldsymbol{v}_{\text{BF}}\boldsymbol{v}_{\text{PA}}^T. \tag{6.26}$$

Note that the precoder (6.26) has rank one, and can be viewed as power allocation $\boldsymbol{v}_{\text{PA}}$ followed by transmit beamforming $\boldsymbol{v}_{\text{BF}}$ pointing in the approximate MBER direction. Also, note that $\mathbf{v}_{PA}$ pre-mixes the two streams with different allocated powers in the sense of approximate MBER using OSIC. We will refer to this scheme as OSIC with beamforming. It

is worth noting that the solution in (6.26) is not necessarily unique due to an approximation introduced in Appendix E. Substituting (6.26) into (6.25), we obtain the approximate average BER as

$$\overline{P}_{IC}^{BF}(\gamma_s;\boldsymbol{h}_1,a) \approx \frac{3}{20}\exp\left\{-\frac{4}{5}\gamma_s\|\boldsymbol{h}_1\|^2(1+|a|^2)\right\}, \tag{6.27}$$

which does not experience error floors. Comparing (6.27) with the performance results of power allocation in Appendix D (cf. (D.5)), we conclude that power allocation alone cannot eliminate error floors in ill-conditioned TIMO channels, while power allocation together with beamforming can overcome the error floors.

Remarks:

- *Comparison with Existing Methods:* The precoder in (6.26) mixes two BPSK streams into a single 4-ary PAM. The receiver is assumed to use the in-phase component of the received signal for BPSK signal reception. In [23], a precoder that mixes two BPSK streams into one QPSK stream is proposed for TIMO spatial multiplexing. We note that different precoder receiver structures are required for the two approaches. In summary, the more complex ML receiver in [23] would be expected to have higher performance.

- *Feedback Overhead and Complexity Issues:* From (6.26), only an estimate of a is required at the transmitter, which can be obtained using (6.11). Operations performed at the transmitter are also trivial.

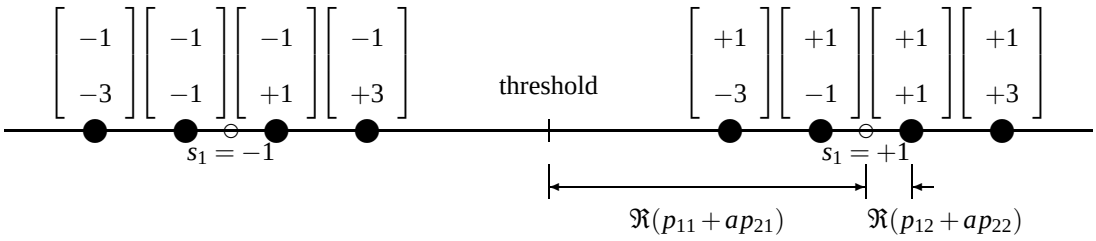

Figure 6.1. Signal space diagram for 4-PAM with precoding in ill-conditioned channels.

6.4.3 Extension to High-Order Modulations

6.4.3.1 Extension to M-ary PAM

Denote the set of possible amplitudes of an M-ary PAM signal as $\{A_m\}_{m=1}^{M}$, with A_m taking discrete values

$$A_m = (2m - 1 - M)d, \qquad m = 1, 2, \cdots, M,$$

where $2d$ is the distance between adjacent signal amplitudes [84]. A signal space diagram of the equalization output (6.23) of quaternary PAM is illustrated in Fig. 6.1, where only two signal points of s_1 are shown for brevity. By similar argument in Section 6.4.2, we obtain an approximate precoder as

$$\boldsymbol{P}_b = \sqrt{2}(M^2+1)^{-1/2}(1+|a|^2)^{-1/2} \begin{bmatrix} 1 \\ a^* \end{bmatrix} \begin{bmatrix} M & 1 \end{bmatrix}. \tag{6.28}$$

We note that (6.28) includes (6.26) as a special case when $M = 2$.

6.4.3.2 Extension to QPSK

We consider extension to QPSK as an example. Fig. 6.2 shows a signal space diagram of the equalization output (6.23), where for brevity of illustration purposes, only one point of s_1 is shown. Without loss of generality, we assume $p_{11} + ap_{22} \stackrel{\text{def}}{=} \rho_1 \geq 0$. Denote

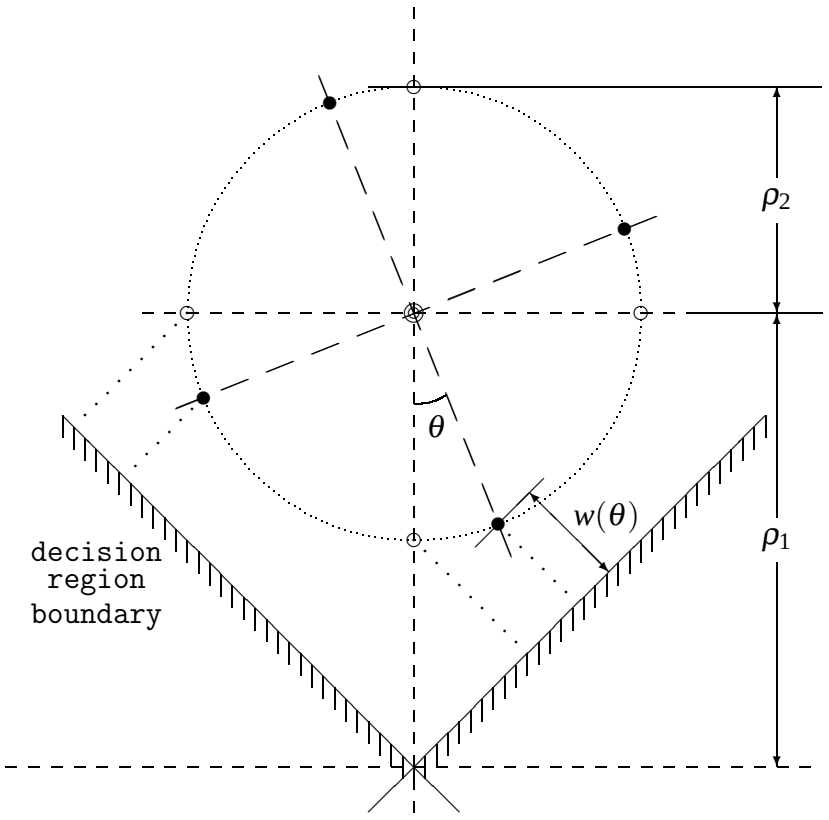

Figure 6.2. Signal space diagram for QPSK with precoding in ill-conditioned channel.

$p_{12}+ap_{22} \stackrel{\text{def}}{=} \rho_2 e^{j\theta}$, where $\theta \in [0, \pi/4)$ is assumed without loss of generality. At moderate-to-high SNR's, the BER is dominated by contributions from the set of closest points to the decision region boundary, denoted as $w(\theta)$ in Fig. 6.2. The average BER can be approximated by

$$\bar{P}(\gamma_s;\theta) \approx \frac{1}{4} Q\left(\sqrt{2\gamma_s w^2(\theta)}\right) \stackrel{\text{def}}{=} \tilde{P}(\gamma_s;\theta).$$

From Fig. 6.2, we calculate $w(\theta)$ as

$$w(\theta) = \frac{\sqrt{2}}{2}\left[\rho_1 - \rho_2\left(\sin\theta + \cos\theta\right)\right].$$

Since $d\tilde{P}(\gamma_s;\theta)/d\theta < 0$, we have

$$\arg\min_{\theta} \tilde{P}(\gamma_s;\theta) = 0,$$

i.e., $p_{12} + ap_{22}$ is also real positive. Following the same argument as in Appendix E, we obtain an approximate MBER precoder for QPSK as

$$\boldsymbol{P}_b = \sqrt{\frac{2}{5}}(1+|a|^2)^{-1/2} \begin{bmatrix} 1 \\ a^* \end{bmatrix} \begin{bmatrix} 2 & 1 \end{bmatrix}, \tag{6.29}$$

which is the same as that of BPSK. We note that this result applies directly to 4-QAM with a single amplitude level [84], since it is just a rotated version of QPSK.

Remark: Extension to higher order 2-dimensional modulations may be conducted in a similar manner. Performance gains for higher order 2-dimensional modulations using transmit beamforming need to be investigated in future work.

6.5 Numerical Results and Discussions

We compare BER performance of the proposed MBER power allocation method for ZF, SIC and OSIC receivers with two existing precoding methods in well-conditioned and ill-conditioned channels, respectively. In addition, comparison of OSIC with MBER transmit beamforming as proposed in Section 6.4 is also made. The channel model in Section 2.1.2 is used in simulations. We assume linear transmit and receive antenna arrays. The following parameters are chosen: $N_r = 4$ receive antennas; transmit and receive antenna spacings expressed in wavelength are 0.5 and 10, respectively; angles of arrival/departure of deterministic component are $\pi/6$ and 0, respectively; angle spread 10°; $K = 8$ dB for Ricean fading channels; and BPSK modulation is used for the purposes of comparison with [28].

6.5.1 Rayleigh Fading

Fig. 6.3 is a plot of the average BER for a variety of transceivers in an uncorrelated Rayleigh fading channel. To clarify the plot, performances of ZF with power allocation and SIC

without power allocation are not shown since they are nearly identical to that of MMSE precoding/decoding; OSIC without power allocation (also not shown) has performance close to that of ZF with MBER precoding. We observe that at a BER of 10^{-3}, the proposed power allocation scheme offers 0.6, 1.4 and 0.8 dB gains over ZF, SIC and OSIC receivers, respectively. Both SIC and OSIC with power allocation outperform precoding schemes, e.g., at a BER of 10^{-3}, OSIC with power allocation offers 1.0 dB and 1.9 dB SNR gains over MBER precoding with ZF equalization and MMSE precoding/decoding, respectively. We can also see that OSIC with MBER beamforming, though designed for ill-conditioned channels, outperforms OSIC without power allocation at SNR's larger than 5 dB.

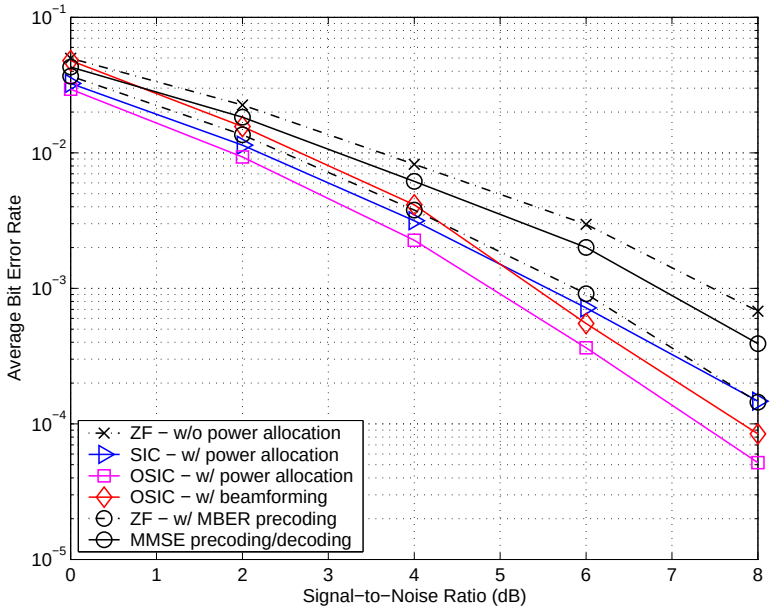

Figure 6.3. Average BER performance in uncorrelated Rayleigh fading TIMO channel ($N_t = 2$, $N_r = 4$).

Fig. 6.4 illustrates average BER performance in correlated Rayleigh fading. Similar relationships among ZF, SIC, OSIC and precoding schemes as in uncorrelated Rayleigh fading channels are observed. It is also shown that OSIC with beamforming outperforms

all other schemes at SNR's larger than 7 dB.

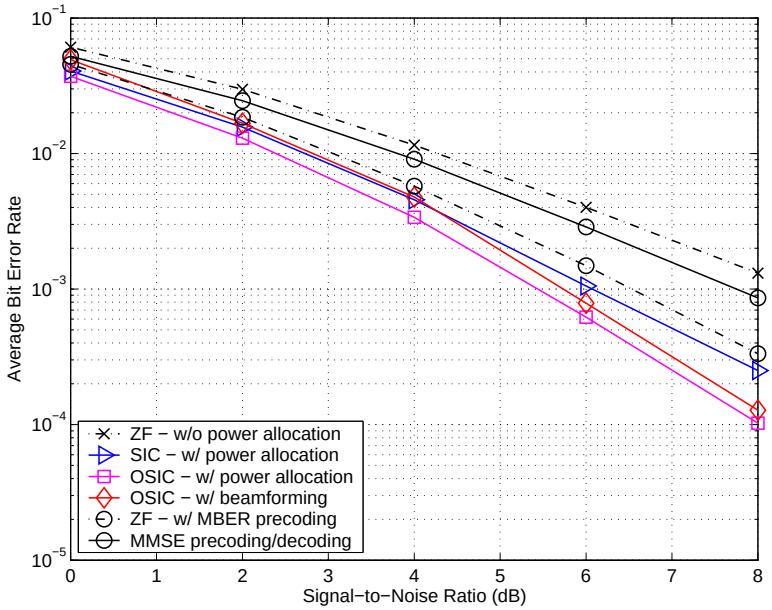

Figure 6.4. Average BER performance in correlated Rayleigh fading TIMO channel ($N_t = 2$, $N_r = 4$).

6.5.2 Ricean Fading

Figs. 6.5 and 6.6 illustrate average BER's in uncorrelated and correlated Ricean fading channels, respectively. Performance of SIC without power allocation (not shown) is nearly identical to that of MMSE precoding/decoding. Again, SIC and OSIC with power allocation outperform precoding schemes. We also observe that the proposed OSIC with MBER beamforming offers significant gain over power allocation and precoding schemes shown: at a BER of 10^{-3}, 7.0 dB SNR gain over OSIC with power allocation in uncorrelated fading, and 8.5 dB in correlated fading are observed. This is as excepted since in Ricean fading, due to the existence of a line-of-sight (LOS) component, the channel matrix is likely to be ill-conditioned.

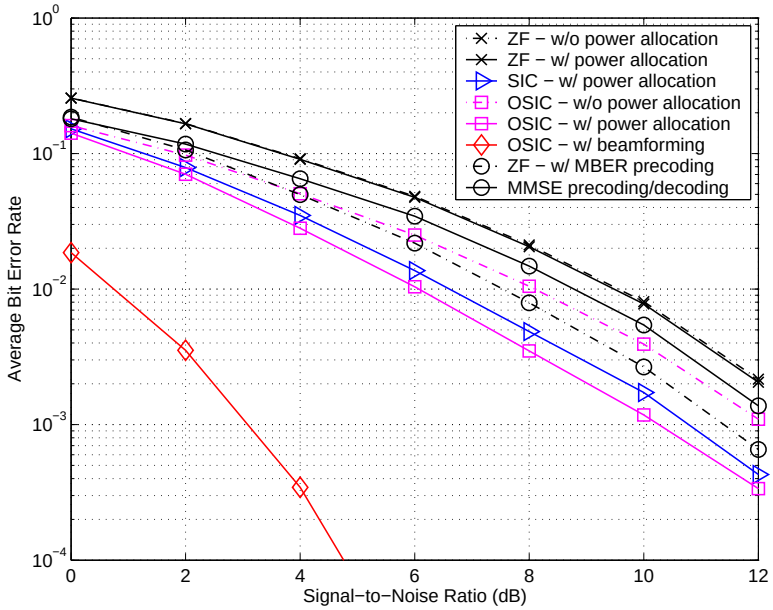

Figure 6.5. Average BER performance in uncorrelated Ricean fading TIMO channel ($N_t = 2$, $N_r = 4$, $K = 8$ dB).

6.6 Conclusion

Minimum BER (MBER) transmit power allocation and beamforming for TIMO spatial multiplexing are proposed in this chapter. It is shown that SIC and OSIC with approximate MBER (AMBER) power allocation outperform existing precoding schemes in Rayleigh fading channels, e.g., at a BER of 10^{-3}, OSIC with AMBER power allocation offers 1.0 dB and 1.9 dB SNR gains over MBER precoding with ZF equalization and MMSE precoding/decoding, respectively. The proposed OSIC with AMBER transmit beamforming eliminates error floors and offers superior performance over both power allocation and precoding schemes in Ricean fading channels, e.g., at a BER of 10^{-3}, OSIC with AMBER beamforming offers 7.0 dB and 8.5 dB SNR gain over OSIC with AMBER power allocation in uncorrelated and correlated Ricean fading, respectively. Compared to more general

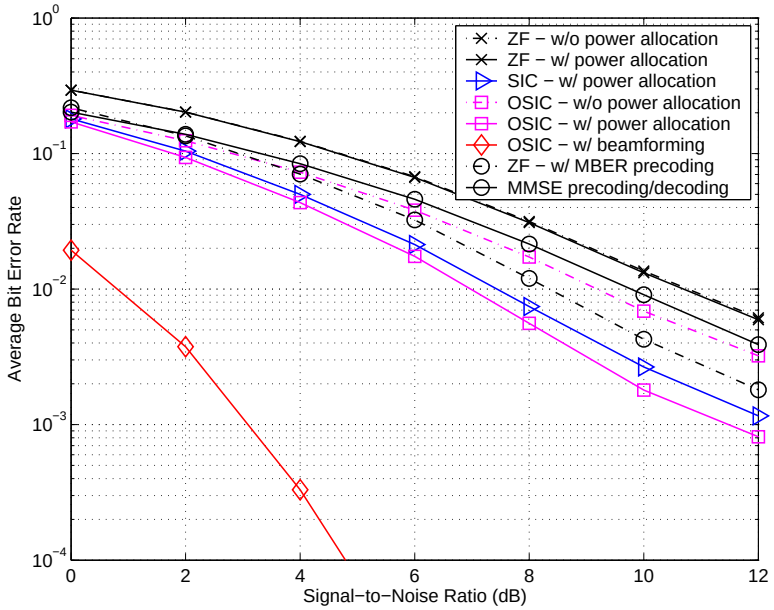

Figure 6.6. Average BER performance in correlated Ricean fading TIMO channel ($N_t = 2$, $N_r = 4$, $K = 8$ dB).

precoding methods, the proposed schemes reduce both complexity and feedback overhead and improve error rate performance.

Chapter 7

Summary, Conclusions and Future Work

In this chapter, we summarize the major contributions in this thesis, and suggest possible future directions which could be extensions of the research presented in this thesis.

7.1 Summary and Conclusions

After providing motivation in Chapter 1, an overview of wireless channel model, multicarrier and MIMO wireless communications is provided in Chapter 2.

Chapter 3 focuses on optimization of transmit redundancy for OFDM transmission to tradeoff performance, complexity and bandwidth efficiency. In Section 3.3, we analyzed redundancy issues in OFDM transmission using a guard interval of CP and ZP as well as no guard interval. It is found that redundancy introduced in OFDM transmission is closely related to system performance and complexity. In Section 3.4, a new system design criterion based on the channel matrix condition number is proposed. This criterion is then applied to the design of an AZP-OFDM, as well as a modification to reduce equalization complexity. An algorithm based on inverse iteration of power method is provided for the choice of the ZP length. Simulation results show that the proposed AZP-OFDM offers robust performance over a large range of channel time dispersion (delay spread) while

keeping the implementation complexity low.

In Chapter 4, optimization of transmit power for CP-OFDM is investigated. This is motivated by the analytical performance comparison between CP-OFDM and CP-SC in Section 4.4, where it is shown that uncoded CP-OFDM is inferior to CP-SC in frequency-selective channels. In Section 4.3, power allocation for CP-OFDM is formulated and solved using a variety of criteria, particularly minimum BER (MBER) and its approximation (AMBER). Algorithms to find MBER and AMBER power allocation solutions are also given in Section 4.3. In Section 4.4, a framework for analytical performance comparison between CP-SC and CP-OFDM is proposed and applied to asymptotic performance comparison among a variety of schemes. It has been established that uncoded CP-OFDM is inferior to ZF-equalized CP-SC, CP-OFDM with EG power allocation has the same performance at ZF-equalized CP-SC, and CP-OFDM with AMBER power allocation outperforms ZF-equalized CP-SC. In Section 4.5, performance degradation of power allocation due to imperfect CSI feedback is analyzed; special cases of CSI uncertainty, including delayed CSI, noisy CSI and covariance feedback are discussed.

In Chapter 5, power allocation is applied to MIMO spatial multiplexing systems. A variety of signal reception methods of MIMO spatial multiplexing, including ZF, SIC and OSIC, as well as their error rate performance are reviewed in Section 5.2. Assuming perfect CSI available at the transmitter, power allocation using an AMBER criterion is then applied to MIMO spatial multiplexing in Section 5.3. Compared with general precoding methods, the proposed power allocation enables interference cancellation and detection ordering under an MBER criterion, with significant reduction in both feedback overhead and processing complexity. In Section 5.4, performance degradation of power allocation with noisy CSI and power feedback is analyzed. The analysis is used to develop a modified AMBER power allocation scheme that uses the variance of the feedback, with the

capability of mitigating error propagation in interference cancellation. Simulation results in Section 5.5 show that SIC and OSIC employing MBER power allocation have the potential to offer superior performance over existing precoding schemes. For example, in a correlated Ricean fading channel, at a BER of 10^{-3}, MBER power allocation for OSIC offers, respectively, 2.0 and 4.0 dB SNR gains over MBER precoding for ZF equalization and MMSE precoding/decoding.

Chapter 6 investigates transmit optimization for TIMO spatial multiplexing, which is a special case of MIMO with two transmit antennas. In Section 6.2, signal reception methods discussed in Section 5.2 are customized for TIMO. Based on performance analysis, a model of ill-conditioned TIMO channel is proposed, which is an example of a "pinhole" channel. AMBER power allocation proposed in Chapter 5 is then applied, and closed-form solution as well as performance analysis are provided in Section 6.3. Section 6.4 is dedicated to transmit optimization for ill-conditioned TIMO channels. An approximate MBER transmit beamforming method is proposed which is shown to eliminate error floors in ill-conditioned channels. Simulation results in Section 6.5 show that the proposed approximate MBER transmit beamforming scheme offers superior performance in fading channels. For example, in uncorrelated Rayleigh fading, at a BER of 10^{-3}, OSIC with AMBER power allocation offers 1.0 dB and 1.9 dB SNR gains over MBER precoding with ZF equalization and MMSE precoding/decoding, respectively; in Ricean fading channels, at a BER of 10^{-3}, OSIC with AMBER beamforming offers 7.0 dB and 8.5 dB SNR gain over OSIC with AMBER power allocation in uncorrelated and correlated Ricean fading, respectively.

7.2 Future Directions

In this section, we discuss several issues that remain to be explored, as well as possible extensions of the results in this thesis.

7.2.1 Effects of/Robustness to Imperfect Knowledge

Although this thesis has investigated imperfect channel knowledge issues of power allocation for OFDM and MIMO spatial multiplexing, several open problems remain regarding imperfect knowledge.

- In Section 3.4, we have assumed that the channel is known perfectly. It is therefore of interest to investigate the effects of imperfect channel knowledge on the performance of AZP-OFDM. Matrix perturbation theory [97] may be used in the analysis. Based on the analysis, robustification of AZP-OFDM may be considered.

- The modified MBER power allocation for MIMO spatial multiplexing proposed in Section 5.4 assumes perfect knowledge of the variance of noisy feedback. One may consider the effects of imperfect estimates of the noise variance.

- Transmit beamforming for ill-conditioned TIMO channels proposed in Section 6.4 also assumes perfect estimation of the parameter a. Therefore, effects of and robustification to imperfect estimate/feedback of a require further investigation.

7.2.2 Partial versus Full CSI for Transmit Optimization

Transmit power allocation for MIMO spatial multiplexing can be viewed as a way of exploiting partial/imperfect CSI at the transmitter (CSIT). It is of interest to compare power allocation (exploiting partial CSI) with existing precoding schemes that rely on full CSI.

While numerical comparisons in terms of error rate performance have been provided in Chapter 5, a fundamental question is: what potential capacity is lost by employing power allocation versus precoding? To be specific, using notations in Chapter 2, capacity of a MIMO channel is given by [79]

$$C = \max_{\text{trace}\{\boldsymbol{P}\boldsymbol{P}^H\} \le N_t} \log_2 \det\left(\boldsymbol{I}_{N_t} + \gamma_s \boldsymbol{\Lambda} \boldsymbol{W}^H \boldsymbol{P}\boldsymbol{P}^H \boldsymbol{W}\right), \tag{7.1}$$

where $\boldsymbol{W}$ and $\boldsymbol{\Lambda}$ are eigenvector and eigenvalue matrices of $\boldsymbol{H}^H\boldsymbol{H}$, respectively.

- No CSIT. By choosing $\boldsymbol{P} = \boldsymbol{I}_{N_t}$, we have

$$C_{no} = \sum_{k=1}^{N_t} \left(1 + \gamma_s \lambda_k^2\right) \text{ bits/sec}, \tag{7.2}$$

  where $\lambda_k^2 \stackrel{\text{def}}{=} [\boldsymbol{\Lambda}]_{k,k}$.

- Full CSIT. The capacity-achieving precoder is given by $\boldsymbol{P} = \boldsymbol{W}\boldsymbol{D}$, where $\boldsymbol{D} \stackrel{\text{def}}{=} \text{diag}\{d_1, \cdots, d_{N_t}\}$ and d_k's are obtained as $d_k = \sqrt{\left(\mu - \gamma_s^{-1}\lambda_k^{-2}\right)_+}$, where μ is chosen to satisfy the transmit power constraint, i.e., $\sum_{k=1}^{N_t} d_k^2 = \text{trace}\{\boldsymbol{P}\boldsymbol{P}^H\} \le N_t$. The capacity of MIMO with full CSIT is given by

$$C_{full} = \sum_{k=1}^{N_t} \log_2\left(1 + \gamma_s \lambda_k^2 d_k^2\right) \text{ bits/sec}. \tag{7.3}$$

- Partial CSIT. For transmit power allocation, the precoding matrix, $\boldsymbol{P}$, is constrained to be diagonal. The capacity of MIMO with power allocation is given by

$$C_{partial} = \max_{\text{trace}\{\boldsymbol{P}^2\} \le N_t} \log_2 \det\left(\boldsymbol{I}_{N_t} + \gamma_s \boldsymbol{H}^H \boldsymbol{H} \boldsymbol{P}^2\right) \text{ bits/sec}. \tag{7.4}$$

Obviously, $C_{no} \le C_{partial} \le C_{full}$. The potential capacity loss due to power allocation needs to be quantified.

7.2.3 Cross-Dimension Transmit Optimization

Multiple dimensions are explored to meet the increasing requirement of high data rates, including space, time and frequency. Recently, cooperative communication has been proposed that achieves performance improvement via multi-user cooperation [70]. It if of interest to consider the joint optimization of resource allocation among multiple dimensions as well as multiple users. Some interesting problems are discussed next.

- Joint space-frequency power allocation for MIMO-OFDM systems. In [78], power allocation for an OFDM-MIMO system is investigated, where the MIMO system is used for transmit-receive diversity, and power allocation is conducted along frequency dimension only. It is of interest to consider joint space-time power allocation for MIMO-OFDM spatial multiplexing systems. This can be viewed as an extension of results of Chapters 4 and 5 in thesis.

- Joint space-time power allocation for transmit diversity systems. Generally transmit diversity does not require CSIT. When CSIT is available and exploited, array gain offered by multiple transmit antennas can be achieved [79]. One interesting problem is how to optimize transmit power to trade off between array gain and feedback overhead when it is difficult/expensive to acquire full CSIT.

- Multi-user joint power allocation. This thesis has investigated power allocation among subcarriers and transmit antennas of a single (virtual) user. Traditionally, power control has been widely employed in multi-user communications to allocate transmit power among different users. One may therefore consider joint transmit power allocation and power control to gain further performance improvement.

Appendix A

SER Depends on Unbiased SNR in Frequency-Flat Channels

Obviously, scaling of the received signal affects only amplitude-modulated signals, not phase- or frequency-modulated signals. Denoting the k-th constellation point as s_k, the unbiased received signal is given by $r = s_k + \eta$, where the noise term η has probability density function (pdf) $f_\eta(\eta)$. Denote the unbiased decision-point SNR as $\gamma_u = \frac{\mathrm{E}\{|s_k|^2\}}{\mathrm{E}\{|\eta|^2\}}$. The conditional probability of correct decision is given by

$$P(c|s_k) = \int_{\mathscr{D}_k} f_\eta(r - s_k)dr, \tag{A.1}$$

where $\mathscr{D}_k$ denotes the decision region for s_k. The average SER, as a function of γ_u, is given by averaging (A.1) over all constellation points, i.e.,

$$\begin{aligned} P_s(\gamma_u) &= \sum_k P(s_k)\left[1 - P(c|s_k)\right] \\ &= 1 - \sum_k P(s_k)P(c|s_k), \end{aligned}$$

where $P(s_k)$ is the *a priori* probability of s_k.

Now we consider a scaled version of r,

$$r' = \alpha r = \alpha s_k + \underbrace{\alpha\eta}_{\eta'},$$

where α is a scaler determined by the receiver. The biased decision-point SNR is given by

$$\begin{aligned}\gamma_b &= \frac{\mathrm{E}\{|s_k|^2\}}{\mathrm{E}\{|r'-s_k|^2\}} \\ &= \frac{\gamma_u}{(1-\alpha)^2\gamma_u+\alpha^2}.\end{aligned}$$

The pdf of η' is $f_{\eta'}(\eta') = \frac{1}{\alpha} f_\eta\left(\frac{\eta'}{\alpha}\right)$. Similar to the unbiased case, we calculate the conditional probability of correct decision as

$$\begin{aligned}P'(c|s_k) &= \int_{\mathscr{D}'_k} f_{\eta'}(r'-\alpha s_k)dr' \\ &= \int_{\mathscr{D}'_k} f_\eta\left(\frac{r'}{\alpha}-s_k\right)\frac{dr'}{\alpha}.\end{aligned}$$

where $\mathscr{D}'_k$ denotes the decision region of s_k in the biased case. It is easily seen that the biased decision region D'_k is also a scaled version of D_k. By a change in variables, we have

$$P'(c|s_k) = \int_{\mathscr{D}_k} f_\eta(z-s_k)dz \equiv P(c|s_k).$$

Therefore, the SER in the biased case is given by

$$P'_s(\gamma_b) = 1-\sum_k P(s_k)P'(c|s_k) \equiv P_s(\gamma_u),$$

i.e., the SER performance of frequency-flat channel is determined by the unbiased SNR.

Appendix B

Solution of A Class of Convex Optimization Problems

We solve a class of constrained convex optimization problems, which can be found in, e.g., [15, 74], for some special cases. Consider

$$\begin{cases} \min \sum_{k=0}^{N-1} f_k(x_k) \\ \text{subject to } \sum_{k=0}^{N-1} x_k = C;\ x_k \geq c_k,\ (k = 0, \cdots, N-1), \end{cases}, \tag{B.1}$$

where $f_k(\cdot)$'s are convex and continuously differentiable; C and c_k's are constants. The solution set is nonempty only if

$$C \geq \sum_{k=0}^{N-1} c_k. \tag{B.2}$$

It is readily verified that the constraints define a convex solution set. Therefore, the above optimization problem is convex, for which the Kuhn-Tucker conditions are sufficient and necessary for optimality. Introducing Lagrange multipliers $\{\mu_k\}_{k=0}^{N-1}$ for the inequality constraints, and multiplier ν for the equality constraint, we obtain the Lagrangian

$$\mathscr{L} = \sum_{k=0}^{N-1} f_k(x_k) + \sum_{k=0}^{N-1} \mu_k(c_k - x_k) + \nu \left(C - \sum_{k=0}^{N-1} x_k \right). \tag{B.3}$$

The Kuhn-Tucker conditions are given by

$$\begin{cases} \frac{d\mathscr{L}}{dx_k} = \frac{df_k(x_k)}{dx_k} - \mu_k - \nu = 0 \\ \sum_{k=0}^{N-1} x_k = C \qquad\qquad , \quad (k = 0, 1, \cdots, N-1). \\ x_k \geq c_k; \quad \mu_k \geq 0; \quad \mu_k(c_k - x_k) = 0 \end{cases} \tag{B.4}$$

Eliminating the slack variable μ_k in (B.4), we obtain the alternative optimality conditions

$$\begin{cases} \frac{df_k}{dx_k} \geq \nu \\ \sum_{k=0}^{N-1} x_k = C, \quad x_k \geq c_k \quad , \quad (k = 0, 1, \cdots, N-1). \\ \left(\frac{df_k}{dx_k} - \nu\right)(c_k - x_k) = 0 \end{cases} \tag{B.5}$$

Since $f(x)$ is convex, $d^2 f(x)/dx^2 > 0$, therefore $df(x)/dx$ is monotone increasing. Denote $g_k(\cdot)$ as the inverse function of df_k/dx_k, which is also monotone increasing. Consider the condition (B.5). If there exists a solution of $df_k/dx_k = \nu$ such that $x_k = g_k(\nu) \geq c_k$, the conditions in (B.5) are satisfied, and hence such a solution solves the original optimization problem (B.1). Otherwise, $\nu < df_k/dx_k$, and we have $x_k = c_k$ according to the third condition in (B.5). We note that the existence and uniqueness of such a solution is guaranteed since df_k/dx_k's are monotone increasing. Therefore, the solution of (B.1) is given by

$$x_k^* = \max\{c_k, g_k(\nu)\}, \tag{B.6}$$

where ν is chosen to satisfy the equality constraint in (B.1), i.e.,

$$\sum_{k=0}^{N-1} \max\{c_k, g_k(\nu)\} = C, \tag{B.7}$$

which can be solved numerically. Since $\sum_{k=0}^{N-1} \max\{c_k, g_k(\nu)\}$ is monotone increasing, such ν exists and is unique as long as the feasibility condition (B.2) is satisfied.

Appendix C

Proof of Claim 5.1

We make the following observations.

1. Conditioned on $\hat{\boldsymbol{H}}$, $\boldsymbol{h}_k$ is distributed as $\mathcal{N}(\hat{\boldsymbol{h}}_k, \sigma_h^2 \boldsymbol{I}_{N_r})$.

2. $\boldsymbol{\Upsilon}^{\perp}_{\hat{\boldsymbol{H}}_{(k+1)}}$ has rank $N_r - N_t + k$, and eigenvalue decomposition,

$$\boldsymbol{\Upsilon}^{\perp}_{\hat{\boldsymbol{H}}_{(k+1)}} = \boldsymbol{U} \begin{bmatrix} \boldsymbol{I}_{N_r - N_t + k} & \boldsymbol{0} \\ \boldsymbol{0} & \boldsymbol{0} \end{bmatrix} \boldsymbol{U}^H. \tag{C.1}$$

3. Denote $\boldsymbol{v} = \boldsymbol{U}^H \boldsymbol{h}_k$. Conditioned on $\hat{\boldsymbol{H}}$, $\boldsymbol{v}$ is distributed as $\mathcal{N}(\boldsymbol{U}^H \hat{\boldsymbol{h}}_k, \sigma_h^2 \boldsymbol{I}_{N_r})$. Furthermore, by denoting $(\cdot)_{\Re} = \Re\{(\cdot)\}$ and $(\cdot)_{\Im} = \Im\{(\cdot)\}$, we have, conditioned on $\hat{\boldsymbol{H}}$,

$$\boldsymbol{v}_{\Re} \sim \mathcal{N}\left(\Re\{\boldsymbol{U}^H \hat{\boldsymbol{h}}_k\}, \frac{\sigma_h^2}{2} \boldsymbol{I}_{N_r}\right), \quad \boldsymbol{v}_{\Im} \sim \mathcal{N}\left(\Im\{\boldsymbol{U}^H \hat{\boldsymbol{h}}_k\}, \frac{\sigma_h^2}{2} \boldsymbol{I}_{N_r}\right), \quad \mathbb{E}\left\{\boldsymbol{v}_{\Re} \boldsymbol{v}_{\Im}^T\right\} = \boldsymbol{0},$$

where the facts $\boldsymbol{U}_{\Re} \boldsymbol{U}_{\Re}^T + \boldsymbol{U}_{\Im} \boldsymbol{U}_{\Im}^T = \boldsymbol{I}_{N_r}$ and $\boldsymbol{U}_{\Re} \boldsymbol{U}_{\Im}^T = \boldsymbol{U}_{\Im} \boldsymbol{U}_{\Re}^T$ have been used.

4. We have

$$\tilde{g}_k^2 = \left\| \boldsymbol{\Upsilon}^{\perp}_{\hat{\boldsymbol{H}}_{(k+1)}} \boldsymbol{h}_k \right\|^2 = \boldsymbol{h}_k^H \boldsymbol{\Upsilon}^{\perp}_{\hat{\boldsymbol{H}}_{(k+1)}} \boldsymbol{h}_k = \boldsymbol{v}^H \begin{bmatrix} \boldsymbol{I}_{N_r - N_t + k} & \boldsymbol{0} \\ \boldsymbol{0} & \boldsymbol{0} \end{bmatrix} \boldsymbol{v} = \sum_{l=1}^{N_r - N_t + k} \left(v_{\Re,l}^2 + v_{\Im,l}^2 \right). \tag{C.2}$$

Therefore, conditioned on $\hat{\boldsymbol{H}}$, $\tilde{g}_k^2$ is the sum of squares of $2(N_r - N_t + k)$ independent real Gaussian random variables with variance $\sigma_h^2/2$, which is chi-square distributed with $2(N_r - N_t + k)$ degrees of freedom. The noncentrality parameter is calculated to be

$$\hat{\boldsymbol{h}}_k^H \boldsymbol{U} \begin{bmatrix} \boldsymbol{I}_{N_r - N_t + k} & \boldsymbol{0} \\ \boldsymbol{0} & \boldsymbol{0} \end{bmatrix} \boldsymbol{U}^H \hat{\boldsymbol{h}}_k = \hat{\boldsymbol{h}}_k^H \boldsymbol{\Upsilon}^{\perp}_{\hat{\boldsymbol{H}}_{(k+1)}} \hat{\boldsymbol{h}}_k = \hat{g}_k^2.$$

This establishes Claim 5.1.

Appendix D

Transmit Power Allocation for Ill-Conditioned TIMO Channels

Similar as in Section 6.3, we apply power allocation (6.12) and (6.13) to ill-conditioned channels (6.10). The estimate of the transmitted signal using ZF equalization is given by

$$\begin{aligned}\begin{bmatrix} y_1 \\ y_2 \end{bmatrix} &= \boldsymbol{H}^{\dagger}\boldsymbol{r} = \boldsymbol{H}^{\dagger}\boldsymbol{H}\boldsymbol{P}\boldsymbol{s} + \boldsymbol{H}^{\dagger}\eta \\ &= \frac{1}{1+|a|^2}\left(\begin{bmatrix} 1 & a \\ a^* & |a|^2 \end{bmatrix}\begin{bmatrix} p_1 s_1 \\ p_2 s_2 \end{bmatrix} + \frac{\boldsymbol{h}_1^H \eta}{\|\boldsymbol{h}_1\|^2}\begin{bmatrix} 1 \\ a^* \end{bmatrix}\right). \end{aligned} \tag{D.1}$$

We observe that $y_2 = a^* y_1$ in (D.1). It suffices to consider

$$y_1' \stackrel{\text{def}}{=} (1+|a|^2)y_1 = p_1 s_1 + a p_2 s_2 + \frac{\boldsymbol{h}_1^H \eta}{\|\boldsymbol{h}_1\|^2}.$$

A signal space diagram is illustrated in Fig. D.1. We assume for now s_1 is detected first, and consider the opposite detection order later. Similar to the analysis in Section 6.4.1, we obtain the approximate average BER

$$\begin{aligned}\bar{P}(\gamma_s; \boldsymbol{h}_1, a; p_1, p_2) \approx\ & \frac{1}{20}\exp\left\{-\gamma_s \|\boldsymbol{h}_1\|^2 (p_1 - \Re(a)p_2)^2\right\} \\ & + \frac{1}{20}\exp\left\{-\gamma_s \|\boldsymbol{h}_1\|^2 (p_1 + \Re(a)p_2)^2\right\}\end{aligned}$$

$$+\frac{1}{10}\exp\left\{-\gamma_s\|\boldsymbol{h}_1\|^2(\Re(a)p_2)^2\right\}. \tag{D.2}$$

To minimize (D.2) under the transmit power constraint (6.13), no closed-form solution exists. However, at moderate-to-high SNR, (D.2) can be further approximated as

$$\begin{aligned}\bar{P}(\gamma_s;\boldsymbol{h}_1,a;p_1,p_2) \;\approx\; & \frac{1}{10}\exp\left\{-\gamma_s\|\boldsymbol{h}_1\|^2(p_1-\Re(a)p_2)^2\right\} \\ & +\frac{1}{20}\exp\left\{-\gamma_s\|\boldsymbol{h}_1\|^2(p_1+\Re(a)p_2)^2\right\}. \end{aligned}\tag{D.3}$$

A closed-form solution that approximately minimize (D.3) under the transmit power constraint (6.13) is found to be

$$p_1 = 2|\Re(a)|p_2, \quad p_2 = \sqrt{\frac{2}{1+4[\Re(a)]^2}}. \tag{D.4}$$

The average BER for power allocation (D.4) in ill-conditioned channels can be approximated as

$$\bar{P}_{IC}^{PA}(\gamma_s;\boldsymbol{h}_1,a) \approx \frac{3}{20}\exp\left\{-\frac{2\gamma_s\|\boldsymbol{h}_1\|^2[\Re(a)]^2}{1+4[\Re(a)]^2}\right\}. \tag{D.5}$$

If s_2 is detected first, by similar argumentations, an approximate solution can be obtained as

$$p_1' = \frac{|\Re(a)|}{2}p_2', \quad p_2' = \sqrt{\frac{8}{4+[\Re(a)]^2}}. \tag{D.6}$$

The average BER for power allocation (D.6) in ill-conditioned channels can be approximated as

$$\bar{P}_{IC}^{PA'}(\gamma_s;\boldsymbol{h}_1,a) \approx \frac{3}{20}\exp\left\{-\frac{2\gamma_s\|\boldsymbol{h}_1\|^2[\Re(a)]^2}{4+[\Re(a)]^2}\right\}. \tag{D.7}$$

Comparing (D.7) with (D.5), by assumption $|a| \leq 1$, we know detecting s_1 first is optimal. It is obvious that (D.5) experiences error floors when $\Re(a) \approx 0$. This motivates our study of general precoding scheme for ill-conditioned channels.

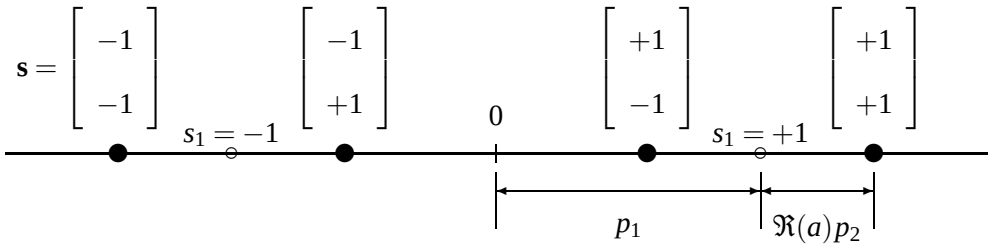

Figure D.1. Signal space diagram for BPSK with transmit power allocation in ill-conditioned channels.

Appendix E

Transmit Beamforming for Ill-Conditioned TIMO Channels

Consider the optimization problem of minimizing (6.25) under the constraint (6.22). Denote $\angle x$ as the phase angle of x. Since phase angles of p_{11}, p_{12}, p_{21} and p_{22} are irrelevant to the power constraint (6.22), we consider optimizing the phase angles first. A few observations are now in order.

1. The optimal p_{11} must be real; otherwise, by multiplying p_{11} by $e^{-j\angle p_{11}}$, $\tilde{P}_{IC}$ is reduced without violating the power constraint, i.e., a better precoder can be found. Therefore, without loss of generality, we have $p_{11} \geq 0$.

2. Similarly, optimal p_{21} satisfies $ap_{21} \geq 0$.

3. For simplicity of notation, denote $x = p_{11} + ap_{21}$, $y = \Re(p_{12} + ap_{22})$, and $\gamma = 2\gamma_s\|\boldsymbol{h}_1\|^2$. By assumption (6.24), we have $x \geq y$. Rewrite $\tilde{P}_{IC}$ in (6.25) as

$$\tilde{P}_{IC} = \frac{1}{20}e^{-\gamma(x-y)^2} + \frac{1}{10}e^{-\gamma y^2}.$$

   Its derivative with respect to y is obtained as

$$\frac{d\tilde{P}_{IC}}{dy} = \frac{1}{10}\gamma(x-y)e^{-\gamma(x-y)^2} - \frac{1}{5}\gamma y e^{-\gamma y^2}. \tag{E.1}$$

We now have two cases:

(a) if $x > 2y$, we have $\frac{d\tilde{P}_{IC}}{dy} < 0$, i.e., $\tilde{P}_{IC}$ is decreasing in y. Therefore, $\tilde{P}_{IC}$ achieves its local minimum when $p_{12} + ap_{22}$ is real and non-negative, because otherwise, by multiplying p_{12} and p_{22} by $e^{-j\angle(p_{12}+ap_{22})}$, a better precoder can be found. Furthermore, both p_{12} and ap_{22} must be real and non-negative by similar argumentation;

(b) otherwise, $y \le x \le 2y$, we have $\frac{d\tilde{P}_{IC}}{dy} > 0$, $\tilde{P}_{IC}$ is increasing in y, and $\tilde{P}_{IC}$ achieves its local minimum at $y = 0$, i.e., $p_{12} + ap_{22}$ is purely imaginary.

Comparing the local minimum values of these two cases,

$$\begin{aligned} \tilde{P}_{IC}|_{\Im(p_{12}+ap_{22})=0} &= \frac{1}{20}e^{-\gamma(x-y)^2} + \frac{1}{10}e^{-\gamma y^2}, \\ \tilde{P}_{IC}|_{\Re(p_{12}+ap_{22})=0} &= \frac{1}{10}e^{-\gamma x^2} + \frac{1}{10}, \end{aligned}$$

it is easily seen that when $p_{12} \ge 0$, $ap_{22} \ge 0$, and $p_{11} + ap_{21} > 2(p_{12} + ap_{22})$, $\tilde{P}_{IC}$ can achieve a global minimum.

Therefore, without loss of generality, the precoder minimizing (6.25) under the power constraint (6.22) satisfies

$$p_{11} \ge 0, \quad p_{12} \ge 0, \quad ap_{21} \ge 0, \quad ap_{22} \ge 0. \tag{E.2}$$

Denote $p_{21} = a^* q_{21}$ and $p_{22} = a^* q_{22}$, where $q_{21} \ge 0, q_{22} \ge 0$. The approximate average BER (6.25) can be written as

$$\begin{aligned} P(\gamma_s; \boldsymbol{h}_1, a; \boldsymbol{P}_b) \approx\ & \frac{1}{10}\exp\left\{-2\gamma_s\|\boldsymbol{h}_1\|^2\left(p_{11} + |a|^2 q_{21} - p_{12} - |a|^2 q_{22}\right)^2\right\} \\ & + \frac{1}{10}\exp\left\{-2\gamma_s\|\boldsymbol{h}_1\|^2\left(p_{12} + |a|^2 q_{22}\right)^2\right\}. \end{aligned} \tag{E.3}$$

By using the method of Lagrange multipliers, the solution to the problem of minimizing (E.3) can be obtained as

$$q_{21} = p_{11}, \quad q_{22} = p_{12}, \quad p_{11} = 2p_{12}. \tag{E.4}$$

To satisfy the power constraint (6.22), we have

$$p_{11} = \sqrt{\frac{8}{5(1+|a|^2)}},\ p_{12} = \frac{1}{2}p_{11},\ p_{21} = a^* p_{11},\ p_{22} = a^* p_{12}, \tag{E.5}$$

from which the precoder (6.26) is obtained.

Bibliography

[1] A. Abdi and M. Kaveh, "A space-time correlation model for multielement antenna systems in mobile fading channels," *IEEE J. Select. Areas Commun.*, vol. 20, no. 3, pp. 550–560, Apr. 2002.

[2] J. Akhtar and D. Gesbert, "A closed-form precoder for spatial multiplexing over correlated MIMO channels," in *Proc. IEEE Global Telecommun. Conf.*, vol. 4, San Francisco, CA, 2003, pp. 1847–1851.

[3] S. M. Alamouti, "A simple transmit diversity technique for wireless communications," *IEEE J. Select. Areas Commun.*, vol. 16, no. 8, pp. 1451–1458, Oct. 1998.

[4] J. B. Andersen, "Array gain and capacity for known random channels with multiple element arrays at both ends," *IEEE J. Select. Areas Commun.*, vol. 18, no. 11, pp. 2172–2178, Nov. 2000.

[5] ANSI, *The DWMT: a Multicarrier Transceiver for ADSL Using M-Band Wavelets*. American National Standards Institute, 1993.

[6] K. L. Baum, T. A. Kostas, P. J. Sartori, and B. K. Classon, "Performance characteristics of cellular systems with different link adaptation strategies," *IEEE Trans. Veh. Technol.*, vol. 52, no. 6, pp. 1497–1507, Nov. 2003.

[7] N. C. Beaulieu, “The evaluation of error probabilities for intersymbol and cochannel interference,” *IEEE Trans. Commun.*, vol. 39, no. 12, pp. 1740–1749, Dec. 1991.

[8] N. Benvenuto and S. Tomasin, “On the comparison between OFDM and single carrier modulation with DFE using a frequency-domain feedforward filter,” *IEEE Trans. Commun.*, vol. 50, no. 6, pp. 947–955, June 2002.

[9] Q. Bi, G. I. Zysman, and H. Menkes, “Wireless mobile communications at the start of the 21st century,” *IEEE Commun. Mag.*, vol. 39, no. 1, pp. 110–116, Jan. 2001.

[10] J. A. C. Bingham, “Multicarrier modulation for data transmission: an idea whose time has come,” *IEEE Commun. Mag.*, vol. 28, no. 5, pp. 5–14, May 1990.

[11] ——, *ADSL, VDSL, and Multicarrier Modulation*. New York, NY: Wiley, 2000.

[12] A. Björck, *Numerical Methods for Least Squares Problems*. Philadelphia, PA: SIAM, 1996.

[13] R. Blum and J. Winters, “On optimum MIMO with antenna selection,” *IEEE Commun. Lett.*, vol. 6, no. 8, pp. 322–324, Aug. 2002.

[14] H. Bölcskei, A. J. Paulraj, K. Hari, and R. Nabar, “Fixed broadband wireless access: state of the art, challenges, and future directions,” *IEEE Commun. Mag.*, vol. 39, no. 1, pp. 100–108, Jan. 2001.

[15] S. Boyd and L. Vandenberghe, *Convex Optimization*. New York, NY: Cambridge University Press, 2004.

[16] J. Brehmer, G. Dietl, M. Joham, and W. Utschick, “Reduced-complexity linear and nonlinear precoding for frequency-selective MIMO channels,” in *Proc. IEEE Veh. Technol. Conf.*, Los Angeles, CA, 2004.

[17] S. Catreux, V. Erceg, D. Gesbert, and R. Heath, "Adaptive modulation and MIMO coding for broadband wireless data networks," *IEEE Commun. Mag.*, vol. 40, no. 6, pp. 108–115, June 2002.

[18] S. Chandrasekaran and A. H. Sayed, "A fast stable solver for nonsymmetric Toeplitz and quasi-Toeplitz systems of linear equations," *SIAM Journal on Matrix Analysis and Applications*, vol. 19, no. 1, pp. 107–139, Jan. 1998.

[19] R. W. Chang, "Synthesis of band-limited orthogonal signals for multichannel data transmission," *Bell Syst. Tech. J.*, vol. 45, pp. 1775–1796, Dec. 1966.

[20] R. S. Cheng and S. Verdú, "Gaussian multiaccess channels with ISI: Capacity region and multiuser water-filling," *IEEE Trans. Info. Theory*, vol. 39, no. 3, pp. 773–785, May 1993.

[21] L. J. Cimini, "Analysis and simulation of a digital mobile channel using orthogonal multiplexed frequency division multiplexing," *IEEE Trans. Commun.*, vol. 33, no. 7, pp. 665–675, July 1985.

[22] J. M. Cioffi, G. P. Dudevoir, M. V. Eyuboglu, and G. D. Forney, "MMSE decision-feedback equalizers and coding — part 1: equalization results," *IEEE Trans. Commun.*, vol. 43, no. 10, pp. 2582–2594, Oct. 1995.

[23] L. Collin, O. Berder, P. Rostaing, and G. Burel, "Optimal minimum distance-based precoder for MIMO spatial multiplexing systems," *IEEE Trans. Signal Processing*, vol. 52, no. 3, pp. 617–627, Mar. 2004.

[24] A. Czylwik, "Adaptive OFDM for wideband radio channels," in *Proc. IEEE Global Telecommun. Conf.*, vol. 1, London, UK, 1996, pp. 713–718.

[25] G. Dahlquist and A. Björck, *Numerical Mathematics and Scientific Computation*. Philadelphia, PA: SIAM, 2003, vol. 2.

[26] O. Damen, A. Chkeif, and J. Belfiore, "Lattice code decoder for space-time codes," *IEEE Commun. Lett.*, vol. 4, no. 5, pp. 161–163, May 2000.

[27] J. W. Demmel, *Applied Numerical Linear Algebra*. Philadelphia, PA: SIAM, 1997.

[28] Y. Ding, T. N. Davidson, Z.-Q. Luo, and K. M. Wong, "Minimum BER block precoders for Zero-Forcing equalization," *IEEE Trans. Signal Processing*, vol. 51, no. 9, pp. 2410–2423, Sept. 2003.

[29] ETSI, *Radio Broadcasting Systems, Digital Audio Broadcasing (DAB) to Mobile, Portable and Fixed Receivers*, 1995.

[30] ——, *Digital Broadcasting Systems for Television, Sound and Data Services: Framing Structure, Channel Coding and Modulation for Digital Terrestrial Television*. Sophia-Antipolis, Valbonne, France: Norme ETSI, document ETS 300 401, European Telecommunications Standards Institute, 1996.

[31] ——, *Channel Models for HIPERLAN/2 in Different Indoor Scenarios*. Sophia-Antipolis, Valbonne, France: Norme ETSI, document 3ERI085B, European Telecommunications Standards Institute, 1998.

[32] ——, *Broadband Radio Access Networks (BRAN): HIPERLAN Type 2 Technical Specification Part 1 – Physical Layer*. Sophia-Antipolis, Valbonne, France: DTS/BRAN030003-1, 1999.

[33] ——, *Broadband Radio Access Networks (BRAN): Functional Requirement for Fixed Wireless Access Systems Below 11 GHz – HIPERMAN*. Sophia-Antipolis, Valbonne, France: ETSI, 2002.

[34] D. Falconer, S. L. Ariyavisitakul, A. Benyamin-Seeyar, and B. Eidson, "Frequency domain equalization for single-carrier broadband wireless systems," *IEEE Commun. Mag.*, vol. 40, no. 4, pp. 58–66, April 2002.

[35] F. R. Farrokhi, G. J. Foschini, A. Lozano, and R. A. Valenzuela, "Link-optimal space-time processing with multiple transmit and receive antennas," *IEEE Commun. Lett.*, vol. 5, no. 3, pp. 85–87, Mar. 2001.

[36] G. J. Foschini and M. J. Gans, "On limits of wireless communications in a fading environment when using multiple antennas," *Wireless Personal Commun.*, vol. 6, no. 3, pp. 311–335, Mar. 1998.

[37] G. J. Foschini, G. D. Golden, R. A. Valenzuela, and P. W. Wolniansky, "Simplified processing for high spectral efficiency wireless communication employing multi-element arrays," *IEEE J. Select. Areas Commun.*, vol. 17, no. 11, pp. 1841–1852, Nov. 1999.

[38] D. Gesbert, H. Bölcskey, D. Gore, and A. J. Paulraj, "Outdoor MIMO wireless channels: Models and performance prediction," *IEEE Trans. Commun.*, vol. 50, no. 12, pp. 1926–1934, Dec. 2002.

[39] D. Gesbert, L. Haumonté, H. Bölcskei, and A. J. Paulraj, "Technologies and performance for non-line-of-sight broadband wireless access networks," *IEEE Commun. Mag.*, vol. 40, no. 4, pp. 86–95, April 2002.

[40] L. Goldfeld, V. Lyandres, and D. Wulich, "Minimum BER power allocation for OFDM in fading channel," *IEEE Trans. Commun.*, vol. 50, no. 11, pp. 1729–1733, Nov. 2002.

[41] G. H. Golub and C. F. van Loan, *Matrix Computations*, 2nd ed. Baltimore, MD: Johns Hopkins University Press, 1989.

[42] D. A. Gore, R. W. Heath, and A. J. Paulraj, "Transmit selection in spatial multiplexing systems," *IEEE Commun. Lett.*, vol. 6, no. 11, pp. 491–493, Nov. 2002.

[43] B. Hassibi and H. Vikalo, "On the expected complexity of sphere decoding," in *Proc. Asilomar Conf. on Signals, Systems and Computers*, vol. 2, Pacific Grove, CA, 2001, pp. 1051–1055.

[44] R. W. Heath, S. Sandhu, and A. Paulraj, "Antenna selection for spatial multiplexing with linear receivers," *IEEE Commun. Lett.*, vol. 6, no. 11, pp. 487–489, Nov. 2001.

[45] R. A. Horn and C. R. Johnson, *Matrix Analysis*. New York, NY: Cambridge University Press, 1999.

[46] IEEE, *IEEE Standard for Wireless LAN Medium Access Control (MAC) and Physical Layer (PHY) Specifications*. The Institute of Electrical and Electronic Engineers, 1997.

[47] ——, *IEEE Standard for Local and Metropolitan Area Networks – Part 16: Air Interface for Fixed Wireless Access Systems*. The Institute of Electrical and Electronic Engineers, 2001.

[48] E. C. Ifeachor and B. W. Jervis, *Digital Signal Processing: A Practical Approach*, 2nd ed. Englewood Cliffs, NJ: Prentice Hall, 2002.

[49] A. P. Iserte, M. A. Lagunas, and A. I. Pérez-Neira, "Robust power allocation for minimum BER in a SISO-OFDM system," in *Proc. IEEE Int. Conf. Commun.*, vol. 2, Anchorage, Alaska, 2003, pp. 1263–1267.

[50] W. Jakes, *Microwave Mobile Communications*. New York, NY: Wiley, 1974.

[51] A. T. James, "Distributions of matrix variates and latent roots derived from normal samples," *The Annals of Math. Stat.*, vol. 35, no. 2, pp. 475–501, June 1964.

[52] G. Jöngren and M. Skoglund, "Utilizing quantized feedback information in orthogonal space-time block coding," in *Proc. IEEE Global Telecommun. Conf.*, vol. 2, San Francisco, CA, 2000, pp. 995–999.

[53] G. Jöngren, M. Skoglund, and B. Ottersten, "Combining bemforming and orthogonal space-time block coding," *IEEE Trans. Info. Theory*, vol. 48, no. 3, pp. 611–627, Mar. 2002.

[54] D. Kim and G. L. Stüber, "Residual ISI cancellation for OFDM with application to HDTV broadcasting," *IEEE J. Select. Areas. in Commun.*, vol. 16, no. 8, pp. 1590–1599, Oct. 1998.

[55] E. G. Larsson, G. Ganesan, P. Stoica, and W.-H. Wong, "On the performance of orthogonal space-time block coding with quantized feedback," *IEEE Commun. Lett.*, vol. 6, no. 11, pp. 487–489, Nov. 2002.

[56] X. Li, H. C. Huang, A. Lozano, and G. J. Foschini, "Reduced-complexity detection algorithms for systems using multi-element arrays," in *Proc. IEEE Global Telecommun. Conf.*, vol. 1, San Francisco, CA, 2000, pp. 1072–1076.

[57] Z. Liu, Y. Xin, and G. B. Giannakis, "Linear constellation precoding for OFDM with maximum multipath diversity and coding gains," *IEEE Trans. Commun.*, vol. 51, no. 3, pp. 416–427, Mar. 2003.

[58] D. Love, R. Heath, W. Santipach, and M. Honig, "What is the value of limited feedback for MIMO channels," *IEEE Commun. Mag.*, vol. 42, no. 10, pp. 54–59, Oct. 2004.

[59] D. J. Love and R. W. Heath, "Limited feedback precoding for spatial multiplexing systems," in *Proc. IEEE Global Telecommun. Conf.*, vol. 4, San Francisco, CA, 2003, pp. 1857–1861.

[60] G. P. McCormick, *Nonlinear Programming: Theory, Algorithms, and Applications*. New York, NY: Wiley, 1983.

[61] B. McNair, L. J. Cimini, and N. Sollenberger, "A robust timing and frequency offset estimation scheme for orghogonal frequency division multiplexing (OFDM) systems," in *Proc. IEEE Veh. Technol. Conf. 1999 Spring*, 1999, pp. 690–694.

[62] P. J. W. Melsa, R. C. Younce, and C. E. Rohrs, "Impulse response shortening for discrete multitone transceivers," *IEEE Trans. Commun.*, vol. 44, no. 12, pp. 1662–1672, Dec. 1996.

[63] S. K. Mitra, *Digital Signal Processing: A Computer-Based Approach*, 2nd ed. New York, NY: McGraw-Hill, 2001.

[64] A. F. Molisch and M. Z. Win, "MIMO systems with antenna selection," *IEEE Microwave Mag.*, vol. 5, no. 1, pp. 46–56, Mar. 3004.

[65] D. H. Morais, *Fixed Broadband Wireless Communications–Principles and Practical Applications*. Englewood Cliffs, NJ: Prentice Hall, 2004.

[66] R. J. Muirhead, *Aspects of Multivariate Statistical Theory*. New York, NY: Wiley, 1982.

[67] B. Muquet, Z. Wang, G. B. Giannakis, M. de Courville, and P. Duhamel, "Cyclic prefixing or zero padding for wireless multicarrier transmissions?" *IEEE Trans. Commun.*, vol. 50, no. 12, pp. 2136–2148, Dec. 2002.

[68] S. H. Nam, O.-S. Shin, and K. B. Lee, "Transmit power allocation for a modified V-BLAST system," *IEEE Trans. Commun.*, vol. 52, no. 7, pp. 1074–1079, July 2004.

[69] A. Narula, M. J. Lopez, M. D. Trott, and G. W. Wornell, "Efficient use of side information in multiple-antenna data transmission over fading channels," *IEEE J. Select. Areas Commun.*, vol. 16, no. 8, pp. 1423–1436, Oct. 1998.

[70] A. Nosratinia, T. E. Hunter, and A. Hedyat, "Cooperative communication in wireless networks," *IEEE Commun. Mag.*, vol. 42, no. 10, pp. 74–80, Oct. 2004.

[71] H. Ochiai and H. Imai, "On the distribution of the peak-to-average power ratio in OFDM signals," *IEEE Trans. Commun.*, vol. 49, no. 2, pp. 282–289, Feb. 2001.

[72] S. Ohno and G. B. Giannakis, "Optimal training and redundant precoding for block transmissions with application to wireless OFDM," *IEEE Trans. Commun.*, vol. 51, no. 12, pp. 2113–2123, Dec. 2002.

[73] R. O'Neill and L. Lopes, "Performance of amplitude limited multitone signals," in *Proc. IEEE Veh. Technol. Conf.*, vol. 3, Stockholm, Sweden, 1994, pp. 1675–1679.

[74] E. N. Onggosanusi, A. M. Sayeed, and B. D. van Veen, "Efficient signaling schemes for wideband space-time wireless channels using channel state information," *IEEE Trans. Veh. Technol.*, vol. 52, no. 1, pp. 1–13, Jan. 2003.

[75] A. Oppenheim and R. Schafer, *Discrete-Time Signal Processing*. Englewood Cliffs, NJ: Prentice Hall, 1989.

[76] D. P. Palomar, J. M. Cioffi, and M. A. Lagunas, "Joint Tx-Rx beamforming design for multicarrier MIMO channels: A unified framework for convex optimization," *IEEE Trans. Signal Processing*, vol. 51, no. 9, pp. 2381–2401, Sept. 2003.

[77] A. Papoulis, *Probability, Random Variables, and Stochastic Processes*, 3rd ed. New York, NY: McGraw-Hill, 1991.

[78] A. Pascual-Iserte, A. I. Pérez-Neira, and M. A. Lagunas, "On power allocation strategies for maximum signal to noise and interference ratio in an OFDM-MIMO system," *IEEE Trans. Wireless Commun.*, vol. 3, no. 3, pp. 808–820, May 2004.

[79] A. Paulraj, R. Nabar, and D. Gore, *Introduction to Space-Time Wireless Communications*. New York, NY: Cambridge University Press, 2003.

[80] A. J. Paulraj, D. A. Gore, R. U. Nabar, and H. Bölcskey, "An overview of MIMO communications—a key to gigabit wireless," *Proc. IEEE*, vol. 92, no. 2, pp. 198–218, Feb. 2004.

[81] A. J. Paulraj and C. B. Papadias, "Space-time processing for wireless communications," *IEEE Signal Processing Mag.*, vol. 14, no. 6, pp. 49–83, Nov. 1997.

[82] A. Peled and A. Ruiz, "Frequency domain data transmission using reduced computational complexity algorithms," in *Proc. IEEE Int. Conf. Acoustic, Speech and Signal Processing*, vol. 5, 1980, pp. 964–967.

[83] G. C. Porter, "Error distribution and diversity performance of a frequency differential PSK HF modem," *IEEE Trans. Commun. Technology*, vol. 16, no. 4, pp. 567–575, Aug. 1968.

[84] J. G. Proakis, *Digital Communications*, 4th ed. New York, NY: McGraw-Hill, 2001.

[85] T. S. Rappaport, *Wireless Communications: Principles and Practice*. Englewood Cliffs, NJ: Prentice Hall, 1996.

[86] F. Rey, M. Lamarca, and G. Vázquez, "Transmit filter optimization based on partial CSI knowledge for wireless applications," in *Proc. IEEE Int. Conf. Commun.*, Anchorage, Alaska, 2003, pp. 2567–2571.

[87] B. Saltzberg, "Performance of an efficient parallel data transmission system," *IEEE Trans. Commun. Technology*, vol. 15, no. 6, pp. 805–811, Dec. 1967.

[88] H. Sampath, P. Stoica, and A. Paulraj, "Generalized linear precoder and decoder design for MIMO channels using the weighted MMSE criterion," *IEEE Trans. Commun.*, vol. 49, no. 12, pp. 2198–2206, Dec. 2001.

[89] S. Sanayei and A. Nosratinia, "Antenna selection in MIMO systems," *IEEE Commun. Mag.*, vol. 42, no. 10, pp. 68–73, Oct. 2004.

[90] H. Sari, G. Karam, and I. Jeanclaude, "Frequency-domain equalization of mobile radio and terrestrial broadcast channels," in *Proc. IEEE Global Telecommun. Conf.*, vol. 1, San Francisco, CA, 1994, pp. 1–5.

[91] A. Scaglione, G. B. Giannakis, and S. Barbarossa, "Redundant filterbank precoders and equalizers - part 1. unification and optimal designs," *IEEE Trans. Signal Processing*, vol. 47, no. 7, pp. 1988–2006, July 1999.

[92] A. Scaglione, P. Stoica, S. Barbarossa, G. B. Giannakis, and H. Sampath, "Optimal designs for space-time linear precoders and equalizers," *IEEE Trans. Signal Processing*, vol. 50, no. 5, pp. 1051–1064, May 2002.

[93] A. Sendonaris, E. Erkip, and B. Aazhang, "User cooperation diversity–part i: System description," *IEEE Trans. Commun.*, vol. 51, no. 11, pp. 1927–1938, Nov. 2003.

[94] S. Shakkottai, T. S. Rappaport, and P. C. Karlsson, "Cross-layer design for wireless networks," *IEEE Commun. Mag.*, vol. 41, no. 10, pp. 74–80, Oct. 2003.

[95] D. Shiu, G. J. Foschini, M. J. Gans, and J. M. Kahn, "Fading correlation and its effect on the capacity of multielement antenna systems," *IEEE Trans. Commun.*, vol. 48, no. 3, pp. 502–513, Mar. 2000.

[96] Y. Song, "*Multiple-Input Multiple-Output Wireless Communication Systems with Cochannel Interference*," Ph.D. dissertation, Dept. of Electrical and Computer Engineering, Queen's University, 2003.

[97] G. W. Stewart and J. Sun, *Matrix Perturbation Theory*. San Diego, CA: Academy Press, 1990.

[98] G. L. Stüber, J. R. Barry, S. W. McLaughlin, Y. Li, M. A. Ingram, and T. G. Pratt, "Broadband MIMO-OFDM wireless communications," *Proc. IEEE*, vol. 92, no. 2, pp. 271–294, Feb. 2004.

[99] V. Tarokh and H. Jafarkhani, "On the computation and reduction of the peak to average power ratio in multicarrier communications," *IEEE Trans. Commun.*, vol. 48, no. 1, pp. 37–44, Jan. 2000.

[100] V. Tarokh, H. Jafarkhani, and A. R. Calderbank, "Space-time block codes from orthogonal designs," *IEEE Trans. Info. Theory*, vol. 45, no. 5, pp. 1456–1467, July 1999.

[101] V. Tarokh, N. Seshadri, and A. Calderbank, "Space-time codes for high data rate wireless communication: performance criterion and code construction," *IEEE Trans. Info. Theory*, vol. 44, no. 2, pp. 744–765, Mar. 1998.

[102] E. Telatar, "Capacity of multi-antenna Gaussian channels," *European Trans. Telecommun.*, vol. 10, no. 6, pp. 585–595, Nov.-Dec. 1999.

[103] M. Toeltsch and A. F. Molisch, "Efficient OFDM transmission without cyclic prefix over frequency-selective channels," in *Proc. IEEE Int. Symposium on Personal, Indoor and Mobile Radio Commun.*, vol. 2, 2000, pp. 1363–1367.

[104] V. Vadde and S. Gray, "Partial response signaling for enhanced spectral efficiency and RF performance in OFDM systems," in *Proc. IEEE Global Telecommun. Conf.*, vol. 5, San Antonio, Texas, USA, 2001, pp. 3120–3124.

[105] N. Wang and S. D. Blostein, "Power loading for CP-OFDM over frequency-selective fading channels," in *Proc. IEEE Global Telecommun. Conf.*, vol. 4, San Francisco, CA, 2003, pp. 2305–2309.

[106] Z. Wang and G. B. Giannakis, "Wireless multicarrier communications," *IEEE Signal Processing Mag.*, vol. 17, no. 3, pp. 29–48, May 2000.

[107] S. Weinstein and P. Ebert, "Data transmission by frequency-division multiplexing using the discrete Fourier transform," *IEEE Trans. Commun.*, vol. 19, no. 5, pp. 628–634, Oct. 1971.

[108] M. Win and J. Winters, "Virtual branch analysis of symbol error probability for hybrid selection/maximal-ratio combing in Rayleigh fading," *IEEE Trans. Commun.*, vol. 49, no. 11, pp. 1926–1934, Nov. 2001.

[109] P. W. Wolniansky, G. J. Foschini, G. D. Golden, and R. A. Valenzuela, "V-blast: An architecture for realizing very high data rates over the rich-scattering wireless channel," in *Proc. ISSSE-98*, Pisa, Italy, 1998, pp. 295–300.

[110] D. Wulich and L. Goldfeld, “Reduction of peak factor in orthogonal multicarrier modulation by amplitude limiting and coding,” *IEEE Trans. Commun.*, vol. 47, no. 1, pp. 18–21, Jan. 1999.

[111] X.-G. Xia, “Precoded and vector OFDM robust to channel spectral nulls with reduced cyclic prefix length in single transmit antenna systems,” *IEEE Trans. Commun.*, vol. 49, no. 8, pp. 1363–1374, Aug. 2001.

[112] K. Yu and B. Ottersten, “Models for MIMO propagation channels: a review,” *Wiley Journal on Wireless Communications and Mobile Computing*, vol. 2, no. 7, pp. 653–666, Nov. 2002.

[113] Y. Zhao and S. G. Haggman, “Sensitivity to Doppler shift and carrier frequency errors in OFDM systems — the consequences and solutions,” in *Proc. IEEE Veh. Technol. Conf.*, vol. 3, Atlanta, Georgia, 1996, pp. 1564–1568.

[114] S. Zhou and G. B. Giannakis, “Optimal transmitter eigen-beamforming and space-time block coding based on channel mean feedback,” *IEEE Trans. Signal Processing*, vol. 50, no. 10, pp. 2599–2613, Oct. 2002.

[115] ——, “Optimal transmitter eigen-beamforming and space-time block coding based on channel mean feedback,” *IEEE Trans. Signal Processing*, vol. 50, no. 10, pp. 2599–2613, Oct. 2002.

[116] ——, “Adaptive modulation for multi-antenna transmissions with channel mean feedback,” in *Proc. IEEE Int. Conf. Commun.*, vol. 4, Anchorage, Alaska, 2003, pp. 2281–2285.